PARTICULATE MATTER EMISSION CHARACTERIZATION FROM A NATURAL GAS HIGH-PRESSURE DIRECT-INJECTION ENGINE

by

BRONSON DAVID PATYCHUK

BASc., The University of British Columbia, 2010

A THESIS SUBMITTED IN PARTIAL FULFILLMENT OF
THE REQUIREMENTS FOR THE DEGREE OF

MASTER OF APPLIED SCIENCE

in

THE FACULTY OF GRADUATE STUDIES

(Mechanical Engineering)

THE UNIVERSITY OF BRITISH COLUMBIA

(Vancouver)

April 2013

© Bronson David Patychuk, 2013

Abstract

Stringent regulations have been enacted to reduce particulate matter (PM) emissions from heavy-duty compression-ignition (CI) engines. New regulations (Euro VI) restrict PM mass and particle number concentration. To help meet these regulations, a greater understanding of the physical and chemical characteristics of the PM is desired. This thesis is concerned with the mobility, morphology (by electron microscopy), mass (filter sampling), light scattering and semivolatile content of the particles.

Natural gas has become an increasingly attractive transportation fuel for both environmental and economic reasons. One technology to utilize gaseous fuels in heavy-duty engines is Westport Innovations Inc.'s High Pressure Direct Injection (HPDI™) system. This is a system where the natural gas is directly injected late in the compression stroke and ignition of the natural gas is provided by a diesel pilot.

PM emissions were characterized from a heavy-duty Cummins ISX engine converted to single cylinder operation and operating under HPDI™ fueling. Tests were performed to observe the effects of speed and load combinations, the effects of operating parameter variations (Injection timing, equivalence ratio, gas supply pressure, EGR % and diesel injection mass) and the effects of fuel premixing on the PM emissions.

Engine load was more important than speed for qualitatively grouping the PM emission characteristics (mass, number, semi-volatile fraction). The exception is at low engine speeds where low mass and number concentrations were observed, along with nearly constant particle sizes, across different loads.

The effects of the input parameter variations were analyzed with response surface methods. The PM emissions were more sensitive to changes in the input parameters than the gaseous emissions. Equivalence ratio, engine power and injection pressure were the most important parameters for PM mass emissions. Overall, the PM emissions varied monotonically with the input parameters and no local PM emission minima were observed.

Partially premixing some of the natural gas before ignition can reduce PM emissions by over 80% at some conditions at the expense of cycle-to-cycle variability and pressure rise rates. Some optimized equivalence ratios and EGR percentages were developed to improve the stability of combustion.

Table of Contents

Appendices

List of Tables

List of Figures

List of Abbreviations, Acronyms and Nomenclature

ATDC – After Top Dead Center
BC – Black Carbon
CI – Compression Ignition
CNG – Compressed Natural Gas
CPC – Condensation Particle Counter
DE – Diesel Exhaust
DMA - Differential Mobility Analyzer
DOC – Diesel Oxidation Catalyst
DPF – Diesel Particulate Filter
EC – Elemental Carbon
EGR – Exhaust Gas Recirculation
EPA – Environmental Protection Agency
EQR – Equivalence Ratio
EU – European Union
FID – Flame Ionizing Detector
GISFC – Gross Indicated Specific Fuel Consumption
GPW – Gas Pulse Width
GRP – Gas Rail Pressure
HPDI – High Pressure Direct Injection
LNG – Liquefied Natural Gas
LPM – Liters Per Minute
NDIR – Non-Dispersive Infrared
NG – Natural Gas
NGV – Natural Gas Vehicles
NMHC – Non Methane Hydrocarbons
NOx – Nitrogen Oxides
NTDE – New Technology Diesel Exhaust
OC – Organic Carbon
PAH – Polycyclic Aromatic Hydrocarbons
PM – Particulate Matter
PN – Particle Number
PPW – Pilot Pulse Width
PSEP – Pulse Separation
SCR – Selective Catalytic Reduction
SI – Spark Ignited
SMPS – Scanning Mobility Particle Spectrometer
SVOC – Semi Volatile Organic Carbon
TAC – Toxic Air Contaminant
TEM - Transmission Electron Microscope
TD - Thermodenuder
TDE – Traditional Diesel Exhaust
TEOM – Tapered Element Oscillating Microbalance
uHC – Unburnt Hydrocarbons
ULSD – Ultra Low Sulfur Diesel

A - Area
d_a – Projected aggregate diameter
DR – Dilution ratio
D_f – Fractal dimension
E_1 – Electric field
f - Frequency, also VOC/SVOC fraction
γ – Ratio of specific heats
L - Length
m - Mass
N – Engine speed
n_p – Number of primary particles
θ – Crank angle degrees
P – Pressure
Q - Net heat release, also volumetric flow rate
r - Radius
R_f – Projected radius
r_p – Primary particle radius
V – Cylinder volume, also voltage
$W_{c,ig}$ – Gross indicated work per cycle
Z_p - Particle Mobility

Acknowledgments

I would first like to thank my supervisor, Dr. Steven Rogak, for providing me with the opportunity to complete my research at UBC. His expertise and guidance throughout my time at UBC was invaluable and I have great appreciation for his contributions to my work. I have really enjoyed this project and became a better engineer over the last three years. This is in large part due to his help. Thank you.

I also want to thank all of the fellow researchers I have had the pleasure of working with during my research, especially Ehsan Faghani, Brian Just, James Montgomery, Arka Soewono, Kiego Karakama, Arminta Chicka and Christie Lagally. I need to specifically single out Hugo Tjong for all of his help with the Matlab codes to process the engine and TEM data.

While still on the topic of colleagues, I need to thank my Formula UBC teammates. Especially Erik Roy for showing me how to run engine dynos and Mike Rooney, Terence Hui and Andrew Reimer for keeping me honest.

Thanks to all of the support staff at UBC; Bob Parry for keeping the engine running along with Glenn Jolly and Sean Buxton for helping troubleshoot and fix all of the electrical gremlins.

Being able to work with an industry partner throughout this project kept things exciting and purposeful. I need to thank Dr. Gordon McTaggart-Cowan, Dr. Ning Wu and Dr. Phil Hill at Westport Innovations for their support and feedback throughout the project.

Finally, I need to thank my family. I owe everything to them. The support from my parents, Barb and Gerry is the reason I could get to this point.

Thanks!

1 Motivation, Scope and Objectives

Compression Ignition (CI) engines are found in a majority of heavy-duty on and off road transportation applications, as well as an increasingly large percentage of light-duty vehicles. These engines' combination of reliability, fuel economy and power has led to their widespread use. However, when compared with spark-ignited (SI) engines, CI engines emit relatively high levels of pollutants affecting local air quality and respiratory health, especially, nitrogen oxides (NOx) and particulate matter (PM).

These emissions can have serious and complex effects on both human health and the environment. As such, these emissions have been increasingly regulated in recent years. Upcoming PM regulations are extremely stringent and will encapsulate more than just the PM mass concentrations. To meet these emission levels, a more thorough understanding of the physical and chemical characteristics of the PM as well as the effects of different engine operating conditions have on these emissions is needed.

This thesis focuses on characterizing the PM emissions from a natural gas fueled High Pressure Direct Injected (HPDI) CI engine. Chapter 1 describes the key issues that motivate the objectives of this thesis. Chapter 2 describes the experimental apparatus used for the study. Chapter 3 contains the experimental results and Chapter 4 offers discussion, recommendations and conclusions derived from this work.

1.1 Emissions from Compression Ignition Engines

CI engines ignite a fuel in a compressed cylinder to produce work. Ideally, the only products of combustion would be carbon dioxide (CO_2), water vapor (H_2O) and any excess air from within the cylinder. However, due to imperfect real conditions "other products are formed, due to incomplete combustion, reactions at temperature and pressure, combustion of engine lubricating oil and oil additives or combustion of non-hydrocarbon components of diesel fuel" (Majewski, 2012)

The most common of these pollutants have been regulated by various governments throughout the world (EPA, 2012) (European Commision, 2012) and are nitrogen oxides (NOx), unburned hydrocarbons (uHCs) (this also includes methane emissions (CH_4)), carbon monoxide (CO) and particulate matter emissions (PM).

In addition to these regulated emissions, many other chemicals are emitted at smaller concentrations, these include "inorganic ions, single-ring aromatics, PAHs, nitroPAHs, alkanes, alcohol and organic acids, hopanes/ steranes, carbonyls, metals and elements" (Khalek, Bougher, Merritt, & Zielinska, 2011). While these pollutants are typically found at low concentrations, they can be comparatively quite toxic (CARB, 2013)

1.1.1 Emission Regulations

Emission regulation for heavy duty vehicles began in 1974 in North America and standardized across Europe in 1998 (Environmental Protection Agency, 2012) (European Commision, 2012). These limits have been steadily tightened over the years to the stringent levels seen today. The regulations for PM emissions have been reduced by a factor of 36 since 1992, similarly, the NOx limits have been reduced by a factor of 20.

Table 1 shows the limits for these pollutants since 1992. The EPA limits in North America show similar reductions.

	Year	CO	HC	NOx	PM	PN
		g/kWh				*#/kWh*
Euro I	1992	4.5	1.1	8.0	0.36	
Euro II	1996	4.0	1.1	7.0	0.25	
Euro II	1998.	4.0	1.1	7.0	0.15	
Euro III	2000	2.1	0.66	5.0	0.10	
Euro IV	2005	1.5	0.46	3.5	0.02	
Euro V	2008	1.5	0.46	2.0	0.02	
Euro VI	2013	1.5	0.13	0.4	0.01	8.0×10^{11}

Table 1 - European Heavy Duty Emission Limits – adapted from http://www.dieselnet.com/standards/eu/hd.php

Of most interest to this study is the restriction of particle number introduced in the EURO VI standard. This is motivated by the possibility that health related effects from PM emission are more sensitive to PM number than mass; this motivates the desire for size measurements in this study. This will be further discussed below.

1.1.2 PM from CI engines

PM refers to many different chemical species that appear as solid or liquid particles once the engine exhaust has been diluted and cooled. While this encompasses a large variety of different species, the PM consists primarily of carbonaceous ‘soot’ particles as well as absorbed organic carbon. There are also other aerosols such as ash particles, metallic abrasion particles, sulfates and silicates (Khalek et al., 2011).

The carbonaceous soot particles typically are agglomerations of smaller 'primary' particles (ex: Figure 1).The agglomerates vary in size from 20nm up to 2 microns. However, the individual primary particles are more uniform in size.

The formation of soot is a complicated process. It occurs in hot, fuel rich zones (in the fuel jet for a diffusion flame in a CI engine) where the fuel undergoes pyrolysis and decomposes into various combustion products (such as methyl radicals (CH_3*) or acetylene (C_2H_2)). These intermediates can combine to form aromatic rings (PAHs) that will bond with each other and eventually form "nuclei" (~6 rings and a diameter of 1.5-2nm). The hot, reactive surface of these particles will readily accept gas-phase hydrocarbons leading to their growth to the size of "primary particles" (6-40 nm). These initial particles will go on and agglomerate to form the soot aggregates seen in the exhaust.

The soot concentrations within the cylinder are many times greater than seen in the exhaust. Throughout the entire formation process, soot is also being oxidized in leaner, high temperature areas. The balance between these 2 processes results in the final PM emissions.

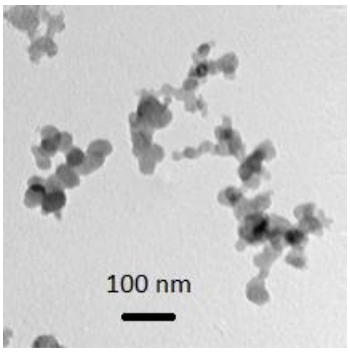

Figure 1 - Typical PM Aggregate from the HPDI Engine

In addition to this solid 'Elemental' or 'Black' carbonaceous soot, there is Semi-Volatile Organic Carbon (SVOC) present in the PM. These organic compounds are typically alkanes (Seigneur, 2009) and can exist in either the gaseous phase or condense to form individual nucleation mode particles or as coating on solid particles. For this study, SVOCs are defined as chemicals which are found as solid particles below 200°C and in the gaseous phase above this temperature. These volatiles are usually assumed to be formed by unburned lubrication oil which has worked its way past the cylinder rings or impurities such as sulfur in the fuel. Depending on engine operating conditions, the semi-volatile fraction can vary between 10-90% of the total mass of the PM (Heywood, 1988).

1.1.3 Health Effects of PM Emissions

PM emission regulations have been driven by the respiratory health effects. Diesel exhaust (DE) has long been known to be harmful and can produce both cancerous and noncancerous health effects: In 1989, IARC classified DE as a "probable" human carcinogen (Group 2A) and has recently reclassified DE as "carcinogenic to humans" (Group 1) (Silverman et al., 2012). The U.S. EPA in 2002 classified diesel exhaust as "likely to be carcinogenic to humans," and in 2000 as a "mobile source air toxin." Diesel

exhaust PM was specifically listed as a “toxic air contaminant” (TAC) by California EPA in 1998. (Hesterberg, Long, Lapin, Hamade, & Valberg, 2010)

The particulates in the DE are the primary cause of these negative health effects and their effects on the human body are influenced by the PM surface area and the presence of adsorbed transitional metals and organics (Ristovski et al., 2012).

It is a “consistently reported result in the toxicological literature is that particle mass is not a very appropriate metric for describing the ability of particles to induce oxidative stress and inflammation” (Günter Oberdörster, Stone, & Donaldson, 2007). For example, the inflammatory response of rodents exposed to particles (G Oberdörster, 2000) was better correlated with surface area correlated than particle mass. “An increased particle surface area per unit mass dose provides an increase in the availability of adsorbed toxic substances and provides a locus for which catalytic chemistry can occur” (Ristovski et al., 2012). As the surface area to mass ratio increases with smaller particles sizes, the size and number of PM emissions is important in evaluating the health effects of emitted PM from CI engines.

The organic fraction of the PM is also important to the overall toxicity of the exhaust (Ayres et al., 2008; Valavanidis, 2008) where “relatively tiny masses of transition metals and organic species [when compared to the total mass of the PM] may make a major contribution” to the overall health effects.

1.1.4 CI Engine Aftertreatment Strategies

These large reductions in pollutant concentrations have been met with a large number of different technologies in both in-cylinder reductions and aftertreatment strategies. These can be classified into 3 main categories:

- In-cylinder + engine design changes
- Fuel + lubricant changes
- Aftertreatment

In-cylinder and engine include electronic direct injection, multiple pulsed injection, high injection pressures, advanced EGR, variable valve actuation and variable geometry turbochargers. Until the 2004 emission regulations, CI engine manufacturers could meet the emission limits with engine modifications.

With the introduction of the 2007/EURO V emission regulations, the PM and NOx limits were so low that aftertreatment of the exhaust became necessary. While there are differences between various manufacturers’ solutions, the industry standard solution is to use a diesel oxidation catalyst (DOC) for HC control, a diesel particulate filter (DPF) for PM control and selective catalytic reduction (SCR) for NOx control (Hesterberg et al., 2011).

DOCs are filled with honeycomb shaped substrates coated with platinum or palladium. These metals act as catalyst to oxidize the CO and HC emissions to CO_2 and H_2O. They can reduce the CO and NMHC emissions by up to 90%

DPFs remove the PM by filtering the exhaust. Like a DOC, the DPF has a ceramic substrate, but with alternating entrances/exits that are blocked off to force the flow through the filter walls. The solid particles are deposited on the wall and collection of up to 90% of the PM mass can be achieved. As theses filters fill up over time, they must be 'regenerated'. This can be done passively (if the exhaust temperature is hot enough to oxidize the captured PM) or actively by artificially increasing the exhaust temperature with late fuel injection. This regeneration process consumes additional fuel, and along with the increased back pressure of the filter, causes a slight reduction in the overall efficiency of the engine.

SCRs use a catalyzed substrate along with a chemical reductant to reduce the NOx emissions by up to 90% by converting NO and NO_2 to N_2 and H_2O. For automotive applications, the chemical reductant is a urea fluid, which is thermally converted by exhaust temperatures, to ammonia (NH_3). This then reacts with the NOx in the presence of a ceramic catalyst. As this fluid is consumed during operation, it must be periodically refilled by the vehicle operator.

Aftertreatment technologies are sensitive to impurities to the fuel and require the use of ultralow sulfur diesel (ULSD)(<15ppm), which was mandated by EPA in 2006 (EPA, 2001). Additionally, the soot morphology will also have an effect on DPFs (Lapuerta, Oliva, Agudelo, & Boehman, 2012). The light off temperature will be altered by the soot composition. The light-off temperature is the mostly dependant on the magnitude of the soot's active surfaces. Smaller primary particles have higher specific surface areas, which leads to increased reactivity and increased oxidation under filter regeneration.

Aftertreatment adds cost and maintenance requirements and can negatively affect the fuel economy from the vehicle. For example, at full DPF/SCR system can cost $30,000 (Range of $11,000 to $50,000) per vehicle(MECA, 2009).

1.2 Natural Gas as a Transportation Fuel

In the past 10 years, there has been renewed interest in natural gas fuelled vehicles (NGVs), mainly because natural gas is cheaper than diesel and gasoline. This difference has grown larger in the past 5 years with the development of techniques to extract unconventional or shale gas. This has massively increased the amount of exploitable reserves in North America and across the world. This has both lowered the cost of NG as well as increased its political attractiveness in promoting energy independence (Stevens, 2012; U.S.-Department-of-Energy, 2012).

Due mainly to these cost savings, the number of natural gas vehicles worldwide has been increasing by 22% annually since 2001 (Natural Gas Vehicle Global, 2012). In Europe, some of these have been passenger cars, but in North America these have been almost exclusively fleet vehicles, primarily light and medium duty trucks powered by compressed natural gas (CNG).

Natural gas is chemically and physically very different from gasoline and diesel; this leads to important technological impacts.

Natural gas, when used as a transportation fuel, typically produces lower levels of pollutants than gasoline or diesel. NG has the lowest carbon / energy ratio of any hydrocarbon. This leads to reduced tailpipe CO_2 emissions (however, losses during extraction and processing may counteract this on a well-to-wheel analysis (Burnham, Han, & Clark, 2011)). Traditionally, NG vehicles have emitted lower concentrations of other criteria pollutants such as NOx, PM and HCs due to this low carbon/hydrogen ratio. However with increasingly stringent emission regulations, this advantage is shrinking in comparison with petroleum fueled vehicles.

Natural gas is much more resistant to ignition than either diesel or gasoline (octane rating of around 120 depending on composition) (Kubesh, King, & Liss, 1992). For SI engines, this allows for increased theoretical efficiency by increasing the compression ratio (by raising the knock limit), however under standard CI engine temperatures and pressures, NG will not reliably self-ignite. This forces the requirement of a forced ignition system for proper engine operation. This can be in the form of a dual-fuel pilot ignition, a spark plug or a hot surface such as a glow plug.

Natural gas can be stored on a vehicle as a compressed gas (CNG) at pressures between 200 and 250bar (giving energy density of ~9MJ/L) or as a liquid in cryogenic tanks at temperatures below -162^{o}C (LNG; energy density 22 MJ/L). The energy density is still less than that of diesel or gasoline (about 35 MJ/L) (US Department of Energy, 2012). In addition to the additional volume of fuel required, these gaseous fuels required more complicated storage systems; either high pressure tanks or cryogenic systems that must be cylindrical in shape leading to packaging issues. Altogether, natural gas requires 2 to 6 times the space for equivalent levels of energy storage (Bell, 2012). Currently, light and medium duty vehicles (engines up to 12L) are almost exclusively powered by CNG due to simpler storage and refueling requirements, whereas larger engines employ LNG for the increased power density.

1.3 High Pressure Direct Injection (HPDI™) Natural Gas Engines

This thesis focusses on the HPDI™ system developed by Westport Innovations Inc. This uses a small diesel pilot to ignite a directly injected NG jet. Both the diesel and pilot fuels are injected late in the compression stroke with a short delay between the 2 injections. This delay is referred to as the pulse separation (PSEP) and is shown schematically in Figure 2. This thesis will refer to ‘traditional’ HPDI combustion, which designates a PSEP greater than 0.3ms. This allows for the diesel pilot to diffuse and provide an ignition source for the natural gas jet. As both fuels are directly injected and burn as diffusion flames, the engine can utilize diesel-like compression ratios and maintain diesel-like efficiencies.

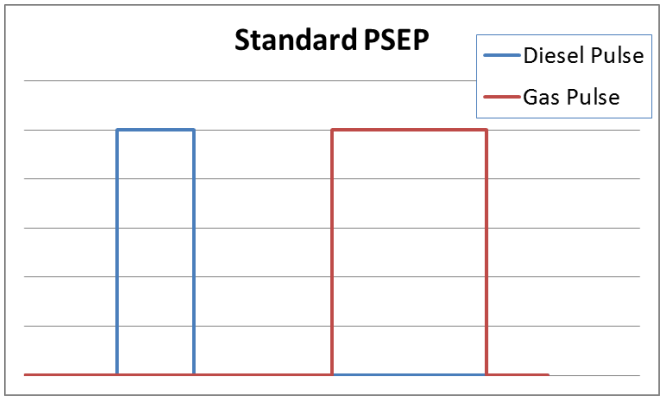

Figure 2 - PSEP Schematic

A key attribute of this technology is the use of a single injector for both fuels. This allows the installation of the system into an unmodified engine head. The injector itself has a dual concentric needle design. The diesel is injected through small holes at the bottom of the injector and is controlled by an inner needle. Surrounding the diesel needles is a larger gas needle to control the natural gas flow through a second ring of holes. These 2 needles can be controlled independently. Figure 3 shows a schematic of these needles schematically and a photo of the entire HPDI injector.

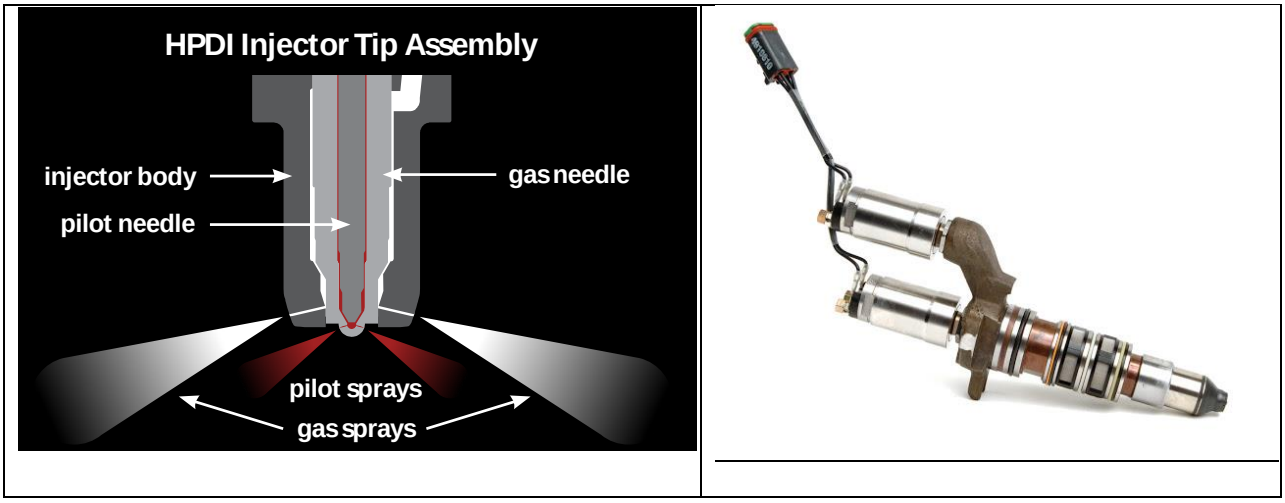

Figure 3 - HPDI Injector Schematic and Picture (www.westport.com)

1.4 Engine PM Emission Studies

There has been considerable progress in reducing the mass emission from diesel vehicles in recent years. Since Euro V/EPA 2007 regulations, the main driving force for this reduction has been the introduction of aftertreatment devices such as DPFs and SCRs. The implementation of these technologies has sufficiently changed the emission characteristics of these engines that (Hesterberg et al., 2011) has defined the PM emissions from post-Euro V/EPA 2007 diesel engines as New Technology Diesel Exhaust (NTDE) as the PM emissions with DPFs and SCRs are fundamentally chemically and physically different from traditional diesel exhaust (TDE).

In contrast to the introduction of aftertreatment in recent years, in-cylinder and engine based changes have been less drastic. This study focuses solely on in-cylinder PM emissions so literature from TDE is still relevant.

There have been a number of studies using a scanning mobility particle spectrometer (SMPS) to determine number concentrations and size distributions from diesel exhaust. Some of the earliest studies were performed by Abdul-Khalek and Kittelson. They investigated the PM size distributions from a 4L medium duty engine certified to US 1994 emissions levels. They observed PM size distributions with 2 peaks, both lognormally distributed, and attributed the small particles to the "volatilization of lube oil metallic ash components and subsequent nucleation of these materials during the expansion stroke" (Abdul-Khalek & Kittelson, 1998).

(Desantes, Bermúdez, García, & Fuentes, 2005) investigated the influence of injection pressure (IP), start of injection (SOI) and exhaust gas recirculation (EGR) on the aerosol exhaust particle size distributions from a EURO 3 heavy-duty engine. They found that increasing the injection pressure reduced the accumulation particle number concentrations, however "A sharp increase in the nucleation mode particle number was observed in the case of highest injection pressure for some engine conditions". This trend of reduced mass concentrations, yet increased number concentration with advanced engine technologies continues through other studies.

(Lähde et al., 2011) investigated the effects of injection pressure from a 7.4L stage 3B off-road heavy-duty engine and found "An increase in the injection pressure resulted in an increase in the nonvolatile nucleation mode (core) emission at medium and at high loads. At low loads, the core was not detected. Simultaneously, a decrease in soot mode number concentration and size and an increase in the soot mode distribution width were detected at all loads"

(Armas, Ballesteros, & Gómez, 2008) observed decreases in both mass and number concentrations with increasing injection pressure from a 2.2L light-duty engine. They also investigated the effects of EGR and observed that reducing the EGR percentage led to a "decrease in the soot concentration and the emitted particles and to the movement of the size distribution towards smaller diameters". This is attributed to "[improving] the combustion process owing to a higher oxygen concentration in the intake mass"

(Leidenberger, Mühlbauer, Lorenz, Lehmann, & Brüggemann, 2012) investigated both injection pressure and equivalence ratio (EQR) on aggregate and primary particle size from a 3L light-duty Euro 4 engine. Concluding "an increased injection pressure leads to smaller primary particle sizes" and "an increase of the equivalence ratio supports primary particle growth, but has less influence compared to the injection pressure that leads to decreasing primary particle sizes" They attribute the reduction in primary particle size to an increased ratio of soot oxidation to formation due to the increased turbulence and mixing caused by the increased injection pressure.

(Fino & Russo, 2011) measured PM emissions from a light-duty 2L diesel engine at 0 and 24% EGR levels, measuring a 4X increase in mass concentrations and a 6X increase in particle number. Along with these increases, the aggregate mode diameter increased from 46-76nm.

The properties of PM emissions from HPDI engines have also been studied. (G. P. McTaggart-Cowan, 2006) studied the effects of injection pressure on the PM mass and size distributions. He tested injection pressure of 21 and 31MPa at number of load and speed combinations and found up to a 50% reduction in PM mass. Increasing the injection pressure also led to fewer and smaller particles. However, this effect was less significant than the effect of EGR, which lead to larger and greater number of particles.

The effect of PSEP on the PM emissions was also studied (G. McTaggart-Cowan, Bushe, & Rogak, 2005). They tested modes with a PSEP from -1.2 to 1.0ms at engine speeds from 800-1200 RPM. Decreasing the PSEP reduced the PM emissions by increasing the peak heat release rates and shortening the combustion duration. This reduction in PM was countered by increased NOx. These PM reductions were only observed with EGR, modes without EGR did not see PM improvements.

(Jones, 2004) studied the effect of the diesel pilot on the total PM emissions. She found that on a fractional basis the diesel pilot contributes minimally to the PM emissions under most operating conditions. This means that the majority of the PM from a HPDI engine is actually caused by the natural gas.

However, the majority of these earlier tests were done at lower engine speeds than the proposed modes in this study. This thesis will attempt to extend some of these results to a larger engine operating condition test matrix.

1.5 Objective and Scope

The objective of this project was to characterize the PM emissions from a HPDI engine. The research was mainly experimental using a heavy duty, single cylinder research engine. This thesis will evaluate the PM in the following ways and evaluate under what conditions there are significant deviations from 'typical' HPDI PM:

- Mass Concentrations

  The PM mass concentration is the traditional measurement for PM emissions from engines. This study will analyze the PM mass concentrations with a number of different techniques (gravimetric filters, TEOM, light scattering) and will compare the emission profiles from the HPDI engine with characteristics from traditional diesel engines.
- Number Concentrations

  There is increasing evidence that the PM number concentration, rather than strictly the PM mass is the more important metric for the negative health effects associated with PM emissions. This is especially true for nano (sub-100nm) particles. The number concentration as well as particle size distribution will be evaluated throughout the study for operating conditions which may be potentially more damaging for human health.
- Semi-Volatile Content

  The PM emissions from diesel engines are complex mixtures of many different species. The 2 main constituents are non-volatile elemental (or black) carbon, along with a class

of hydrocarbons that can be described as semi-volatile organic carbon. These volatile compounds can remain in the gas phase, condense onto the non-volatile particles or nucleate to form new particles. The non-volatile fraction of the PM will be harder for after treatment methods to remove, so the ratio between these 2 constituents will be monitored throughout the study.

- Morphology

  PM morphology will have an effect on exhaust after treatment devices. DPF light-off temperatures will be affected by the magnitude of the soot aggregate's active surfaces, which are related to the primary particle sizes.

These PM physical and chemical characteristics will be explored for a variety of conditions:

- Speed and load combinations at standard engine calibrations over the majority of the engine operating range.
- The Effects of EQR, EGR, GRP, Pilot quantity and Injection timing at a single speed and load combination
- Gas and Diesel interactions allowing some of the fuel to premix before ignition

.

Through all of these tests, the engine performance and gaseous emissions are monitored to understand the combustion characteristics in the engine.

As a large number of different measurement techniques used throughout the study, the relative measurements between the instruments will be compared and contrasted and recommendations will be provided on how to best measure the PM over different operating conditions. Additionally, measurement variability is present with experimental research and will be investigated by combining the data sets throughout this study.

2 Experimental Apparatus

2.1 Single Cylinder Research Engine (SCRE)

All tests were performed using a single-cylinder research engine based on a 15L six-cylinder, 4-stroke 400 hp Cummins ISX engine. The cylinders have a compression ratio of 17:1 and a bore and stroke of 137 and 169mm, respectively. The original 6 cylinder engine was modified by deactivating 5 cylinders to run on a single cylinder. A photo of the engine showing only a single exhaust manifold in Figure 4.

A GE eddy-current dynamometer is used to control the speed of the engine and a 30 kW electric motor is used to provide additional torque to overcome any frictional losses and inertia of the deactivated cylinders.

A screw-type compressor supplies high-pressure natural gas. Gas pressure is held at a pressure slightly below the diesel pressure using a dome-loaded regulator. A coriolis mass-flow meter is used on the gas supply (Endress+Hauser Promass 80A). Diesel flow is supplied by a conventional Bosch diesel fuel pump; pressure is set with a back-pressure regulator. Most of the diesel flow is used for injector actuation and returned at low pressure to the small diesel supply tank. This tank sits on an electronic balance, from which the net mass of diesel injected into the engine can be inferred. Further details regarding the test cell setup can be found in Brown (2008).

Figure 4 - ISX 400 SCRE

Natural gas in Vancouver, Canada contains approximately 96% methane with 2% higher hydrocarbons and 2% N_2 + CO_2. The diesel was road-grade ultra-low-sulphur (<15 mg/kg) which met CAN/CGSB-3.520 standards. The cetane number of the diesel ranges from 41 to 45.

2.1.1 In-Cylinder Pressure Measurement

The cylinder pressure is measured with an AVL QC-33 piezoelectric pressure transducer at 1/2 CA° resolution. From this pressure measurement, the indicated mean effective pressure, apparent heat release rate and engine timing can be determined.

The mean effective pressure an engine size independent measure of engine work and is calculated dividing the work per cycle by the cylinder volume. Due to the SCRE's high internal friction (from the deactivated cylinders), brake performance parameters are not representative of the in-cylinder conditions. As a result, the engine operation is measured on the basis of the gross-indicated power. The gross indicated work per cycle $W_{c,ig}$ is the work delivered to the piston over the compression and expansion strokes only. This is calculated from the cylinder pressure data by doing a numerical integration of the pressures and multiplying the average pressure between two consecutive points by the change in volume.

$$W_{c,ig} = \oint P(\theta) \frac{dV(\theta)}{d\theta} d\theta \quad (1)$$

The GIMEP is then:

$$GIMEP = \frac{W_{c,ig}}{N} \quad (2)$$

The apparent net heat release rate Q_n is the rate at which work is done on the piston plus the rate of sensible internal energy change of the cylinder contents.(Heywood, 1988)

$$\frac{dQ_n}{d\theta} = \frac{\gamma}{\gamma - 1} P \frac{dV}{d\theta} + \frac{1}{\gamma - 1} V \frac{dP}{d\theta} \quad (3)$$

Where $Q_{n\,is}$ the net apparent heat release rate, P is the cylinder pressure, V is the cylinder volume and γ is the specific heat ratio of the combustion gasses and is given a value of 1.3.

The engine timing is then specified by the 50% IHR point, which is calculated from the cumulative heat release over the cycle.

For efficiency calculations, the lower heating values of the fuels were used. These values are 48,810 KJ/kg for CNG and 42,772 KJ/kg for the diesel.

2.2 Gaseous Emissions Measurement

Gaseous emissions from the engine are taken downstream of the exhaust surge tank, near the PM system sampling port. The sample is passed through a heated filter, and sent through a temperature

controlled sample line to the AVL CEB-NA emissions bench in the control room. The emissions bench measures total unburned hydrocarbons (uHC), CO_2,O_2, CH_4, CO, and NOx.

The uHC and CH_4 are measured with individual flame ionizing detectors (FID), the NO and NO_2 are measured by chemiluminescence detectors, the O_2 by a paramagnetic detector while the CO and CO_2 are measured by non-dispersive-infrared absorption (NDIR).

The emissions bench was calibrated with a zero, low and high span gas (covering the entire measurement range) at the start of every test day. Following every day, the calibrations were checked again to ensure the instrument drift was less than 5%.

2.3 Particle Emissions Measurement

2.3.1 Particulate Sampling System

The raw engine exhaust must be diluted because it contains PM concentrations too high for most laboratory instruments and so as to approximate the dilution experienced as vehicle exhaust exits a tailpipe. The PM sampling system can have a significant effect on the measured PM from an engine. This is especially true when analyzing the ultra-low emissions from current engines for particle size and number as well as the volatile content (Giechaskiel, Dilara, & Andersson, 2008; Mohr & Lehmann, 2003).

The PM sampling system installed on the SCRE is separate from the gaseous measurement system and is based on a 2-stage system using an ejector diluter and an aging chamber. A schematic of the system is shown in Figure 5.

The PM sampling point is located approximately 6m from the exhaust surge tank and is drawn from the main 3”, insulated, exhaust pipe. A small sample (1-2LPM) is drawn from the exhaust by a venture ejector diluter. This diluter is fed with dry, filtered and pre-heated air. This air is heated to match the exhaust temperature at this point (~70°C depending on engine operating conditions). This is done to prevent the condensation or nucleation of any semi-volatile components in this initial stage. The sample then passes to an aging chamber where it is further diluted with cooler air to bring the sample temperature to 55°C; allowing particle growth and freezing the state of the PM. This temperature is mandated by EU regulations for gravimetric filter measurements (Kryiakis, Vouitsis, & Samaras, 2002). These 2 dilution flows are controlled by a pair of rotameters to maintain a dilution ratio (DR) between 9:1 and 15:1 as well as atmospheric pressure (± 200Pa) in front of the PM instrument sampling location.

The dilution ratio is calculated by comparing the upstream and downstream CO_2 concentrations in the sample. The upstream value is given by the main AVL bench whereas the diluted CO_2 measurement is measured by a California Analytical NDIR analyzer (model 100) connected with the other PM instruments. The dilution ratio is then calculated by:

$$DR = \frac{[CO_{2,wet}] - 0.03}{[CO_{2,LR,DRy}]\left(1 - \frac{[H_2O]}{([CO_{2,dry}] - 0.03)/([CO_{2,LR,dry}] - 0.03)}\right) - 0.03} \quad (4)$$

This corrects for humidity in the sample as well as for the atmospheric concentration of CO_2 (300ppm)

The total length of the system is 5m with a total residence time of ~10s. This sampling time is long enough to ensure adequate mixing and complete evolution of the PM to steady stare conditions. Excess exhaust is vented to the atmosphere.

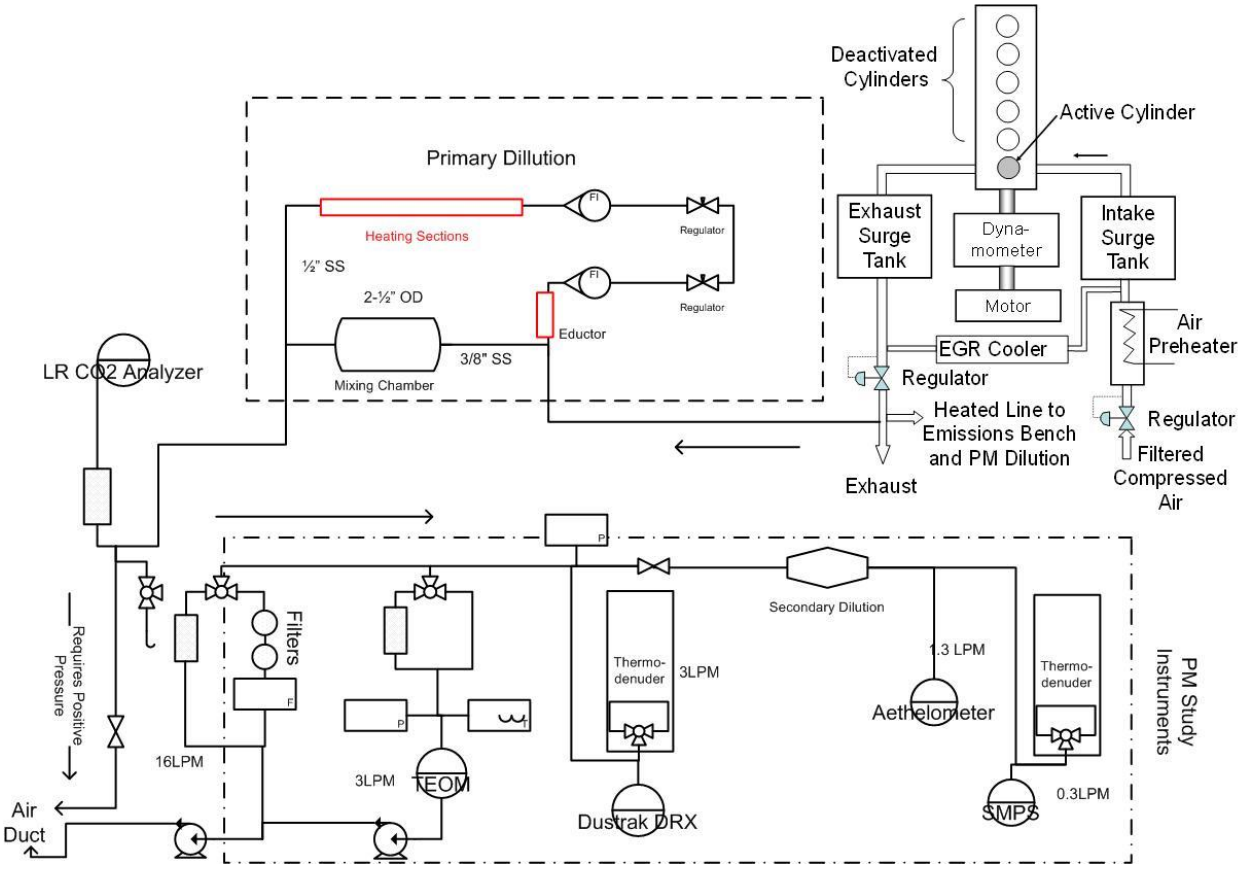

Figure 5 - SCRE PM System Schematic – Engine Schematic Adapted form Brown (2008)

2.3.2 Tapered Element Oscillating Microbalance (TEOM)

The Rupprecht and Patashnick (Model 1105) TEOM provides a continuous mass measurement of the engine PM. Unlike other fast response instruments, which measure an indirect property of the PM to

provide a mass measurement, the TEOM is sensitive to the PM *mass* loading. As this study focused on a wide range of engine operating conditions, the optical and morphological properties of the PM can change and cause these other instruments to produce biased mass measurements.

The instrument draws 3LPM and the air is maintained at 40°C at the sampling chamber for repeatable results.

The TEOM uses a filter mounted on a tapered hollow tube. The exhaust sample passes through this tube and any particulate is deposited on this filter. This tapered element is maintained in a 'clamped-free' oscillation and the frequencies of these oscillations are measured. As PM mass collects on the filter, the natural frequency of the element will change. The mass loading is correlated with this frequency change by:

$$\delta m = K_0 \left(\frac{1}{f_{final}^2} - \frac{1}{f_{initial}^2} \right) \quad (5)$$

Where K_0 is a calibration constant (Patashnick & Rupprecht, 1991)

While the TEOM is the only fast instrument to directly measure PM mass, it has a few disadvantages. The instrument has a relatively slow response time, especially at low PM concentrations. To determine the mass loading rate, the slope of the filter mass is determined. At low concentrations, this slope can be difficult to determine dude to a cyclical oscillation observed in the measurement. Figure 6 shows representative mass loading data for low and high PM concentrations. The magnitude of the oscillations are the same for both plots, however the loading rate is much more difficult to determine for the low concentration condition.

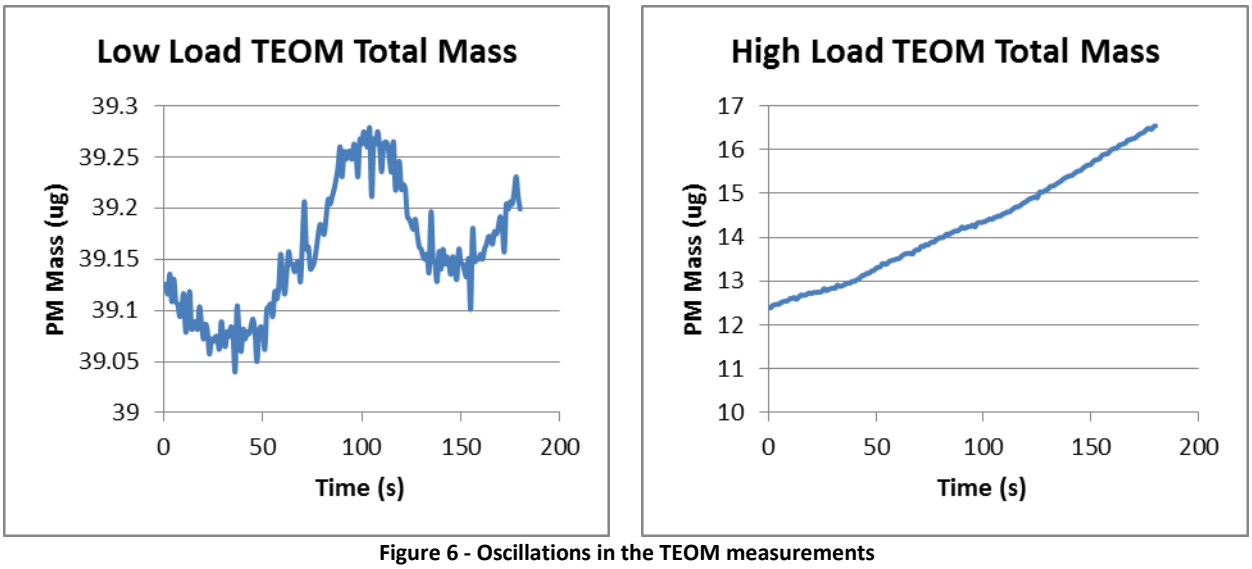

Figure 6 - Oscillations in the TEOM measurements

This behaviour has been observed before by (Kelly & Morgan, 2002) and it was attributed to volatization and devolatization of the loaded PM. However, they observe these effects on much larger time scales then our fluctuations with a period of approximately 100 seconds.

Samples were typically taken for 180 seconds. This will reliably capture emission levels down to 0.01g/kW-hr however; concentrations below this level will be reported inaccurately, as the mass-loading slope is smaller than the cyclical variations in the instrument's response. A further description of the TEOM installed on the SCRE is offered by (Brown, 2008) and (G. P. McTaggart-Cowan, 2006).

2.3.3 DustTrak DRX

The TSI DustTrak DRX™ (Model 8530) uses 90° laser light scattering and a photodetector to measure PM concentrations. The intensity of scattered light by PM particles is dictated by Raleigh theory on account of the small size of the PM particles compared to the wavelength (780nm) of the laser. Thus the intensity of the scattered light is proportional to the sixth power of particle diameter (d^6 or $mass^2$) as well as the refractive index of the particles.

The instrument uses a calibration constant based off of `A1 Test Dust' (ISO 12103-1 A1) to convert the photo detector voltage to a mass. This dust has a mean diameter of approximately 1µm and an extremely broad distribution when compared to diesel PM. Therefore, the instrument is not expected to be perfectly correlated with PM mass. Additionally, if the engine PM morphology or refractive index differs from this calibration aerosol, the measurement will be further biased. For example, (Maricq, 2013) tested the DustTrak with oil droplets and engine PM and observed that the response is compositionally dependant and not fully correlated with mass. However, he remarks on the usefulness of the instrument if the PM characteristics remain relatively constant. Also, it has been previously seen on this engine that with large semi-volatile fractions can cause very large mass overestimations (Patychuk & Rogak, 2012).

Despite these limitations, the instrument has the fastest (1s) response time of any of the instruments used in this study and very low detection limits and provides useful data if its shortcomings are acknowledged.

2.3.4 Scanning Mobility Particle Spectrometer

The TSI Scanning Mobility Particle Spectrometer (SMPS) (Model 3080 Electrostatic Classifier / Model 3025 CPC) provides a high-resolution mobility size distribution. This instrument uses a classifying column (Differential Mobility Analyzer (DMA)) where a scanning electric field allows only a specifically sized particle to pass to a condensation particle counter (CPC). A schematic of the DMA is shown in Figure 7.

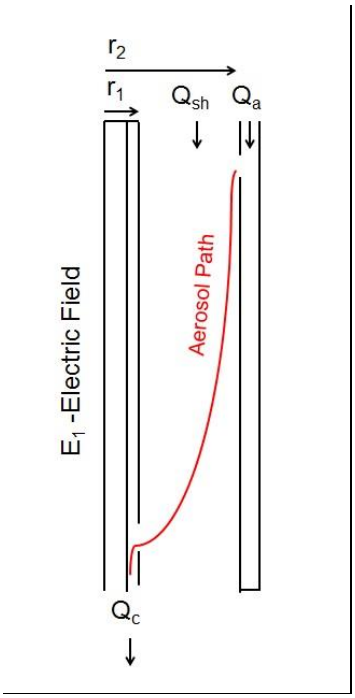

Figure 7 - Aerosol Paths in a DMA – Adapted from (Wang & Flagan, 1990)

The mobility of the particles allowed to pass through the extraction slot is governed by the equations:

$$Z_p^* = \frac{Q_a + Q_{sh}}{2\pi E_1 L} ln \frac{r_2}{r_1} \qquad \beta = \frac{Q_a + Q_c}{Q_{sh} + Q_e}$$
$$Z_{p,max} = Z_p^*(1+\beta) \qquad Z_{p,min} = Z_p^*(1-\beta) \tag{6}$$

Where Z_p^* is the nominal particle mobility that will pass from the inlet and out the exit. Particles of slightly higher and lower mobilities will also be transmitted from the aerosol flow to the classified aerosol flow. These are bounded by $Z_{p,max}$ and $Z_{p,min}$. β denotes the aerosol flows to that of the larger sheath and exhaust flow. E_1 is the electric field at the collector wall and L is the length between the inlet and collector slots. Q_a , Q_c and Q_{sh} are the aerosol, classified aerosol and sheath airflow rates.

The mobility decreases with particle size, so larger electric fields will allow larger particles to pass through the DMA. In practice, the voltage on the central electrode is varied from 0-9000V.

Once the particles exit the DMA, they are the counted by the CPC. The CPC adds butanol vapor to the aerosol stream, in a supersaturation state, to grow the particles. Once the particles have grown to sizes over 1µm, they are detected optically with a laser and photodetector.

A SMPS system can be operated in a stepping or scanning mode. In the stepping mode, the DMA is operated at fixed voltages (and thus particle mobilities) and discretely form a size distribution by operating at a number of different voltages. Due to time response and settling issues with the

instrument, this technique can take up to an hour to complete a full scan (Flagan, 2008), which is quite impractical for most applications. The TSI 3080 SMPS system overcomes this limitation by continuously scanning over the voltage range. Inside the DMA all particles will follow the same trajectories if the ratio of the voltage at any point during its transit to the voltage when it entered the DMA is kept constant. This is only achieved with constant or exponentially ramped voltage.

$$V = V_0 e^{t/\tau_{scan}} \tag{7}$$

This allows the SMPS system to quickly ramp its voltage and create an entire size distribution in 2 minutes while maintaining particle sizing accuracy.

This study used 2 different DMA columns. The TSI 3085 nano-DMA which allows for size measurements from 5-212nms and a custom made long column DMA with a measurement range of 14-650nm. The dimensions of this column and operating parameters of the SMPS are shown in Table 2.

Length	41.29 cm
Inner Radius	0.945 cm
Outer Radius	1.927 cm
Sheath Flow	3 LPM
Aerosol Flow	0.3 LPM
Particle Density	1.2g/cc
Multiple Charge Correction Turned On	

Table 2 - Custom Long Column DMA Dimensions

The SMPS data inversion algorithm uses a mass-mobility assumption where all of the particles are perfect spheres. Thus, the mass measurement will vary with changing particle morphology, especially with low density fractal aggregates (Maricq & Xu, 2004). This can be corrected with post-processing algorithms based on the particles primary particle diameters and fractal dimensions. However, this has not been done for this study. As such, the volumes reported here can be expected to be larger than those inferred for the other instruments.

2.3.5 Thermodenduder

The UBC-developed thermodenuder (TD) allows the other instruments to measure the semi-volatile organic compounds (SVOC) fraction of the PM. The denuder design is similar to Wehner and Burtscher's (Burtscher, Baltensperger, & Bukowiecki, 2001; Wehner & Philippin, 2002) and is shown schematically in Figure 8.

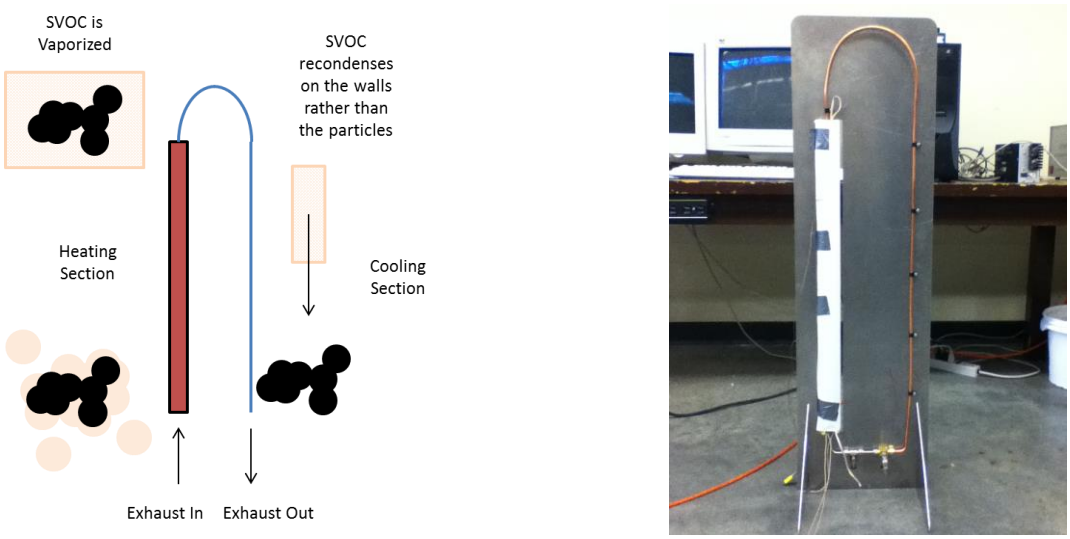

Figure 8 - Thermodenuder Schematic and Photo

The simple design consists of a heating and cooling section. The heating section is 80cm long with an inner diameter of 0.94cm and is temperature controlled with an Omega PID controller and electrical heating tape. The sample is headed to 200°C. This temperature is high enough to vaporize the highly volatile OC, sulphuric acid, ammonium sulfate and bisulfate and some of the low volatility OC in the sample (Burtscher et al., 2001). This was confirmed by varying the evaporator temperature and observing changes in the size distribution of the PM; No changes occurred above 200°C. Figure 9 shows the size distribution changes with changing TD temperature. This size distribution shift around 80°C shows that the semi-volatile fraction consists of a number of different species with different vapor pressures/vaporization temperatures. After the SVOCs have been vaporized, the sample moves to a cooling section. There is an insert between the sections to ensure that laminar flow is maintained. The cooling section is a 160 cm long insulated copper tube with a small inner diameter of 0.30cm and as such, a large surface area-to-volume ratio. As the sample is gradually cooled, the SVOCs will preferentially re-condense onto the tubing walls instead of the aerosol particles, leaving just the non-volatile fraction of the PM to exit the instrument. By switching back and forth between the instrument and a bypass, the semi-volatile fraction can be measured.

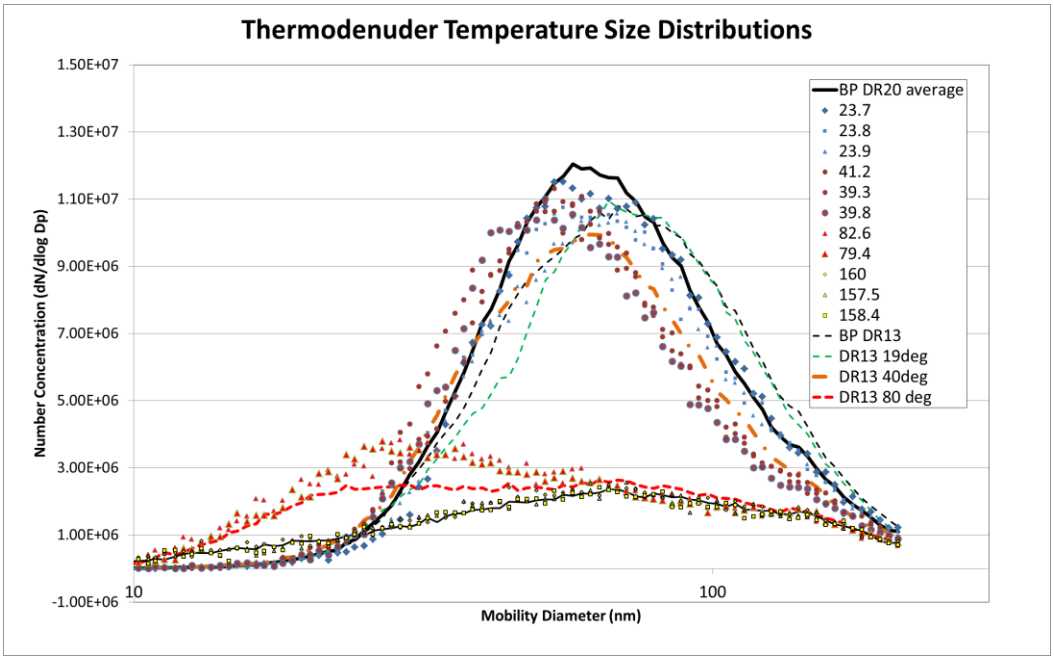

Figure 9 - PM Size Distributions with Varying TD Temperature

Losses for the TD (as a function of temperature and particle size) were determined experimentally and compared with a diffusion loss calculation suggested by (Gormley & Kennedy, 1948) in Figure 10. All results have been corrected for these losses. The effect of this correction is small as the TD has transport efficiency above 90% for particles larger than 30nm. The correction has an effect on the total number concentration, but almost none on the total mass. This is because the majority of the total mass comes from the large particles (function of d^3), where the losses through the denuder are less than 2%.

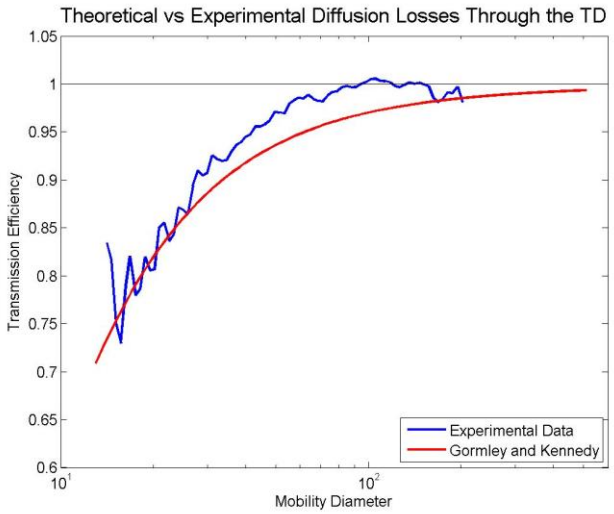

Figure 10 - Particle Losses through the TD

3 Results

The experiments were divided into 3 major blocks with different types of parameter variations:

- Speed and Load combinations in Section 3.1 – Multimode Testing
- The Effects of EQR, EGR, GRP, Pilot quantity and Injection timing in Section 3.2 – Parameter Variations
- Gas and Diesel interactions in Section 3.3 – Effects of Natural Gas Premixing on Emissions

In each of these sections, the mass and number concentrations, the semi-volatile fraction and the particle morphology will be evaluated to characterize the PM emissions from a HPDI engine. Detailed tables of measurements are given in Appendix D.

In Section 3.4, the emission sensitivities to the parameters as determined in section 3.2 were used to assess the amount of measurement variability due to errors in setting operating conditions using Monte Carlo simulations.

The following tables show the test matrices these tests. For all tests the SMPS, TEOM, DustTrak and thermodenuder (A denuded and undenuded measurement were taken for each repeat) were used for PM characterization. For the Multimode tests quartz (for EC/OC analysis), Teflon (for gravimetric analysis) and TEM grid were taken as well.

For the multimode tests, each collection was a minimum of 600 seconds of steady state data collection. These longer tests reduced the sampling uncertainty of the data while allowing sufficient time for the PM to deposit on the gravimetric and quartz filters. For the parameter sweep testing, each data collection was averaged over 180 seconds with the engine running at steady state.

Mode	Speed	GIMEP	EQR	EGR	GRP	Diesel Fuel Mass per Injection	50% IHR	Repeats	Quartz Filters
	rev/min	bar	kg/kg	%	MPa	mg	deg ATDC		
A25	1222	5.1	0.45	20	15.0	8.0	15	2	2
A50	1222	10.7	0.60	15	20.0	10.0	15	2	2
A75	1222	16.3	0.60	15	25.0	8.0	15	2	2
B25	1493	5.5	0.50	20	20.0	12.0	15	2	2
B50	1493	11.0	0.55	20	25.0	19.0	10	2	2
B75	1493	16.6	0.60	20	25.0	10.0	10	2	2
C25	1763	5.2	0.45	15	20.0	10.0	20	2	2
C50	1763	9.1	0.55	20	25.0	10.0	10	2	2
C75	1763	14.1	0.60	20	25.0	8.0	10	2	2
B75 Neg PSEP	1493	16.6	0.70	25	25.0	10.0	10	2	2
B75 0% EGR	1493	16.6	0.60	0	25.0	10.0	10	2	2
Premixed 1	1222	16.3	0.60	0	25.0	8.0	15	2	2
Premixed 2	1222	16.3	0.60	0	25.0	8.0	15	2	2

Table 3 - Multimode and Premixed Test Matrix

Speed	EQR	EGR	Repeats at IHR CA50%=			Pilot	GRP
			5	10	15	mg/inj	Mpa
1493	0.6	0	2	2	2	10	25
1493	0.6	20	2	2	2	10	25
1493	0.45	20	0	2	0	10	25
1493	0.55	20	2	2	2	10	25
1493	0.65	20	2	2	2	10	25
1493	0.7	20	0	2	0	10	25
1493	0.6	20	2	2	2	10	23
1493	0.6	20	2	2	2	10	30
1493	0.6	10	2	2	2	10	25
1493	0.6	30	0	2	0	10	25
1493	0.6	20	0	2	0	min.	25
1493	0.6	20	2	2	2	15	25
1493	0.6	20	0	2	0	20	25
1493	0.55	20	2	2	2	15	25
1493	0.65	20	2	2	2	15	25
1493	0.6	20	2	2	2	15	23
1493	0.6	20	2	2	2	15	30

Table 4 - Parameter Sweep Test Matrix

3.1 MultiMode Testing

This first section will look at the effect of engine speed and load on the PM emissions from the engine. Throughout this section, test conditions based on previous results were used. These were selected as a compromise between performance and efficiency. As the operating parameters (EQR, EGR, GRP, Pilot Mass, Timing) change throughout the speed and load variations (to optimized values) this section will give an overall view of the PM emission over the entire operating range without a specific focus on the operating parameters.

3.1.1 Comparisons with Gaseous Emissions

Before moving into the detailed PM characterization, trade off curves with gaseous emissions can show general emission trends over the operating range. In the following plots, the data points have been colored by their load level and their shape signifies the engine speed.

The PM mass plotted in these charts is reported from the SMPS. Even though the absolute value of this reported mass is biased upwards, it provides the best relative resolution to both the high and low PM concentrations. A more thorough comparison of the relative mass concentrations is shown in Section 3.1.6. All measurements have been normalized by engine power and the PM measurements corrected for dilution. Each point represents a single data collection (There are at least 4 points for each mode).

The engine load is designated by the symbol color (red, blue, green for 25, 50 and 75% load respectively) and by symbol (star, circle and cross for A, B and C) for engine speed.

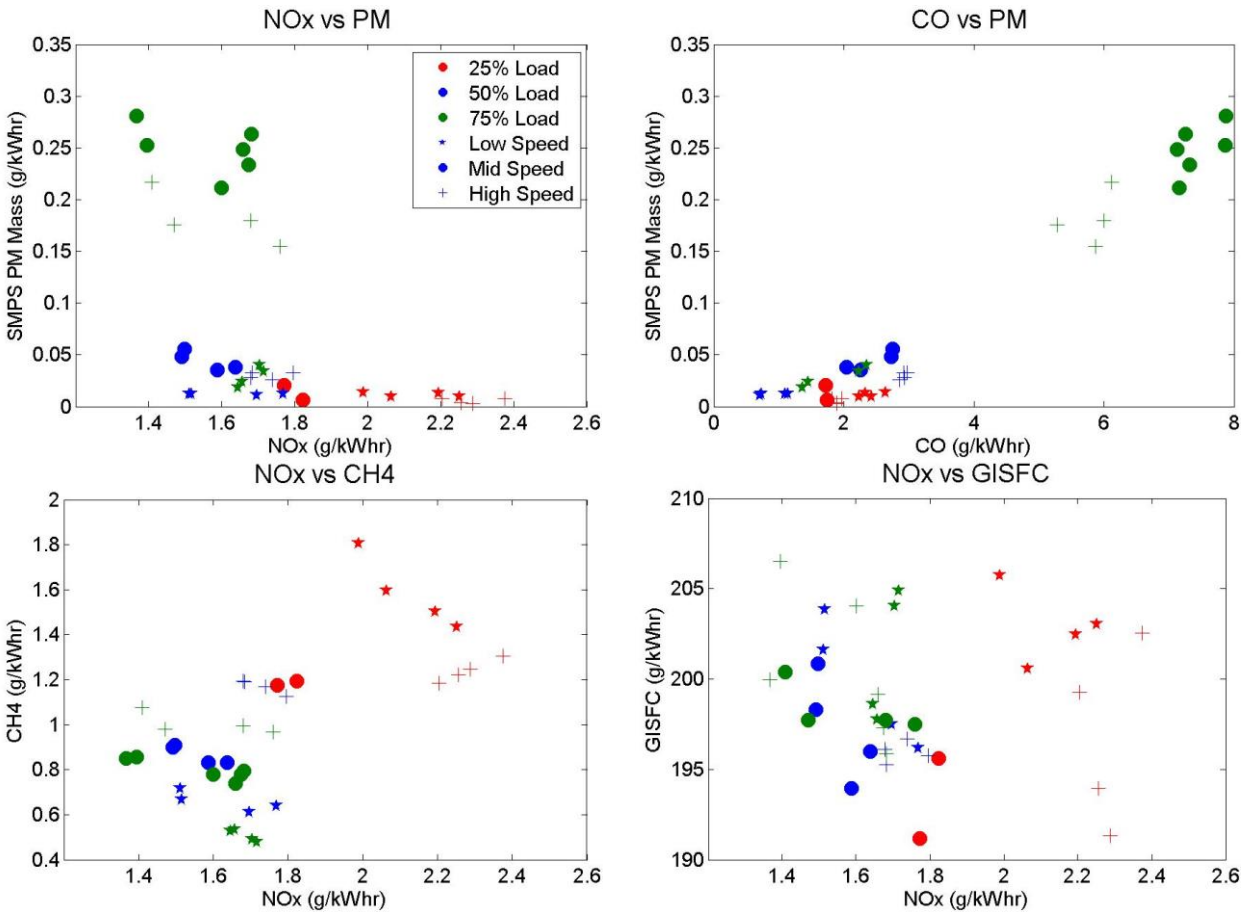

Figure 11 - Emission Trade-off Curves for 9-mode testing (load indicated by color; speed by symbol shape)

The NOx-PM trade off curve for the HPDI emissions closely resembles that of the traditional diesel engine (Johnson, 2008). On a power specific basis, the higher load conditions have much higher PM emissions than the other points along with low NOx emissions. The mid and low loads points have significantly lower PM emissions, with the low load points having higher NOx emissions.

There is a strong correlation between CO and PM emissions. CO emissions are a product of incomplete combustion and are formed in fuel rich (oxygen lacking) environment. Even though the global equivalence ratio is always lean, the fuel rich jet cores still produce some CO. Like the PM, this is mostly a function of load/equivalence ratio. However, as will be demonstrated below, the CO-PM correlation is broken when gas is more premixed before combustion

It is important to remember that the emissions are normalized on a power specific basis. For example, high load conditions have higher combustion tempreatures and NOx emissions compared to lower load modes. However, the increase in NOx emissions is smaller than the increase in power, leading to low, power specific, NOx emissions at high loads.

3.1.2 Mass Concentrations

As seen in the preceding section, the PM mass concentrations are most strongly correlated with engine load/equivalence ratio, with engine speed having a less significant effect. These results are plotted in Figure 12. Mode A75 shows a much lower mass concentration than the other high load conditions.

In addition, the TEOM and DustTrak results are also plotted. This shows that all 3 instruments capture the emission trends, but have different absolute values. As seen in Section 3.1.6, the TEOM measurement has the best correlation with gravimetric filters and is the most trustworthy instrument above loadings of 0.01g/kW-hr.

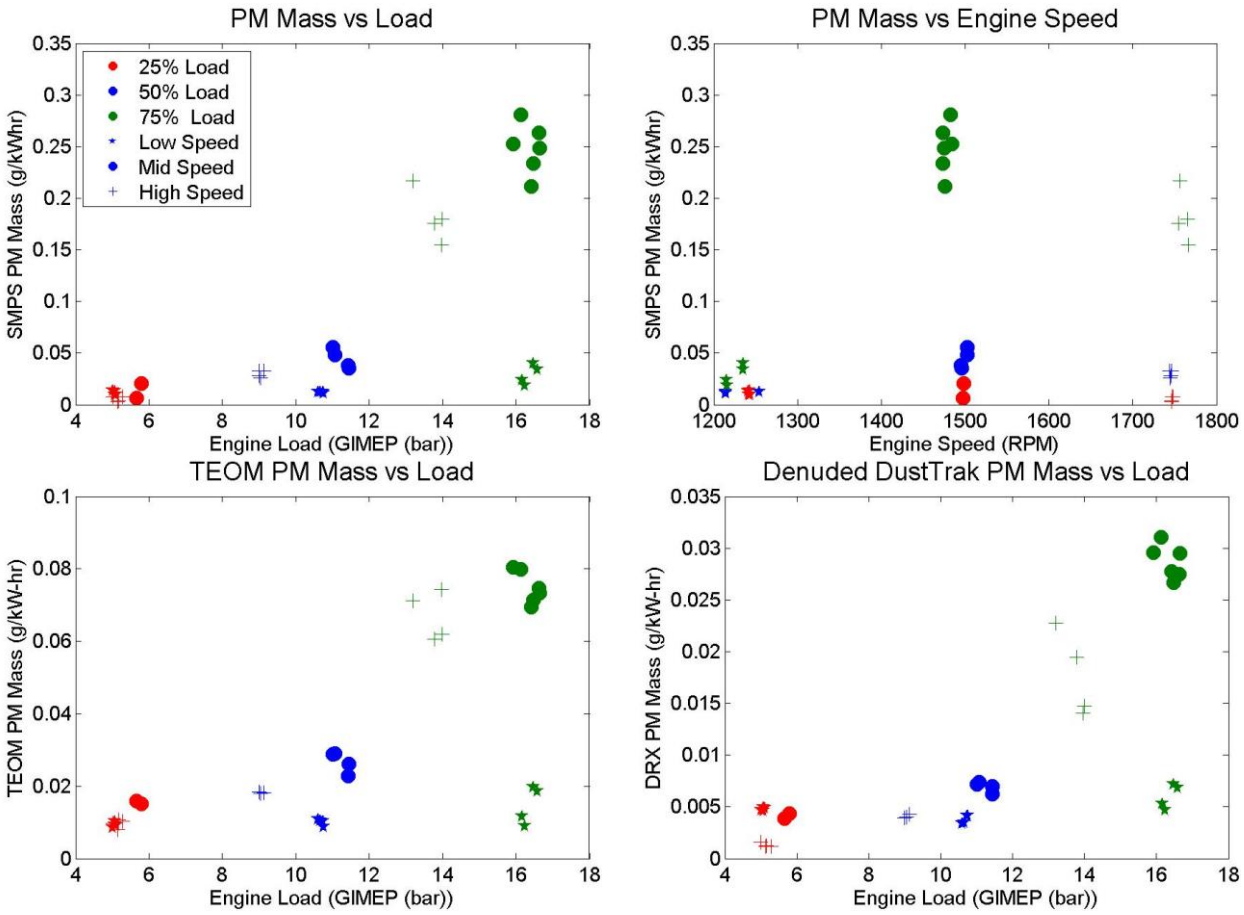

Figure 12 - PM Mass vs Speed and Load

3.1.3 Number Concentrations / Size Distributions

The SMPS provided size and number information of the emitted PM. These results will be analyzed in the following section. Throughout this thesis, the mean particle diameter reported from the SMPS is the geometric mean diameter. This represents the size bin with the highest number concentration. The SMPS size distributions for all 9 modes are shown in Figure 13

These plots show both the size distributions for both the raw PM with the solid line and the non-volatile fraction of the PM after it has pasted through the thermodenuder with the dotted line. The TD loss corrections of Gormely and Kennedy (Section 2.3.5) have been applied to the data; these corrections are actually very small and cannot explain the reduction in particle number concentrations shown in Figure 13. The semi-volatile fraction of the PM is the difference between these 2 lines. The vertical scale for the plots is ΔN/ΔlogDp (# of particles / cc) and has been corrected for dilution. This scaling ensures the area under the curve is proportional to the number of particles in each size bin. The range of this axis is the same for all plots.

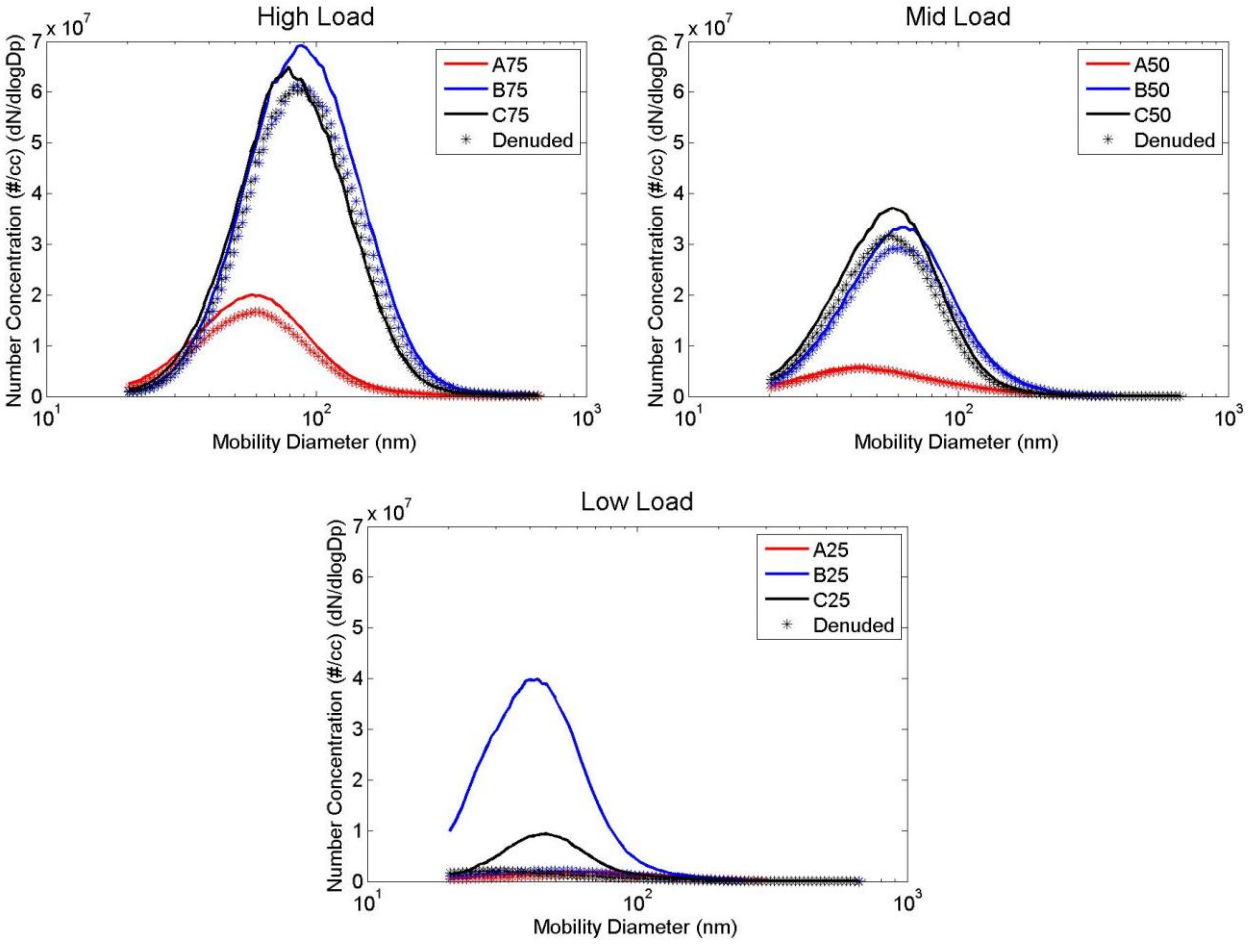

Figure 13 - MultiMode SMPS Size Distributions

Over all modes, the size distributions show lognormal distributions typical of diesel engines (Heywood, 1988) with approximately equal geometric standard deviations (Harris & Maricq, 2001). While the qualitative shapes are the same throughout the cycles, there are some differences in the particles sizes and semi-volatile content.

The mean particle size varies from 40-92nms over our load range. This is comparable to traditional diesel engines where mean particle sizes of 46-110nm (Fino & Russo, 2011), 46nm (Khalek et al., 2011)

40-100nm (Lu, Cheung, & Huang, 2012) and 60-100nm (Burtscher, 2005) are reported in literature from engine out TDE.

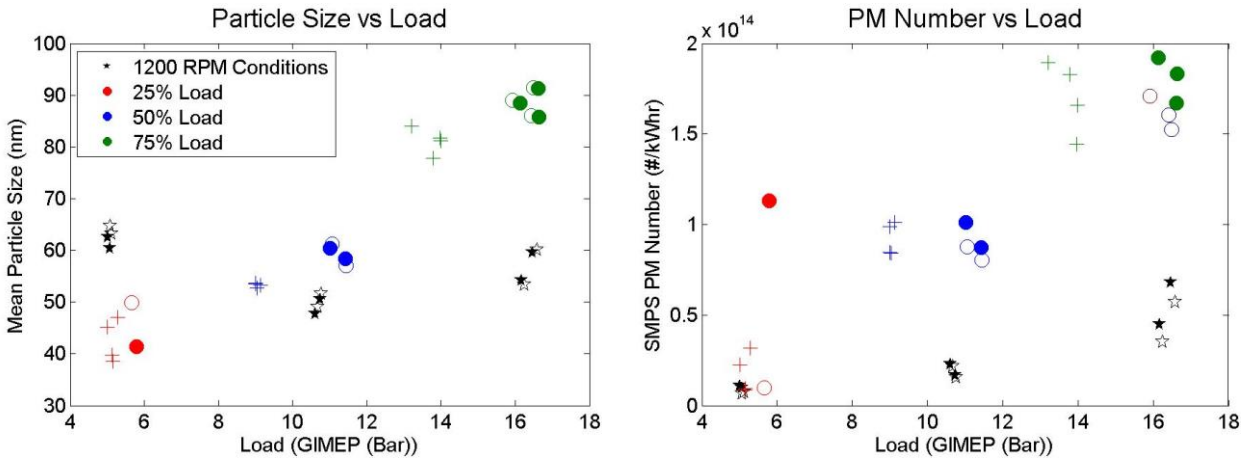

Figure 14 - Mean Particles Size vs Load / PM Mass vs Number

As seen in Figure 14, the mean particles size increases almost linearly with increasing load, for the mid and high speed modes. However, this is not the case for the low load conditions. The mean particle size is almost constant for these 3 points. This provides more justification for the grouping of point A75 with the lower load points. The increased residence times may change the ratio between the PM formation and oxidation. Initially, the longer time scales (immediately after injection) may lead to greater particle growth; later, oxidation may begin to dominate the overall concentrations.

The number concentration vs load plot is similar to the mass concentration data in Figure 12. The lower speed modes have lower number concentrations than the high speed modes at the same load.

More interestingly is the lack of size distribution shifts after the PM has passed through the thermodenuder. In many traditional diesel engines, the semi-volatile fraction appears as small, externally mixed, nucleation mode particles, where the organic carbon vapor condenses to form new particles (as opposed to internally mixed coatings, where the SVOCs condense on existing PM particles). This results in bimodal size distributions with a second peak around 15nm. This is not seen in the HPDI PM. In Figure 14 it can be seen that the mean particles size barely changes when the SVOCs are removed (the difference between the open and closed symbols). This suggests that the semi-volatile particles are externally mixed. Unlike traditional engines, where the externally mixed nucleation mode SVOC particles remain smaller than ~20nm, the particles seen from this engine grow much larger and reach the same size as the non-volatile particles. This could be explained by reduced inception rates of the semi-volatile particles (possible due to the slower PM formation pathways for NG vs diesel). If, when compared to a traditional diesel engine, a similar amount of raw volatile species exist in-cylinder (eg: having a similar amount of lubrication oil entering the cylinder) then this will lead to large particles when these semi-volatile species condense on the fewer number of incepted particles.

The semi-volatile fraction will be further investigated in the following section.

3.1.4 Comparison of Semi-Volatile Fraction Measurements

Given the importance of the semi-volatile content to aftertreatment strategies and human health implications, the semi-volatile content was measured with a number of different measurements. These will be compared and contrasted below.

- Thermodenuder with the SMPS and DustTrak
- Aethalometer BC / TEOM measurement
- Quartz filter offline EC/OC measurement

3.1.4.1 SMPS/DustTrak with the Thermodenuder

As described in Section 2.3.5 the thermodenuder developed for this study removes the semi-volatile fraction of the PM while leaving the non-volatile species. During the multi-mode experiments, the PM stream was either diverted through the denuder or allowed to bypass the instrument. The difference between the 2 measurements was the semi-volatile fraction.

Tests were performed with both the SMPS and DustTrak installed downstream of the TD. Using the SMPS gives size resolved measurements of the SVOC content. The DustTrak is very sensitive to any changes in PM composition and any changes in the refractive index of the particles.

3.1.4.2 Aethalometer –TEOM Comparison

Another technique to measure the semi-volatile content of the PM is to use an Aethalometer (Magee Scientific Model AE22-HS) in conjunction with the TEOM.

The Aethalometer is only sensitive to the black carbon content of the PM. The instrument uses a 880nm laser and photodector to measure the optical attenuation (light transmission) of the PM deposited on a quartz filter. The near-infrared light source is sensitive to only spectrally broad absorption which is typical of optically black particles. PAHs and other semi-volatile particles exhibit other molecular absorption processes which are sensitive to shorter wavelength light and are not detected by the instrument (Hansen, 2005).

The Aethalometer is very sensitive; however it relies on an assumption of a linear change in light absorption with BC mass deposition. The assumption fails when the filter becomes saturated. This set an upper limit of the PM mass concentration the instrument can measure in a 2 minute sample time. Even though the instrument was installed with a pump-and-filter secondary dilution loop, the instrument would become saturated at high loading conditions, giving erroneous results.

As the Aethalometer is only sensitive to the non-volatile black carbon in the PM sample, it can be compared with the TEOM measurement, which is sensitive to the total PM mass. Again, the semi-volatile fraction is the difference between these 2 measurements. Unlike the TD which must be switched on and off, this 2 instrument approach allows the measure the same PM sample simultaneously.

3.1.4.3 Offline Quartz Filter NIOSH 9334

A more accurate semi-volatile content measurement can be made with an offline EC/OC measurement based on the NIOSH 9334 procedure. For this measurement, quartz filters are pre-baked at 550°C for 24 hours to remove any existing volatiles from the filters and stored in a freezer before use. The PM is then deposited on the filters until the filter is visibly black. The sampling time depends on the PM concentration and varied from 10-60 minutes. The samples were then sent to Sunset Labs (http://www.sunlab.com/ , Tigard, OR) for the analysis. Appendix C has more information on the analysis techniques and the raw data from this analysis.

The quartz filter EC/OC data is taken from 2 different samples. The first samples were taken during the multimode and premixed tests. These samples were taken without a quartz-behind-quartz backup filter (McDow & Huntzicker, 1990). The absolute values of these results appeared to overestimate the semi-volatile fraction (given previous data from this engine). As such, a second round of sampling occurred with back up filters. These backup filers provide a correction for the positive sampling artifacts from vaporous organic carbon. Any OC found on the second filter can be assumed to come from species found in the vapor phase and are not part of the semi-volatile fraction of the PM. For the second sampling, only modes B25, B50 and B75 were tested.

The relative amount of OC found on these backup filters was 10-30% of front filter mass; however the relative values from the first test were still valid. To correct for this difference, the relative difference at each load level was subtracted from the initial results (i.e. The difference between the it first and second B50 result will be subtracted from the initial A50 and C50 values).

The relative amount of VOC found on these backup filters was 20-45% of front filter SVOC. In an attempt to combine these two results, a correction was applied to the first results. It was assumed that the fraction of SVOCs to VOCs were constant for each load level (25,50 and 75% load).

$$f{=}mOC{,}Frontmf = \left(\frac{m_{OC,Front}}{m_{OC,Rear}}\right) from\ test\ 2 \tag{8}$$

Then this fraction of OC was subtracted from the found on the filters for the first test.

$$m'_{OC,Front} = m_{OC,Front} - \left(\frac{m_{OC,Front}}{f}\right) at\ test\ 1 \tag{9}$$

Where $m'_{OC,Front}$ is the corrected OC mass on the filter for the initial filters. Then the semi-volatile fraction is calculated by:

$$SVOC\ \%= mOC,Front'mOC,Front'+ mEC,FrontSVOC\ \% = \frac{m'_{OC,Front}}{m'_{OC,Front}+ m_{EC,Front}} \quad (10)$$

The corrected data from the first filter tests still did not match up with the second round of testing or earlier results, however the values were closer. Both rounds of testing had similar EC concentrations on the filters, but there was excess OC on the first round. While the absolute values of the first round of filter testing are biased, the relative differences between modes are still valid.

Both results are shown in Table 5 and the raw data is found in Appendix C.

3.1.4.4 Semi-Volatile Fraction of PM

The results of these analyses are shown in Table 5. The average standard deviations of the analyses are shown in the bottom row.

		Semi-Volatile Fraction (%)								
		SMPS Mass		SMPS Number		Aeth/TEOM		Filter OC/(OC+EC)		
			Load Averaged		Load Averaged		Load Averaged	First Test Corrected	Second Test	Load Averaged
Low Load	A25	25.9	49.2	30.7	62.5	75.3	77.9	73.7		83.5
	B25	67.6		91.2		74.1		87.2	85.9	
	C25	54.2		65.7		84.3		89.4		
Mid Load	A50	4.78	12.9	5.27	12.6	35.5	49.5	70.1		63.6
	B50	10.3		10.6		61.5		59.5	45.0	
	C50	17.4		15.7		51.6		60.5		
High Load	A75	19		18.7		-		64.2		
	B75	12.1	8.5	10.7	7.7	36.4	44.0	37.7	32.6	38.8
	C75	4.9		4.6		51.6		39.8		
	Average σ	6.0		8.8				3.3		

Table 5 – Semi-Volatile Fraction over the 9 Modes

Like the gaseous emissions, the semi-volatile fraction is most strongly correlated with load (again with the exception of Mode A75). The high load conditions have a lower level of SVOCs than the low load conditions. This is consistent with behavior seen in traditional diesel engines (Alander, Leskinen, Raunemaa, & Rantanen, 2004)(Heywood, 1988).

After the backup filter correction, the results also correlate well with results seen on this same engine (Jones, 2004). She measured a semi-volatile fraction of 72.3% at low load and 26.4% at high load with quartz filters at slightly different operating conditions.

Both the online measurements capture the semi-volatile fraction's dependence on engine load, but have discrepancies with the reported absolute value. The magnitude of the Aeth/TEOM measurement is close to the values for the corrected offline measurements. On average, the SMPS and TD underestimates the semi-volatile fraction by 33% when compared to the quartz filter measurements. This is due to the

complex relationship between particle mass and electrical mobility, especially for these coated and uncoated fractal aggregates. This behavior will be further explored in section 3.1.7.

Figure 15 shows the all of the online techniques plotted against the offline analysis. Perfect agreement would lie on the 1:1 line. While the magnitudes of the measurements differ, they all have a slope near unity.

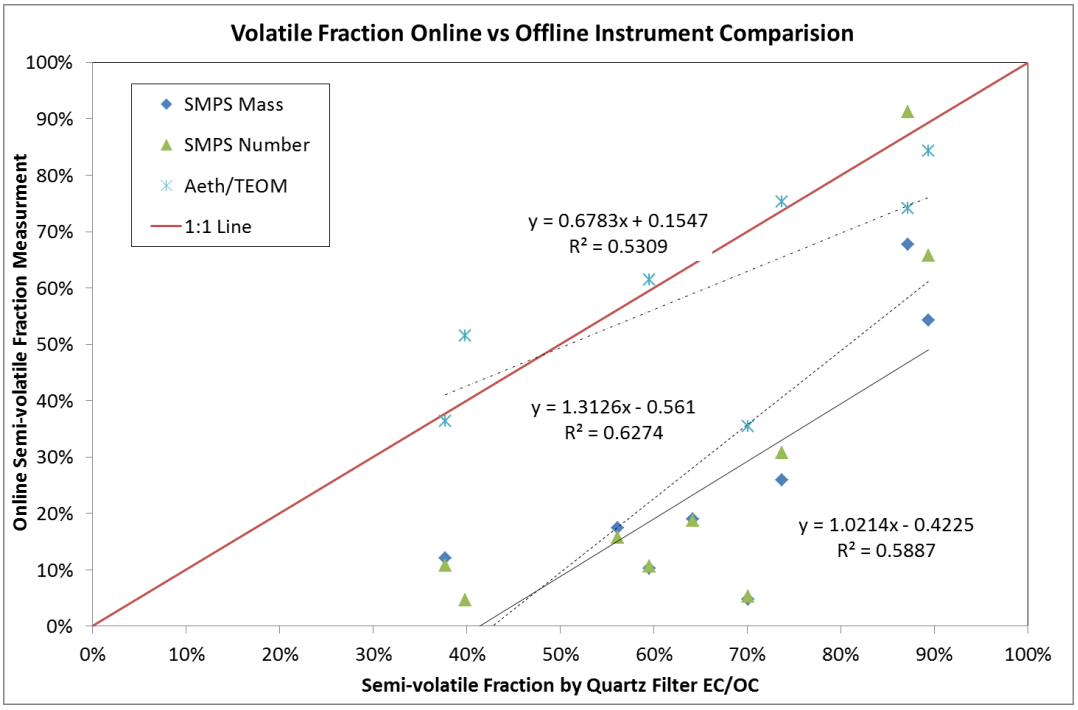

Figure 15 – Semi-Volatile Fraction Measurement Comparisons

3.1.5 Particle Morphology

To inspect the morphology of the soot particles, TEM images were taken at all 9 modes. The particles were deposited on carbon grids (Ted Pella P/N 01813-F, Carbon Type B, 300 Mesh Cu) with a thermophoretic sampler (Just, 2012). For each mode, a minimum of 25 particles were analyzed on a transmission electron microscope (Hitachi H7600). Individual particles were selected with a random grid search to minimize human bias in selecting interesting particles.

The goal of the analysis was to evaluate the primary particle and aggregate sizes from the 9 mode test cycle. A MATLAB image processing code was used to determine aggregate and primary particles size. This was done by isolating individual particles and then turning them into binary images (using a manually adjustable threshold limit) to determine the total aggregate size as well as radius of gyration. Primary particles were measured by taking the average of the height and width of each particle. Depending on the size of the aggregate and the clarity of the particles, between 2 and 15 primaries were measured. The boundaries for some of the smaller primary particles can be somewhat unclear, so there

may be an upward bias in choosing larger primaries with more distinct boundaries. Additional information on this image processing code can be found in Appendix B.

Initially, a 'pan' view is taken in 5 different positions, in a circular pattern on the grid, to get an overall view of the deposited particles. 5 particles from each view are analyzed to get a representative sample of the particles. Figure 16 shows a pan view at 50,000X magnification for a representative low, mid and high load point.

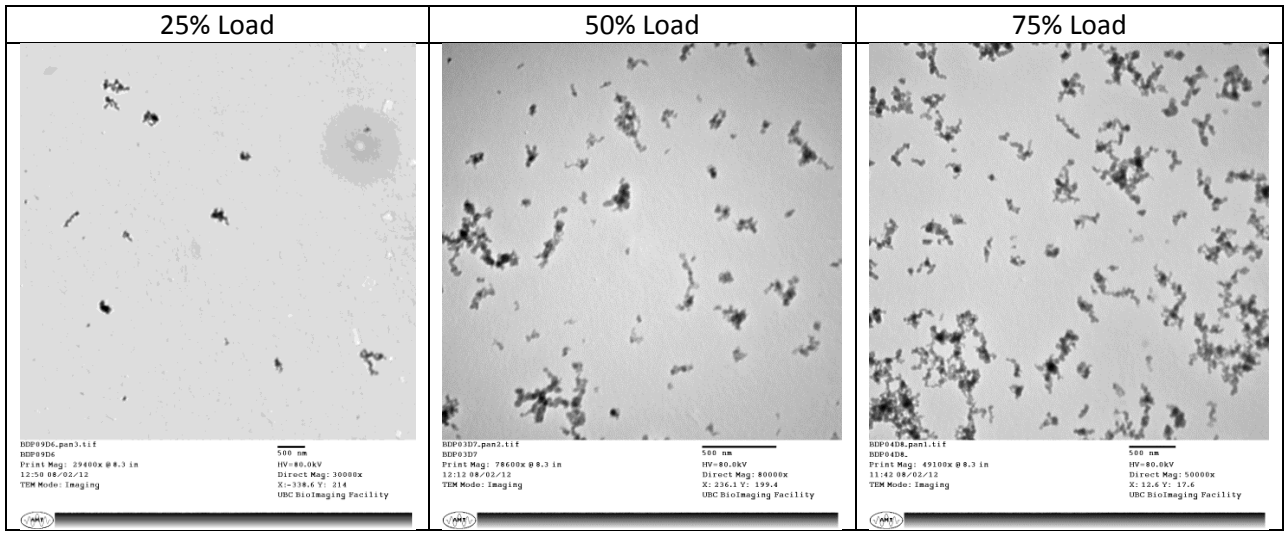

Figure 16 - TEM Pan Images for a Low, Mid and High Load Mode

Figure 17 shows some representative individual particles for these low, mid and high load conditions. Magnification ranges from 80,000X to 400,000X.

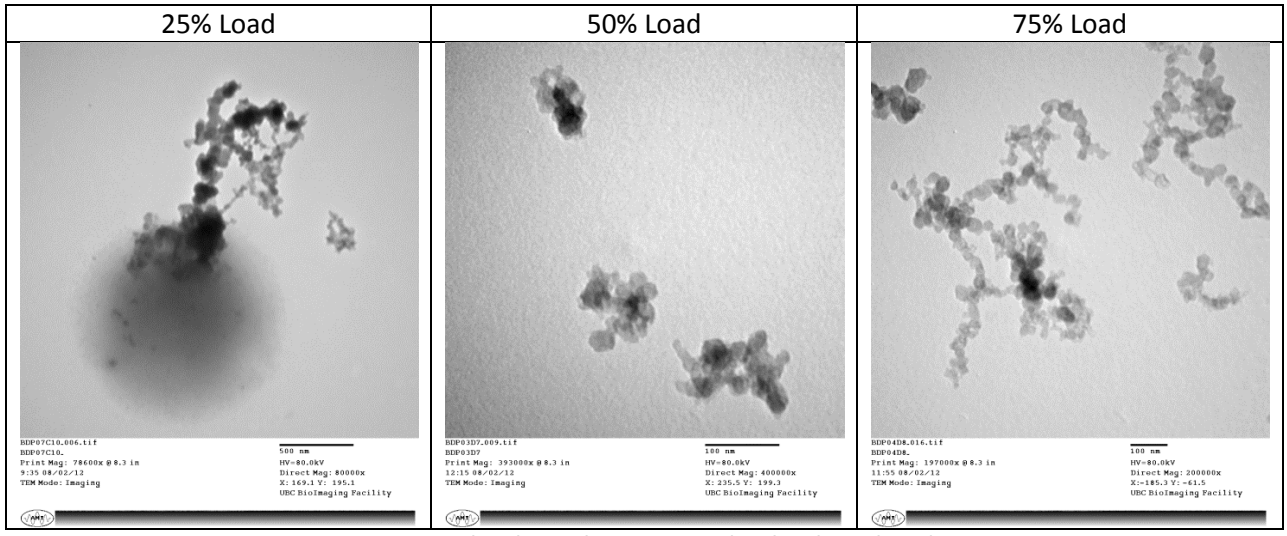

Figure 17 - Isolated Particles at Low, Mid and High Load Modes

Mirroring the results from the SMPS size distributions, the 50% and 75% load points have fairly similar morphology with the large majority of particles being fractal aggregate chains. Similarly, the majority of the particles at the 25% load condition are aggregates; however, there is now the emergence, of what are believed to be, SVOC splotches. An example is shown in the first panel of Figure 17. Semi-volatile particles have been observed in previous diesel PM TEM studies. (Mathis, Kaegi, Mohr, & Zenobi, 2004; Shi, Mark, & Harrison, 2000) observed semi-volatile nucleation mode particles deposited on their TEM grids.

In this study, the observed SVOC particles are quite large (>500nm in diameter), and may be the manifestation of many smaller semi-volatile mode particles which have condensed together (Given that the semi-volatile particles measured by the SMPS are <100nm in diameter). This may continue to support the claim that the externally mixed nucleation mode particles from this HPDI engine grow larger than those found in a traditional diesel engine.

3.1.5.1 Primary Particle and Aggregate Sizing

From the MATLAB based image processing code, aggregate and primary particle sizes were determined. An example of an aggregate image, a converted binary image and measured primary particle lengths are shown in Figure 18

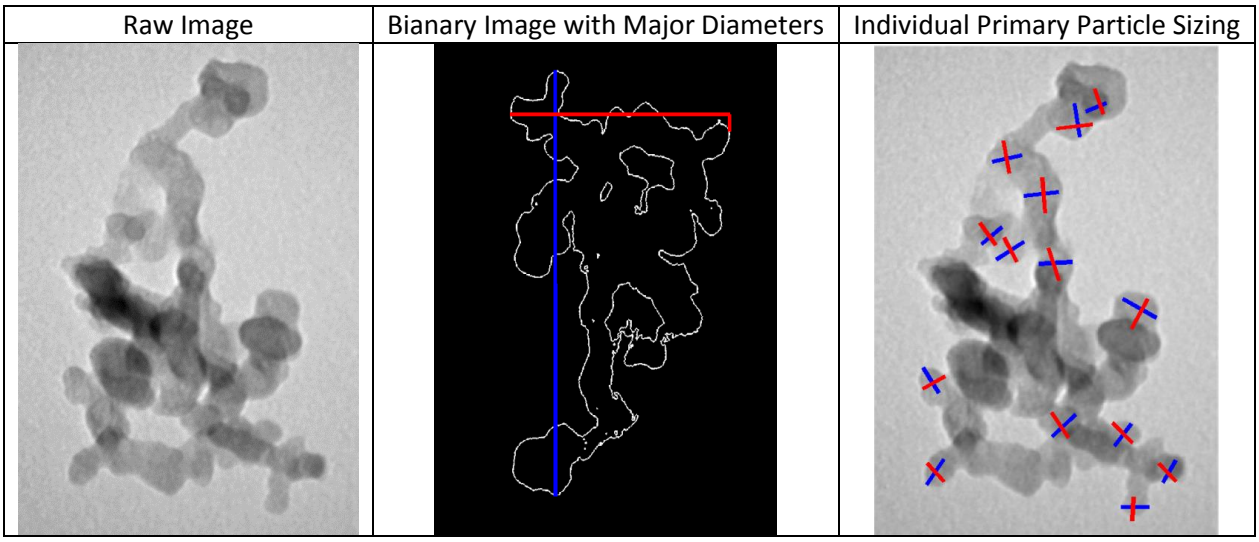

Figure 18 - Image Processing on an Aggregate Image

The tabulated results are shown in Table 6. The projected aggregate diameter (d_a) is calculated from the following equation:

$$d_a = \sqrt{\frac{4A}{\pi}} \qquad (11)$$

Where A is the projected area of the aggregate

(S. Rogak, Flagan, & Nguyen, 1993) have shown that the mobility diameter of an aggregate is approximately equal to the projected aggregate diameter if the particles have a single charge. (A multiple charge correction post-processing algorithm was applied to the SMPS data to remove any multiply charged particles, so the TEM and SMPS data should be comparable)

Representative histograms for the primary particle diameters and the aggregate projected diameters are shown in Figure 19. The aggregate diameter is compared with the mobility diameter distribution measured by the SMPS at this mode.

The projected aggregate diameter measurements are biased upwards compared to the SMPS mean diameters. A comparison between these 2 methods is seen in Figure 20. The median diameters from the TEM imaging are, on average, 29.6 nm larger than from the SMPS for the mid and high speed modes. For these modes, the mean diameters follow the same trend as the SMPS with respect to engine speed and load. The low load modes show an even greater over estimation of 64.2 nm. This upward bias could be caused by a high flow rate through the TPS, which would cause a disproportional amount of large particles to be deposited on the grid due to impaction; however, the flow was controlled with an appropriate critical orifice. Also, there is potential for some human selection bias for larger particles when selecting particles on the microscope.

	Low Load			Mid Load			High Load		
Engine Mode	A25	B25	C25	A50	B50	C50	A75	B75	C75
Median Projected d_A (nm)	123.7	128.6	68.9	61.6	95.5	84.3	102.7	118.6	101.7
Standard Error	14.7	16.4	18.6	13.1	10.7	11.0	11.8	11.3	7.5
d_p (nm)	32.8	29.7	27.2	25.6	27.8	22.6	26.3	30.4	26.4
Standard Error	0.97	0.75	0.67	0.71	0.64	0.40	0.58	0.56	0.48

Table 6 - Particle Size and Primary Particle Diameters

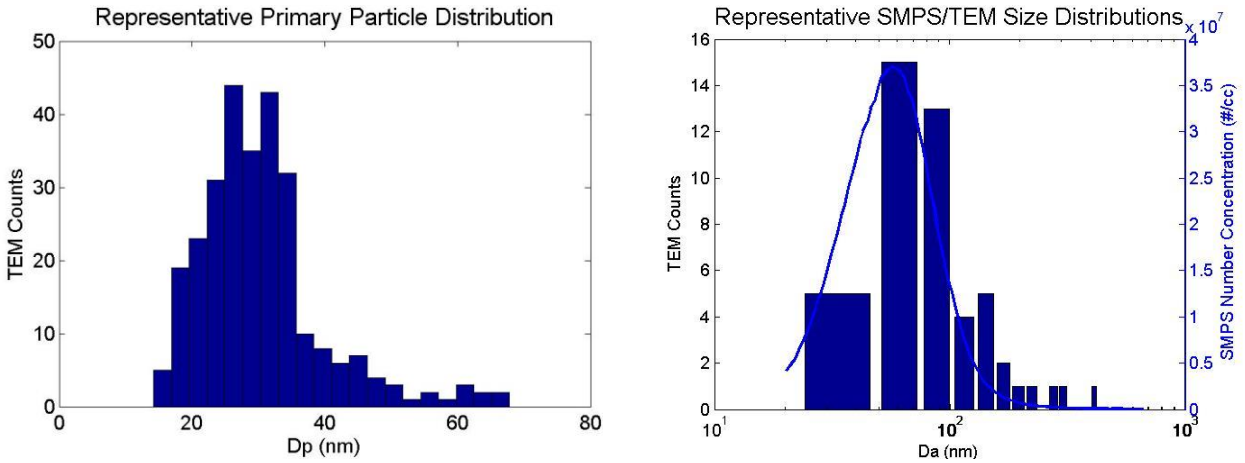

Figure 19 - Primary Particle and Aggregate Diameter Histograms

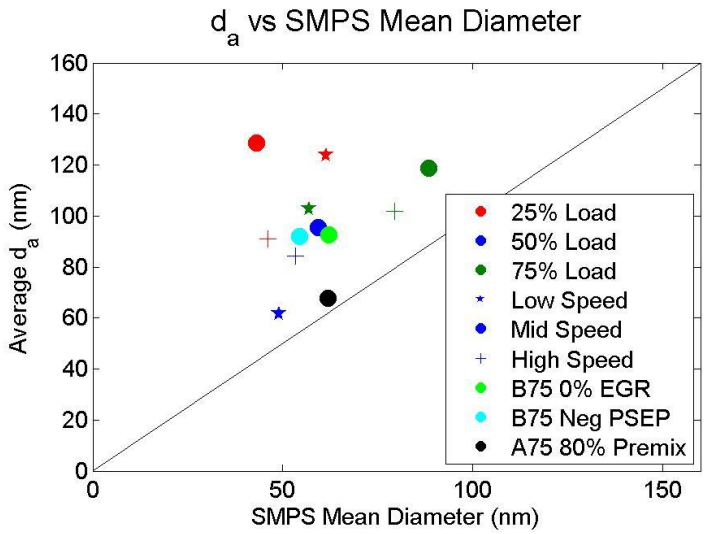

Figure 20 - TEM and SMPS Aggregate Size Comparison

The average primary particle sizes are 23-34nm for all of the modes and are distributed approximately lognormally. Figure 21 shows the primary particle sizes plotted against engine speed and EQR. There is a slight downwards correlation between engine speed and primary particle size. This is caused by the reduced in-cylinder residence times restricting the amount of hydrocarbons that can condense on the soot nuclei, limiting their growth. This phenomenon has been observed in a number of studies on traditional diesel engines (Lapuerta, Martos, & Herreros, 2007; Lu et al., 2012; Neer & Koylu, 2006).

In these referenced diesel studies, it was also observed that increases in the EQR lead to increases in primary particle size. This is explained by increased concentrations of hydrocarbon radicals causing increased particle growth inside the cylinder. This was not seen in this study. A possible explanation could be due to issues with the TEM sampler and the unrepresentative size distributions (compared to the SMPS). Figure 22 shows a correlation between the primary particle size and mean aggregate diameter, with larger primary particles found in larger aggregates. Typically, it is assumed that the primary particles are all the same size from a specific engine (Although (Barone, Storey, Youngquist, & Szybist, 2012) observed similar results to this study). From the parameter sweep study, higher equivalence ratios resulted in to larger mean aggregate diameters. This would suggest that the primary particle size would increase with increasing EQR and would be consistent with diesel engines in literature.

The other operating parameters (Pilot mass, GRP, EGR and timing) did not show any clear trends.

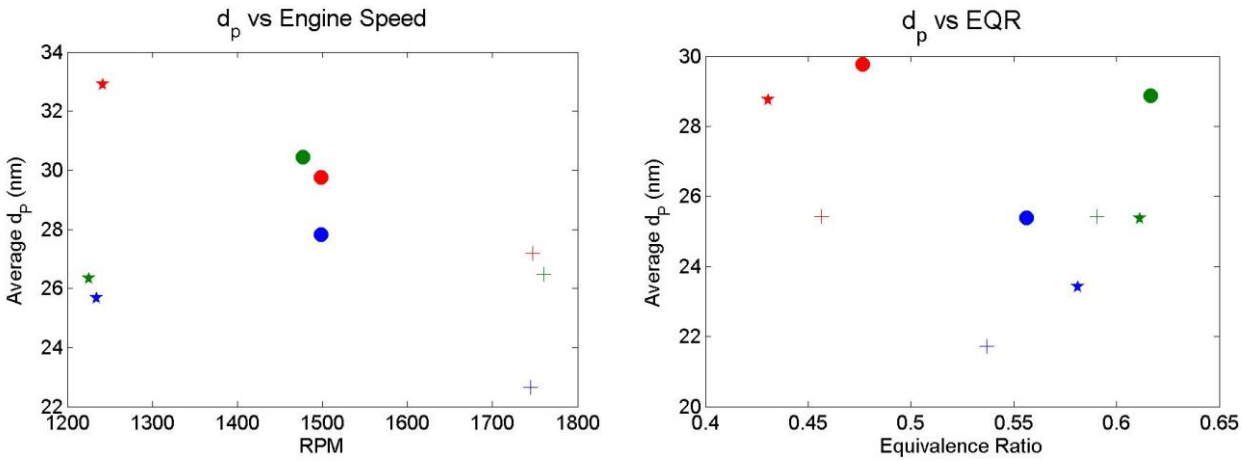

Figure 21 - Primary Particle Diameter as a Function of Speed and EQR

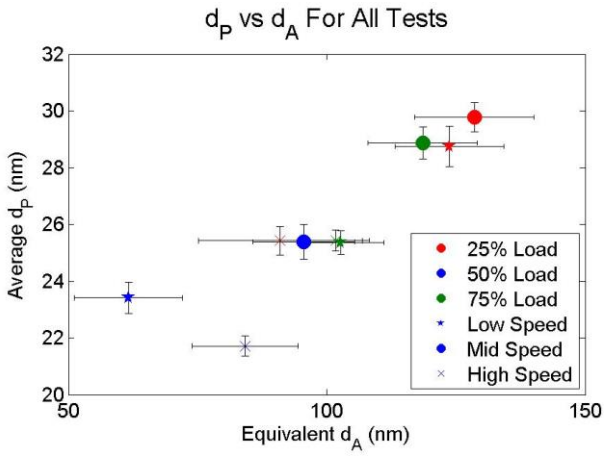

Figure 22 - Particle Diameter vs Primary Particle Size

3.1.6 Instrument Comparisons

The multimode testing provided a large data set allowing a comparison of the PM instruments' differing responses to a wide range of operating conditions and particulate characteristics.

Figure 23 shows the TEOM and Denuded DustTrak results plotted against gravimetric filters, which are the traditional method of PM mass sampling along with still being the 'gold' standard. The TEOM correlates very well with these results. Even the low load conditions match up well due to longer sampling times (10 minute collections, to better match up with the lengthy filter collections).

The denuded DustTrak measurement also has a linear response along with a 30% underestimation when compared to the filters. This is markedly different to the response of the instrument without the TD shown in Figure 24. This demonstrates the need to use a denuder upstream of this instrument.

After some confidence is established in the online measurements with the gravimetric filter comparison, Figure 24 shows these online instruments plotted against each other.

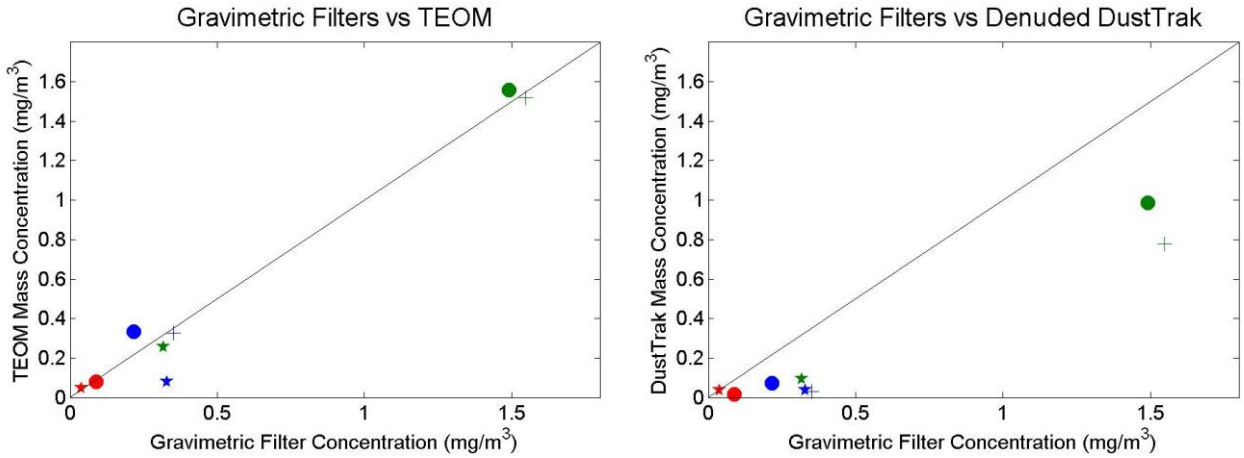

Figure 23 - Instrument Comparison with Gravimetric Filters

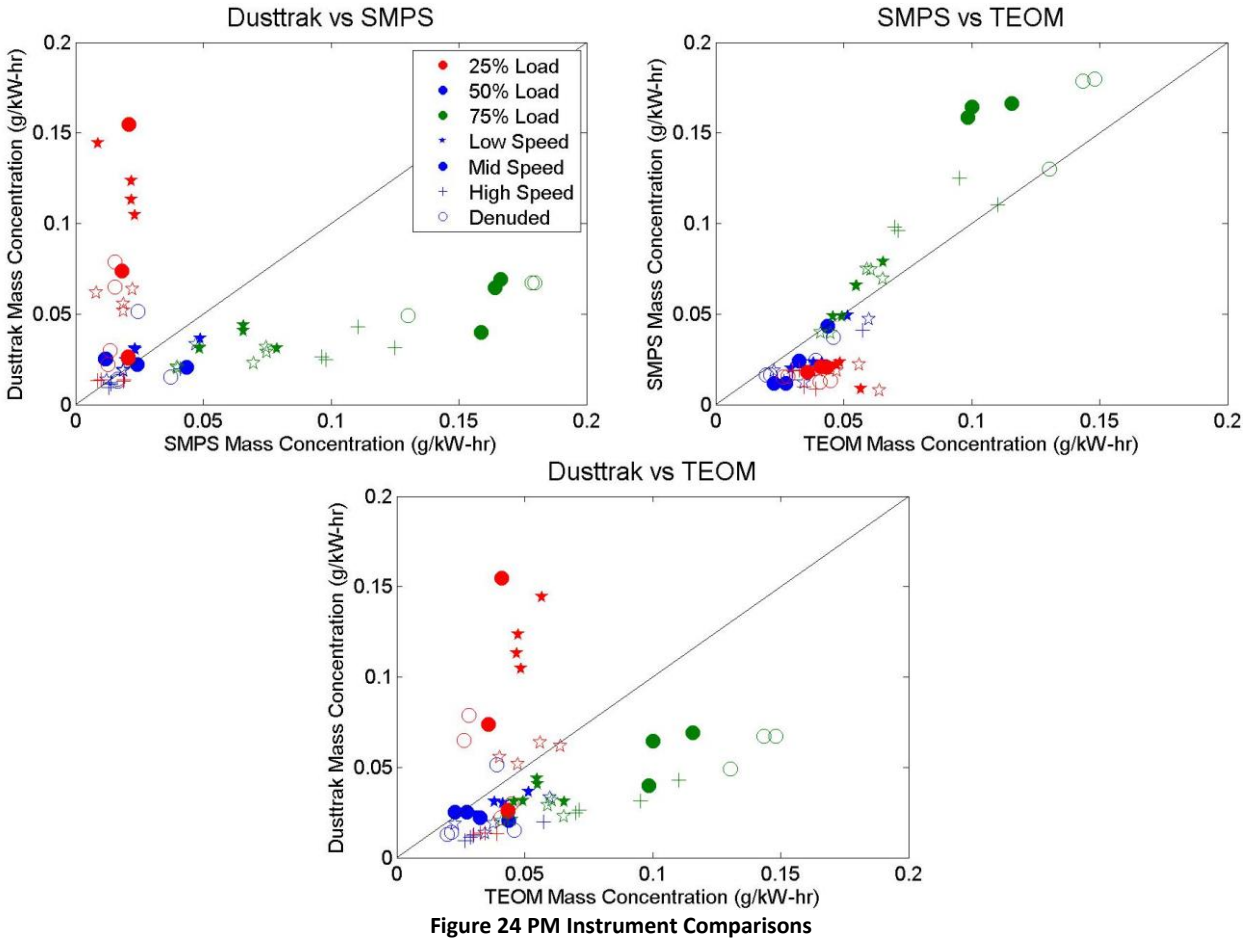

Figure 24 PM Instrument Comparisons

The SMPS and TEOM have an approximately liner response when compared together. As expected, the slope of the correlations is steeper than the 1:1 line as the SMPS over predicts the mass concentrations of fractal aggregates. There is a smearing of TEOM data points around the 0.01g/kW-hr emission level as the sensitivity of the TEOM has trouble resolving these low concentrations. However, as the shape of the PM size distributions are relatively constant throughout the tests, the SMPS gives a consistent mass measurment.

As reported by (Maricq, 2013), the DustTrak, however, shows a distinctly different response to different PM characteristics. At the mid and high load conditions, the DustTrak has a linear, and approximately 30% under prediction in comparison to the TEOM. This is reasonable give that the diesel PM particles are smaller than the calibration dust for the instrument and light scattering's strong dependence on particle size.

At low loads, the DustTrak gives a drastically different response. The DustTrak overestimates the PM at these conditions. This response can be attributed to the refractive index changes caused by the increased amount of SVOC particles in the PM. The semi-volatile fraction mostly manifests itself as externally mixed particles and these particles will have a different refractive index in comparison to the non-volatile, black carbon, particles. These semi-volatile particles scatter more light, leading to mass concentration over estimations. This is seen in the difference between the denuded and undenuded measurements. The measurements with the semi-volatile particles removed are much closer to the mid and high load measurement responses.

Even though the DustTrak is sensitive down to much lower mass concentrations, in comparison to the TEOM, it's response to PM with high levels of SVOCs is troubling. As a recommendation, a thermodenuder should be permanently installed upstream of the instrument. Also, care should be taken when comparing absolute emissions between the DustTrak and TEOM, relative comparisons across test points are safer.

3.1.7 Mobility of Coated Fractal Aggregates

The SMPS does not give a direct measurement of the particle diameter. The instrument measures the electrical mobility (the ratio between the electric charge and aerodynamic drag), which is then converted to an equivalent spherical diameter. As the PM particles emitted from CI engines are non-spherical aggregated chains, this spherical mobility measurement does not properly correlate with the particles mass. This relationship becomes even more complex if there is a condensed SVOC film around the outside of the particle.

The structure of these agglomerates can be described by the fractal dimension. The number of primary particles can be correlated with the outer radius of the agglomerate by: (S. N. Rogak & Flagan, 1992)

$$n_p = \left(\frac{R_f}{r_p}\right)^{D_f} \tag{12}$$

Where n_p is the number of primary particles, R_f is the projected radius (such as from a TEM image) of the fractal aggregate, r_p is the radius of the primary particles and D_f is the fractal dimension.

(S. N. Rogak & Flagan, 1992) showed that the projected area diameters of TiO2 and Si agglomerates are nearly equal to mobility diameters for particles with mobility diameters up to 400 nm and (Kittelson, McMurry, & Park, 2004) showed this also applies to diesel PM particles in the 50-220nm range.

They also proposed that the mass and mobility can be correlated with the following equation:

$$M = k_m \left(\frac{D_{mobility}}{d_p} \right)^{D_{fm}} \tag{13}$$

Where k_m is the mass fractal prefactor and D_{fm} is the mass fractal dimension.

Typically, the fractal dimension and the primary particle size are nearly constant for particles emitted from similar engines. It is then possible to run a correction on the SMPS mobility diameter distributions to provide a better estimation of the particle mass.

However, it becomes more complicated to extract this mass information from measured mobility changes from coated particles (Such as the thermodenuder measurements in this study).

If the spherical mass-mobility assumption is maintained, additional coating condensed onto the particles will be treated as increasing the size of the primary particles and producing a large increase in the overall aggregate size. This is shown in the second image in Figure 25. A more realistic representation of condensed SVOCs coating an aggregate is shown in the third image, where the whole aggregate is coated with a film of uniform thickness 'δ'.

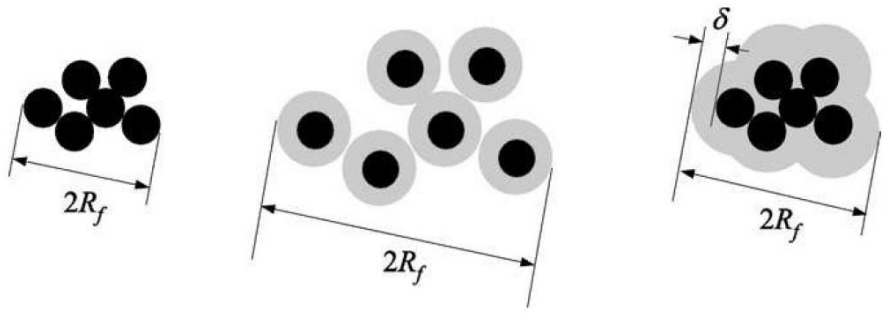

Figure 25 - Aggregate Coating Representations – From Park & Rogak, 2003

(Park & Rogak, 2003) suggested that this can be dealt with a technique of "particle obliteration" where primary particles are lost during the surface growth, leads to a more representative approximation to the mass-mobility relationship for the coated particles. For the obliterated primary method, when the aggregate is coated, the mass is conserved but mobility is recalculated with a reduced number primary particles.

The change in number of primary particles is given by:

$$dn_p = \frac{3D_f}{4\pi(3-D_f)} \left(\frac{R_f^{D_f}}{n_p r_p^3}\right)^{\frac{3}{3-D_f}} \left(\frac{r_p}{R_f} - 1\right) dv \quad (14)$$

Where n_p is the number of primary particles, r_p is the primary particle radius, R_f is the particle outer radius and dv is the change of in particle volume from the coating.

Figure 26 shows the difference in calculated mobility between the individually coated and obliterated primary methods for a particle of arbitrary size with increasing amount of volatile coating. It can be seen that for mass semi-volatile fractions of 50%, there can be a difference in calculated mobility of 15% between the 2 methods.

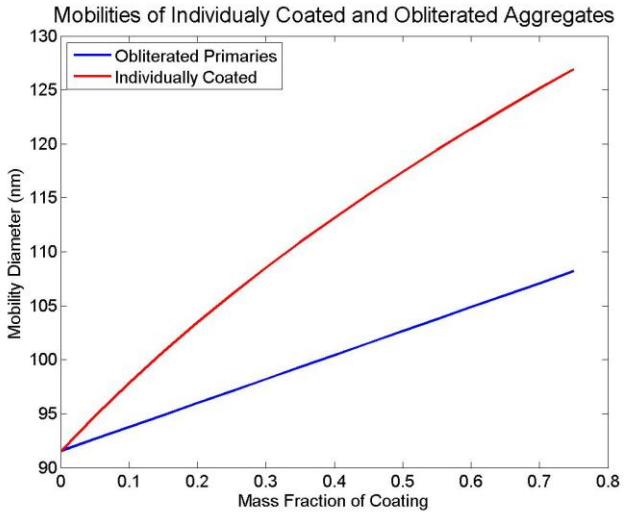

Figure 26 - Mobility Difference in Coating Assumptions with Different Coating Mass Fractions

Given the substantial effect of model assumptions on the mobility-coating relation, it is not easy to obtain reliable coating mass using the SMPS. However, if the soot particles were internally mixed with organic material, the thermodenuder should have caused a mobility diameter reduction of over 10% for the EC/OC ratios observed in this study. The actual change in mobility diameter was several nanometers – far lower than expected for coated particles. This supports the hypothesis that the organic material is externally mixed.

3.2 Parameter Variations at Fixed Speed and Load

Alongside the multimode testing, an input parameter variation study at fixed load and speed was performed to better understand the effects of our controllable inputs on the engine out emissions. This study was based around mode B75 as it represents the highest sooting point attainable on the SCRE hardware. While maintaining the engine load and speed, the EQR, EGR, GRP and Diesel Pilot Mass were varied around the baseline engine calibration. A goal of this test was to search for an optimal engine calibration for the PM. That is, for a PM 'well' or non-linearity in the emission responses of the input parameters. The tested parameter values were highlighted in Table 4. In addition single-parameter sweeps, tests were performed to observe any combination effects between the Pilot Mass, GRP and EQR.

3.2.1 Mass Emissions

Figure 27 shows the PM mass emissions as measured by the DustTrak, TEOM and SMPS with a linear least squares fit though each of the instrument's data points. The fit parameters are shown in Table 7. These fits include all 3 engine timings tested and these are indicated by the shape of the symbol. The filled symbols represent undenuded symbols whereas the open symbols have been passed through the thermodenuder. All of the symbols for the TEOM are filled as the thermodunder was not installed upstream of this instrument.

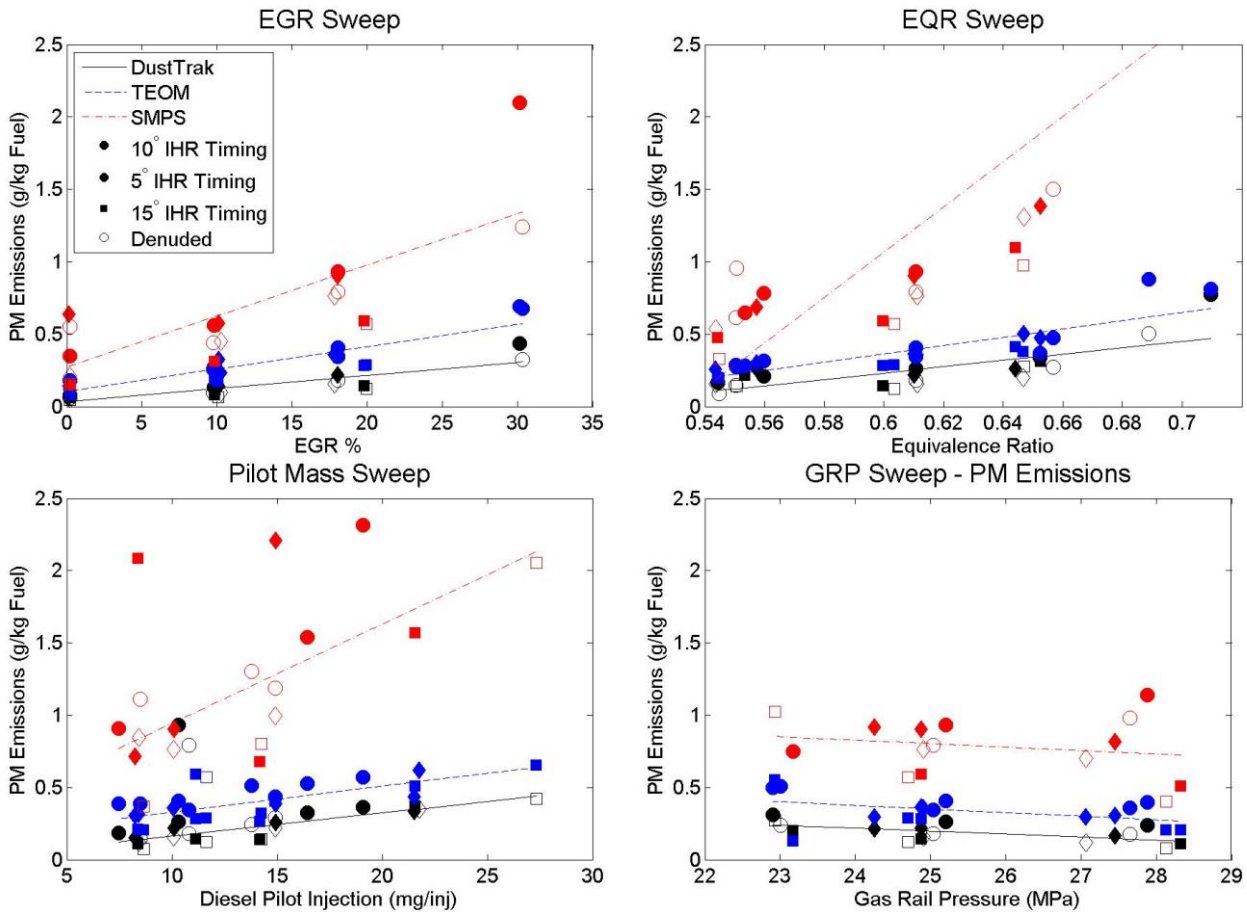

Figure 27 PM Mass Emissions over the Parameter Sweeps

	EGR			EQR			Pilot Mass			GRP		
	Slope	Intercept	R^2	Slope	Intercept	R^2	Slope	Intercept	R^2	Slope	Intercept	R^2
SMPS	0.0443	0.16	0.78	15.62	-8.30	0.86	0.0119	0.302	0.58	-0.02	1.39	0.80
TEOM	0.0159	0.099	0.90	2.84	-1.34	0.86	0.0179	0.151	0.76	-0.02	0.977	0.75
DRX	0.0095	0.030	0.87	2.18	-1.08	0.76	0.0160	0.0024	0.86	-0.02	0.703	0.66

Table 7 - Linear Regression Parameters

The changes in the PM mass emission with the parameter variations are monotonic and the linear fits are fairly reasonable ($r^2 > 0.75$). The biggest deviation from this linear response is seen on the EQR sweep, especially with the SMPS measurement. Figure 28 better shows this response with a larger scale on the y-axis.

This large deviation from the other 2 instruments is caused by changes in the PM morphology. As described later, the mean particle size is growing with higher equivalence ratios. This change in particle size furthers the upward bias in the SMPS' mass-mobility algorithms.

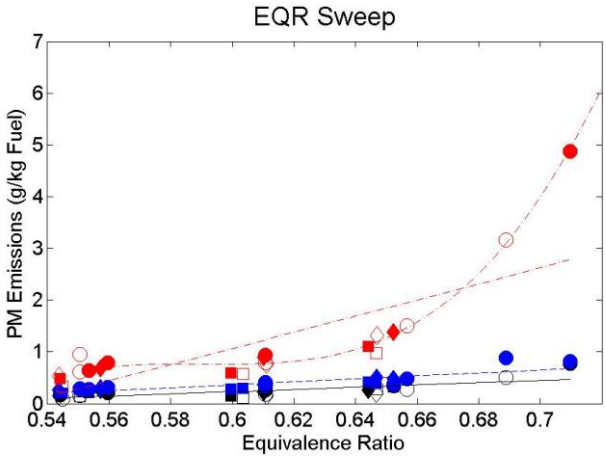

Figure 28 - PM Emissions over the EQR sweep with Non-Linear SMPS Measurement

3.2.2 Response Surfaces

To further understand the relative importance, as well as any combination effects, of the input parameters on the engine emissions, response surface fits were developed (Myers, Montgomery, & Anderson-Cook, 2009). This methodology works for both the PM emissions as well as the gaseous emissions. First Order (linear) fits were applied to all of the tested input parameters as well as the PSEP value. Additionally, a second order fit was applied to the timing as previous results have shown a PM emission maximums near 10° IHR timing (G. P. McTaggart-Cowan, 2006). The form of this equation is:

$$y = \beta_0 + \beta_1 x_1 + \beta_2 x_2 + \beta_3 x_3 \ldots\ldots + \beta_{11} x_1^2 \tag{15}$$

Where β are the partial regression coefficients and x are the input parameters.

The matrix X needs to be inverted to calculated and the least squared estimator of β and is given by:

$$\boldsymbol{b} = (\boldsymbol{X}'\boldsymbol{X})^{-1}\boldsymbol{X}'\boldsymbol{y} \tag{16}$$

(matrix notation)

This then leads to the fitted regression model:

$$\hat{\boldsymbol{y}} = \boldsymbol{X}\boldsymbol{b} \qquad \hat{y} = b_0 + \sum_{j=1}^{k} b_j x_{ij} \quad i = 1,2 \ldots, n \tag{17}$$

In order to apply the response surface methodologies, the natural input variables must be transformed to coded variables. These coded variables are centered across the minimum and maximum values actually seen in our experiment (eg. between 7.45 and 27.3mg/inj for the pilot mass). It is then

normalized to have a mean of 0 and limits of -1 and 1. This allows for the comparison of the relative importance of the 2 variables over the range tested.

Overall, these simple, linear, empirical fits do a good job of predicting these emissions. As a check on the appropriateness of the linear approximations, plots of the residuals of the fits were evaluated in Figure 29 . These showed no systematic trend along with being distributed normally near the mean of the response. There are some deviations from the predicted response at the tail ends of the distribution, indicating that the emissions do not follow a perfectly linear fit, however these first-order models were adequate (and prevent excessive 'over fitting' of the data). The measured and prediced measurements for the NOx and TEOM emissions are shown in Figure 30 further confirming the use of these models. The predicted values are calculated by entering the input parameters, from each tested mode, into the empirical fits; these are then compared to the actual measured values.

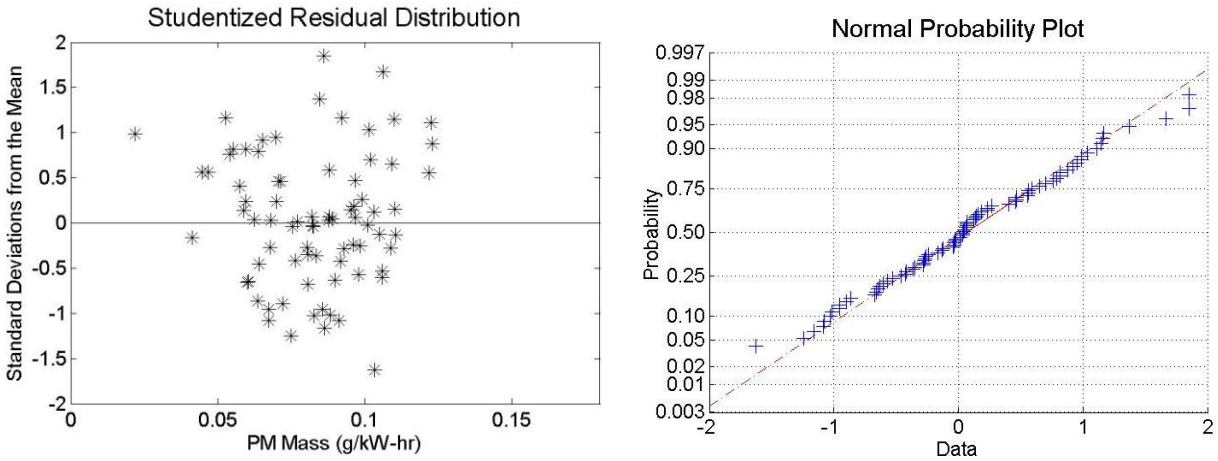

Figure 29 - Residual Analysis for the TEOM Response Surface

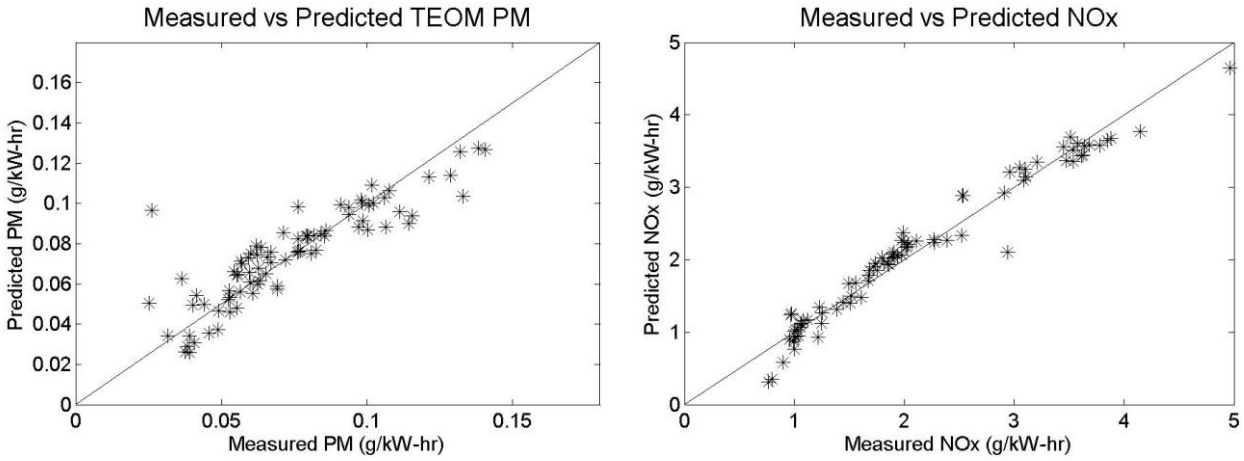

Figure 30 - Measured vs Predicted Emissions from the Response Surface Fits

From these surfaces, the partial derivatives of the emissions with respect to each input can be developed. These then show the relative importance of each parameter to the final emissions.

Table 8 shows the effect of a 1% change in each parameter on both the PM emissions as well as some selected gaseous emissions. For example a 1% increase in the GRP will lead to a 1.55% reduction in the TEOM measurement. Note that as a second order fix is applied to the engine timing, this value will change for different timing values. This chart is calculated for a 50% IHR at 10° ATDC.

% Change in Measurement for a 1% change in Input Parameters						
	Diesel	GRP	EQR	EGR	GIMEP	Timing
DustTrak	0.22	-1.39	3.00	0.99	2.90	1.37
TEOM	0.08	-1.55	2.88	0.80	1.43	1.13
NOx	-0.04	-0.10	-1.69	-1.59	-0.01	-1.78
CO	0.00	-0.38	4.21	0.51	-0.51	0.49
CH4	0.02	0.22	-0.82	0.60	-0.57	0.02
PM Number	-0.04	-0.87	2.20	0.42	-0.02	0.57
Mean PM Diameter	0.03	-0.66	1.06	0.28	-0.25	0.31
GISFC	0.00	0.05	0.28	-0.03	-0.10	0.04

Table 8 - Partial Derivatives of the Input Parameters to the Emissions

Equivalence Ratio, Injection Pressure and Power have the strongest effect on the PM mass emissions. The diesel pilot quantity has the smallest effect. It is interesting to note that the DustTrak is more sensitive to the diesel and power inputs than the TEOM. This suggests that the size or volatility of the PM is affected by these input changes.

An important result from this table is how the PM emissions are much more sensitive to the engine operating conditions that the gaseous emissions.

The slopes between the individual parameter sweeps and the combination sweeps are not significantly different and show no major combination effects. The lack of non-linearities along with the trade-offs with the gaseous emissions suggests the lack of an optimized, engine operating calibration for a PM emission local minima. The minimum EQR, EQR and pilot quantity, along with high GRP will lead to a minimum PM emission level; however, performance and other emissions will be affected.

3.2.3 Size and Number Emissions

In addition to the mass emissions, the number concentration and mean particles size was measured by the SMPS. These results are shown in Figure 31 and Figure 32. The y-axes have been held constant for all charts.

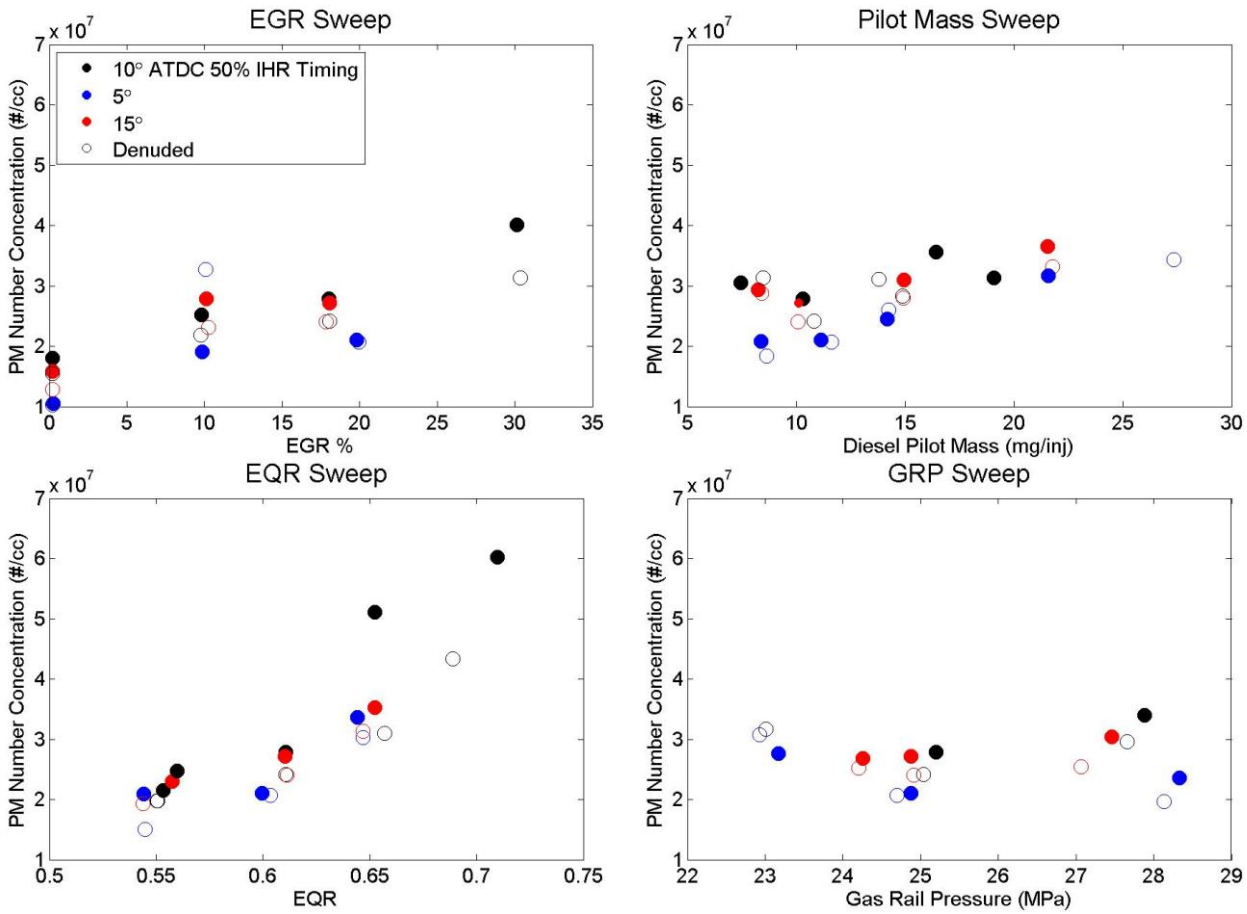

Figure 31 - PM Number Emissions over the Parameter Sweeps

For the parameter sweeps, the emitted particles ranged from 1-7*10^7 particles/cc with a mean particles size from 65-120nm.

The EGR and EQR plots show strongly increasing number concentrations and particle size with the increase in input parameter. This mirrors the results from the previous works on diesel engine PM (Armas et al., 2008; Lähde et al., 2011; Leidenberger et al., 2012). The Pilot and GRP plots do not show such distinct trends. This is in contrast to previous work on diesel engines where EQR is shown to have less of an effect on the size and number of particles then the injection pressure. The injection pressures for common rail engines in these studies are typically higher than 100 MPa where as we are injecting a gaseous fuel at 25 ±3 MPa. Larger pressure differences that are available on the SCRE (leading to increased turbulent mixing) are probably needed to see large reductions in PM. This is an interesting difference in the combustion and PM formation characteristics between HPDI and diesel engines.

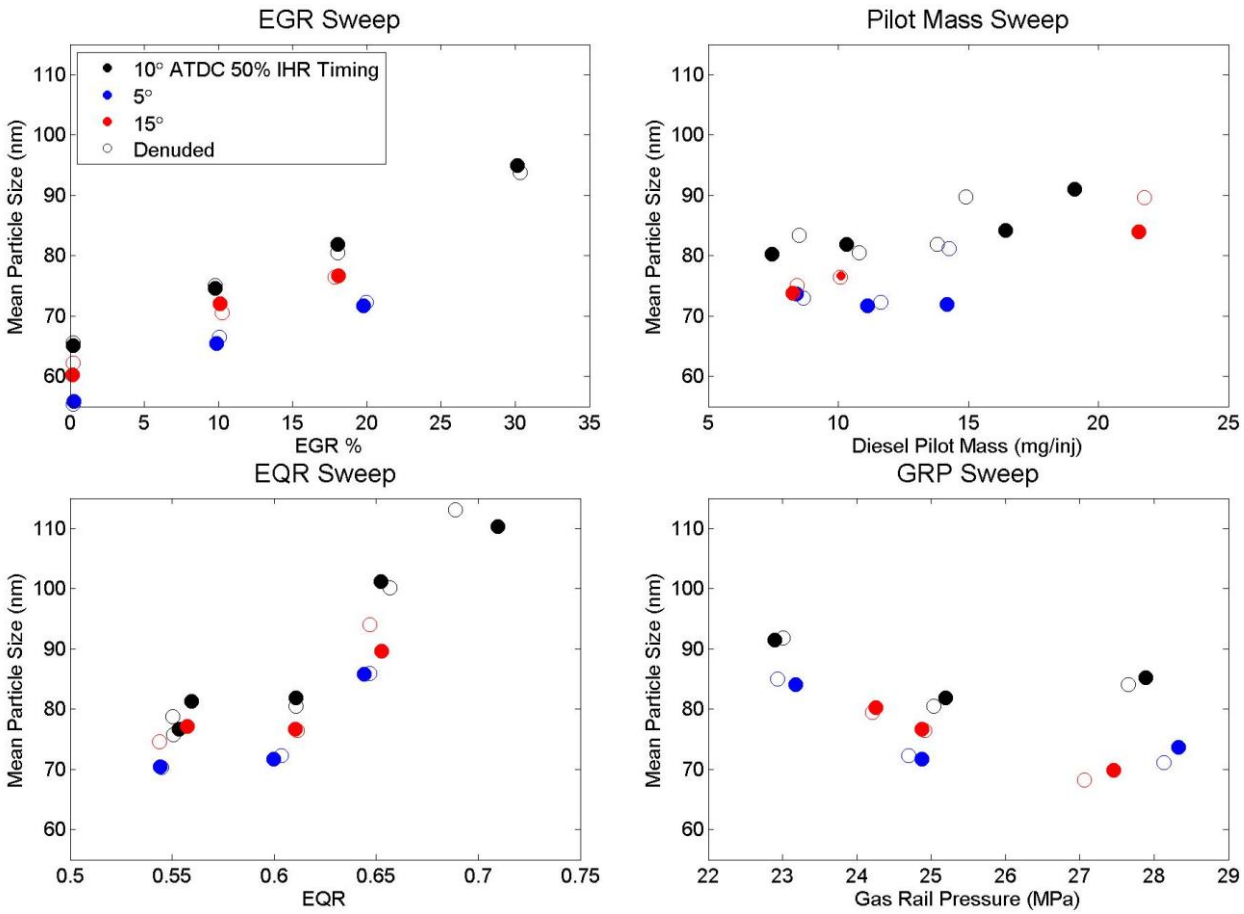

Figure 32 - Mean Particle Size Changes over the Parameter Sweeps

3.2.4 Semi-Volatile Fraction

The semi-volatile fraction was measured with a thermodenuder upstream of both the SMPS and DustTrak for all tests. The DustTrak predicts a semi-volatile fraction higher than the SMPS, yet lower than the offline EC/OC measurements taken during Multimode tests. Figure 34 shows the measured semi-volatile fraction over the parameter sweeps. There is significant scatter in the data, highlighting the difficult in consistently measuring the semi-volatile content of PM with online techniques.

Also, like the Multimode testing, the size distributions shapes are mostly determined by engine load. As such, the qualitative shapes of the distributions are consistent over the parameter sweeps only shifting with mean particles size changes (as described above) or in number with increasing mass (as engine load was constant for all tests). The semi-volatile fraction still appears as externally mixed particles with mean particle sizes near the mean size on the non-volatile particles.

Figure 33 shows some representative size distributions and Figure 34 shows the semi-volatile fraction changes over the parameter sweeps.

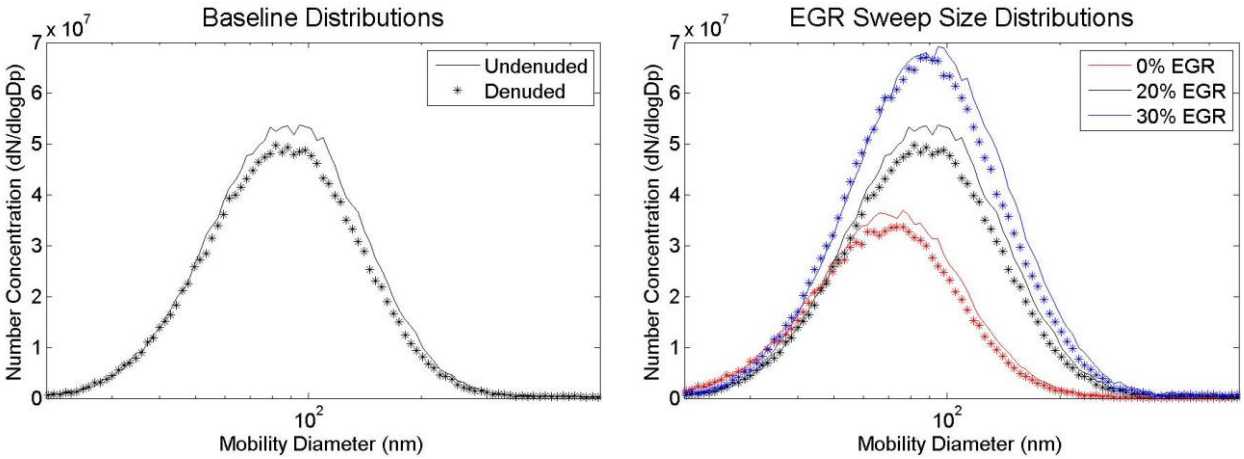

Figure 33 Representative Size Distributions for the Parameter Sweeps

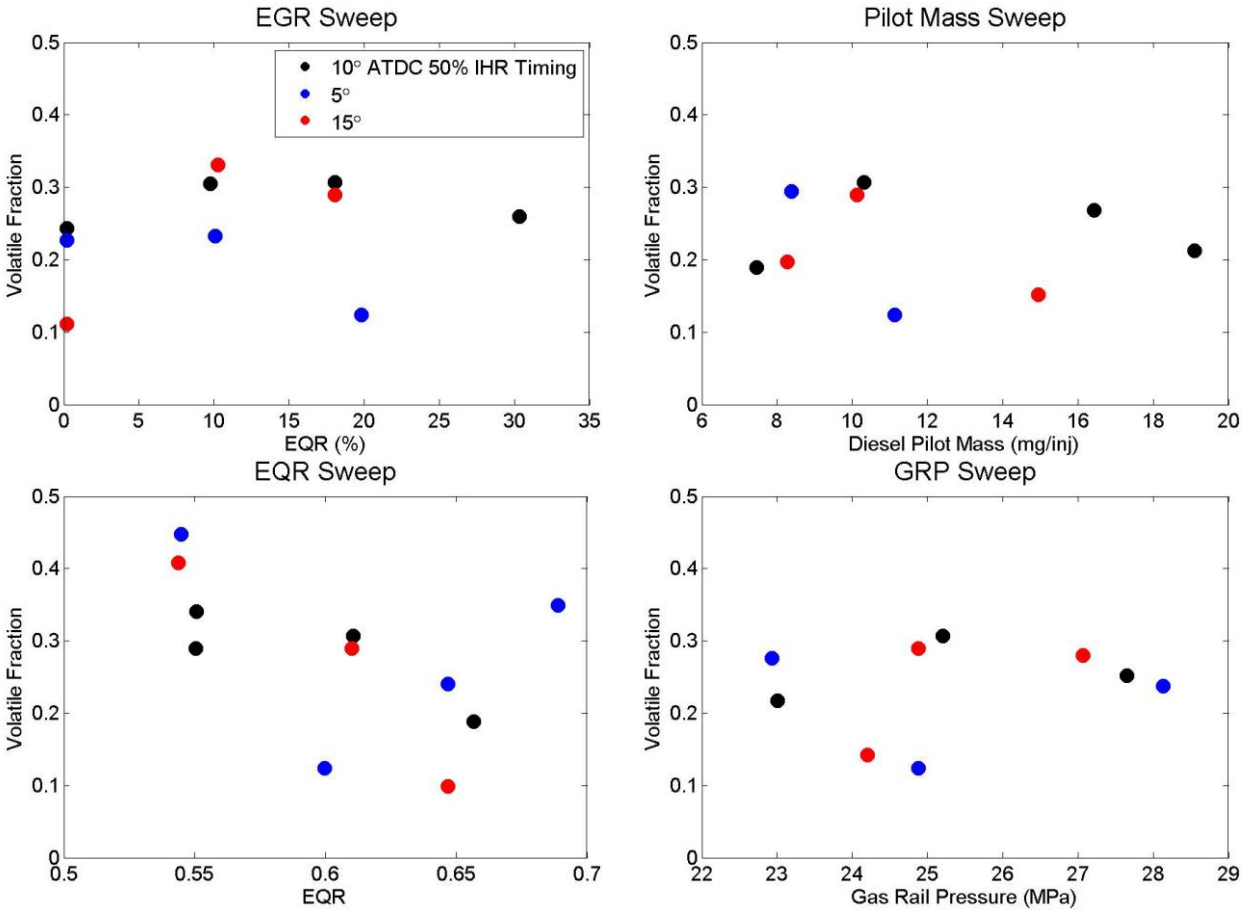

Figure 34 Semi-Volatile Fraction (based on DustTrak) Changes over the Parameter Sweeps

3.2.5 Further Investigation into the 0% EGR Operating Condition

With the prevalence of high efficiency SCRs, which can reduce NOx concentrations by up to 90%(Johnson, 2008), there has been an interest in running engines at lower EGR levels to reduce the PM

emissions. Additional instrumentation was used at the 0% EGR condition to better understand the effects of no EGR on the PM emissions. The results are shown in Table 9.

	0% EGR	Baseline
TEOM PM Mass (g/kW-hr)	0.02	0.07
Number (#/kW-hr)	$7.73*10^{13}$	$1.81*10^{14}$
NOx (g/kW-hr)	4.55	1.58
Semi-Volatile Fraction (%) (Quartz Filter)	56%	38%
Primary Particle Size (nm)	28.0	26.1
Geometric Mean Particle Size (nm)	62.1	85.8

Table 9 - Mode B75 0% EGR vs Baseline Emissions

The effect of running without EGR for an HPDI engine is similar to a traditional diesel engine. There is a large decrease in both PM number and mass concentrations. The mean particle size is also significantly decreased from 85.8 to 62.1nm. As a result of this decreased particle size, the relative drop in number concentration is less than the drop in mass concentration. Unlike the mean particle size, the primary particle size remains constant.

The semi-volatile fraction decreases with increasing EGR. This mirrors results from diesel literature (Fino & Russo, 2011). This could be attributed to the large decrease (71%) in total PM mass associated with running without EGR (greater than the other parameter sweeps). Most of this decease could be EC (with the OC emission rates from burnt lube oil remaining more constant), which would shift the semi-volatile fraction.

There are significant reductions in PM associated with eliminating EGR. However, using traditional injection strategies, thus fundamental combustion characteristics, the NOx-PM trade-off is not broken and very high levels of NOx are emitted. Due to the relative merits and costs of DPFs and SCRs, engine calibrations will need to be tuned for and compromises made with respect to after treatment devices and not just in-cylinder performance.

As seen in the parameter sweep tests, if traditional HPDI combustion behavior is maintained, the emissions do not deviate from the traditional emission trade-off curves. To improve the emissions, the combustion process must be changed. In the next section, the effect of increasing the amount of natural gas premixing is investigated.

3.3 Partial Premixing of Natural Gas at Two Loads

Particulate matter is formed in fuel rich and high temperature areas of the engine cylinder, which are inherent to the diffusion flames in CI engines. This is in contrast to SI engines where the fuel is premixed with the oxidant before combustion. This greatly reduces the fuel (equivalence ratio) stratification within the cylinder and almost eliminates PM emissions. This section will investigate the effects of fuel premixing on the emissions of HPDI combustion. Natural gas can be allowed to premix before combustion by injection it into the cylinder before the diesel pilot has ignited. The parameter varied in these tests is the pulse separation (PSEP). This is defined as the amount of time from the end of the diesel injection until the start of the gas injection. Typically, this value varies from 0.3-1.0ms depending on operating conditions. For these partially premixed tests, the timing is reduced to negative values. This means that the natural gas is injected during or even before the diesel. As the diesel takes some time to vaporize and ignite, the natural gas is given additional time to entrain air and diffuse before combustion.

In this section, 2 different approaches to premixing will be investigated. First, partially premixed tests are performed at mode B75 with the natural gas injection occurring at approximately the same time as the diesel pilot during the late stages of the compression stroke. The second tests focus on injecting the natural gas during the intake stroke, allowing for the natural gas to almost completely mix with the oxidant. This test was performed at a slower speed at mode A75 with 0% EGR.

3.3.1 Mode B75 Partially Premixed

Initial tests with partially premixed combustion focused on keeping all of the engine operating parameters for mode B75 constant while varying the PSEP.

Figure 35 shows the PM and Gaseous emissions trade-offs for the standard Mode B75 engine calibration along with tests at -0.3ms and -1.0ms PSEP. At this condition, the PPW is ~0.65ms. This means the natural gas injection starts during the diesel injection for the -0.3ms points, and before the diesel for the -1.0ms points.

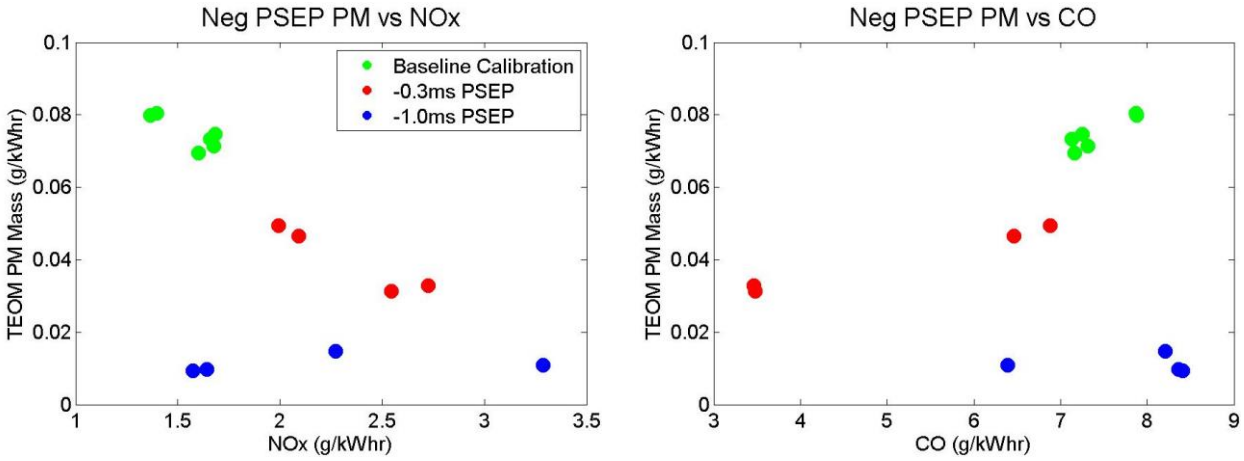

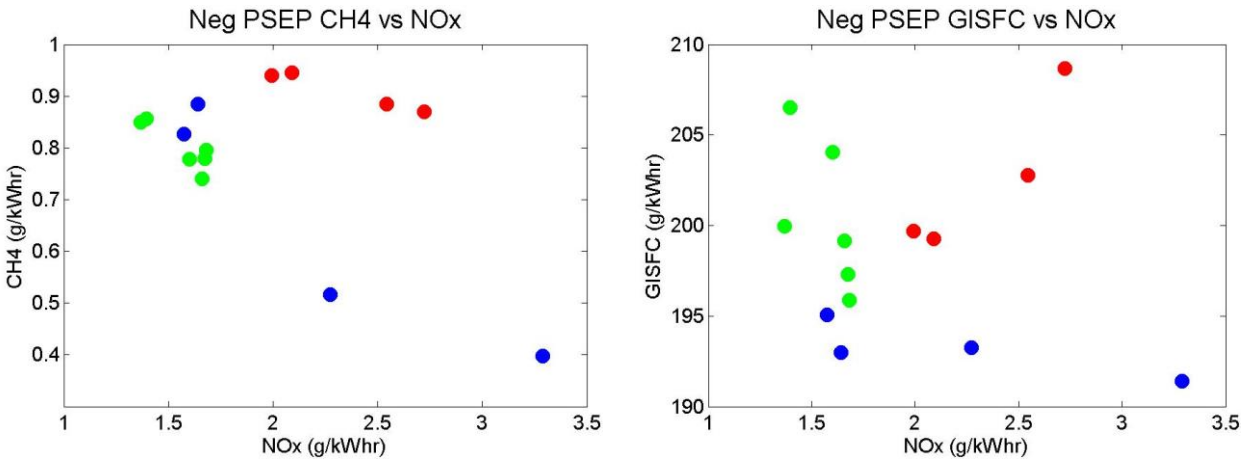

Figure 35 - Mode B75 Partially Premixed Emissions

Decreasing the separation between the natural gas and pilot injections lead to a much more variable combustion event and emission levels. This is seen in the emission variability and will be further investigated with the in-cylinder performance. Even with this increased scatter, trends can be determined from the data.

Introducing premixing breaks the linear relationship between CO and PM emissions. High CO levels remain with the high load conditions; the overall equivalence ratio is held constant, however there are reduced PM emissions. At the lower level of premixing (-0.3ms) the emission level appears to shift along the NOx-PM trade-off curve (Increased NOx emissions accompanying the PM reduction). However, at the higher levels of premixing, there is a downwards shift in this trade-off curve (toward the origin).

An interesting feature of increasing the amount of premixing is the effect on fuel consumption. Decreasing the PSEP initially leads to an increase in fuel consumption, with a peak around -0.5ms. After this point, the fuel consumption decreases. This may be caused by the state of combustion on the diesel pilot when the natural gas reaches it. With standard HPDI combustion, the natural gas jet follows the propagating diesel flame, leading to consistent combustion. As you decrease the separation to the point when both pilot and gas are injected at the same time, the interaction between the two, initially non-reacting, jets decreases the quality of combustion. The natural gas jet may be injected right into the strongest combustion of the igniting diesel pilot causing sharp, inconsistent pressure rises. Further decreasing the 'separation' (injecting the gas before the pilot) lets some more significant premixing occur and the quality of combustion increases.

3.3.2 High EQR/EGR Negative PSEP

As the combustion at these premixed conditions is different than the standard HPDI combustion, it could be expected that the effects of changing the input parameters such as EQR and EGR will have different effects on the emissions.

A parameter search was undertaken to find a combination of engine inputs that would result in improved engine and emissions performance. To reduce the high NOx emissions and the abrupt and

variable pressure rise associated with the negative PSEP points, higher EGR levels were attempted. This lead to high uHC emissions, so the intake charge pressure was reduced, increasing the EQR. These techniques lead to an interesting optimization in emission levels that will be further investigated in this section.

Like the earlier tests, engine speed, load and heat release timing were held constant, but now the EQR was set at 0.7 and the EGR at 25%. For this test, the PSEP was varied from 0.3ms (the baseline calibration) to -0.9ms in 0.2ms increments. Quartz filters for EC/OC analysis and TEM grids for imaging were taken at the most premixed condition.

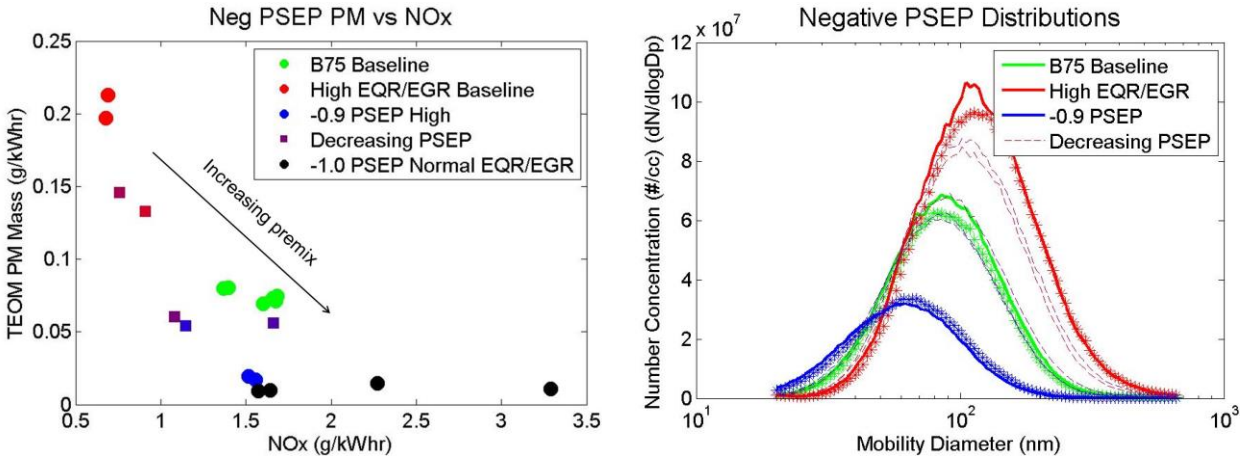

Figure 36 - Negative PSEP PM Emissions and Size Distributions

Figure 36 shows the PM-NOx trade-for this high EQR/EGR PSEP sweep along with the corresponding size distributions. For the PSEP sweep, the color on the plot progressively changes from red to blue with increasing premixing. It can be seen that this optimized set of operating parameters shifts this trade-off curve towards the origin. There is only a minimal increase in the PM emission with the increased EQR and EGR when compared with the baseline calibrations for -1.0ms PSEP. However, both the NOx emissions magnitude and variability are reduced.

The CH_4 emissions follow the same trend as the baseline negative PSEP calibration, increasing initially as the two injection get closer to each other, before decreasing when the NG injection occurs before the pilot. A downside to this combustion strategy is consistently high CO emissions. The concentrations are above than the upper span limit on the CO sensor, leading to uncertain results. While the concentrations are higher than the span limits, the bench is able to extrapolate it's calibration and still report a value. The CO emissions are estimated to get around 12g/kWhr. Fortunately, CO is easily oxidized in the DOC (Johnson, 2008) and should not prove to be a problem in implementation or for regulations.

3.3.2.1 In-Cylinder Pressure Analysis

Figure 37 shows the in-cylinder pressure and heat release rates over the PSEP sweep. With more premixing of the fuel, the heat release becomes much more abrupt. As the 50% IHR timing is held

constant, the abrupt combustion forces the start of combustion to occur later in the cycle. The premixing leads to much higher pressure rise rates, albeit with lower peak pressures as the short combustion duration occurs mostly during the expansion stroke.

This high pressure rise rate comes with increased variability in peak cylinder pressure. Each data collection records 45 cycles and the coefficient of variation in the peak pressure is shown in Table 10. While there is an increase in the peak pressure variation, the variation in the power output remains approximately constant throughout the sweep, suggesting that this increased pressure variation may not be too detrimental to overall engine performance. Figure 38 compares the increase in pressure rise with the reduction in PM. The rate of pressure rise increases with increasing premix up until a PSEP of -0.6ms, after it levels out with peak around 7.5bar/CA degree.

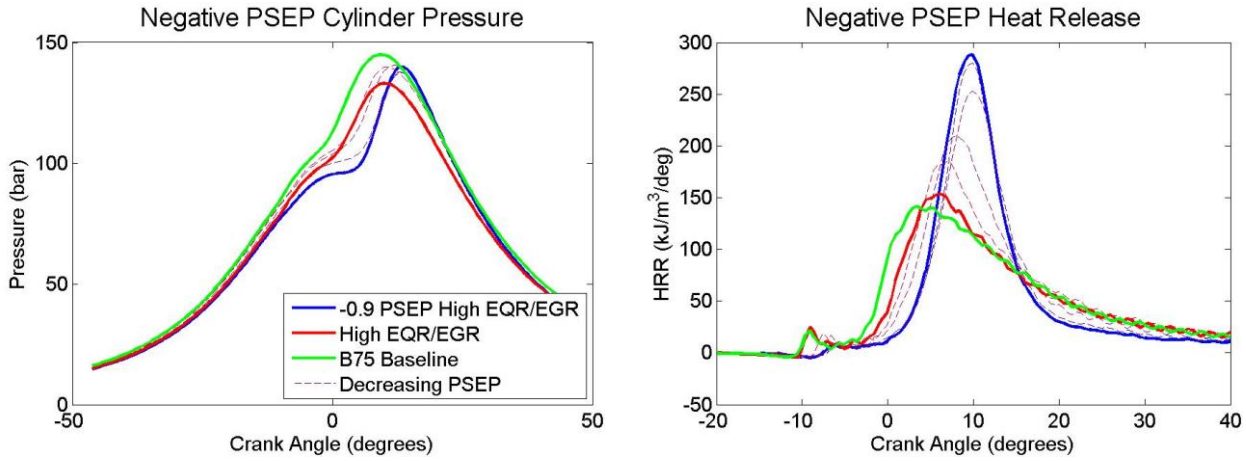

Figure 37 - Negative PSEP Sweep Cylinder Pressure and Heat Release Rate

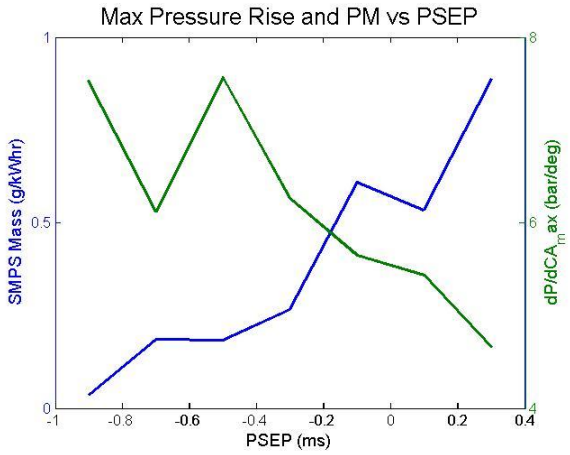

Figure 38 - PM Reduction and Increased Variability of the Neg PSEP Sweep

PSEP (ms)	0.3	0.1	-0.1	-0.3	-0.5	-0.7	-0.9
P_{max} (%)	0.92	1.61	1.26	2.69	3.55	4.40	3.45

Table 10 - Coefficient of Variation of Peak Pressure over the PSEP Sweep

3.3.2.2 Semi-Volatile Fraction

The semi-volatile fraction was measured at the -0.9ms PSEP mode with EC/OC quartz filter analysis and with the TD/SMPS combination. Both methods show an increase in the semi-volatile fraction when compared with the B75 baseline calibration. These results are shown in Table 11. As the input parameters were optimized for the negative PSEP, this larger SVOC fraction could be an effect of the changes in EQR and EGR. However, an increase of this magnitude was not seen in the parameter variation tests (which tested conditions of at least 0.7EQR and 25% EGR). The increased semi-volatile fraction is most likely caused by the increased premixing. (Lev-On et al., 2002) measured the semi-volatile fraction of both diesel fueled and a SI natural gas fueled transit buses over the 'Central Business District' test cycle. The measured semi-volatile fractions were 15% and 90% for the diesel bus and the NG bus respectively. While this test compared different fuels, it demonstrated an increased semi-volatile fraction with the premixed combustion. This change is influenced by the reduced quantities of BC emitted (from the reduced local equivalence ratio with a more constant OC emission rate; altering the EC/OC ratio) it does not fully account for the entire shift.

	Filter Analysis	SMPS Mass	SMPS Mass OC Concentration	SMPS Number
Baseline	37.7%	12.12%	0.032 g/kwhr	10.76%
Negative PSEP	60.5%	22.34%	0.007 g/kwhr	20.66%

Table 11 - Negative PSEP Semi-Volatile Fraction Comparison

3.3.2.3 Morphology

Along with the semi-volatile fraction measurements, TEM grids were taken to examine the particles morphology at this mode. Table 12 shows the measured particle sizes compared to the baseline calibration. There is a reduction in both the mean aggregate sizes as well as the primary particle sizes when compared to the baseline. This is despite the higher EQR and EGR. The effects of the input parameters are changed down to the morphological level. This shows that the fundamental combustion process is quite different compared to the traditional HPDI calibration.

(Barone et al., 2012) analyzed the particle morphology for a direct injected spark ignited (DISI) engine and measured mean particles sizes between 10-15nm. As somewhat expected, the measurements for the negative PSEP mode are between Barone's results and the baseline calibration.

	-1.0ms PSEP High EGR High EQR	B75 Baseline
Primary Particle Size (nm)	23.9	30.5
Geometric Mean Aggregate Size (nm)	61.5	88.7

Table 12 - Negative PSEP Particle Sizes

While the particles are smaller at this operating condition, the general shape of the PM size distribution is similar to the baseline HPDI combustion. It will be seen in the following section that further increasing the percentage of premixed fuel greatly changes size distributions and the morphology of the PM.

3.3.3 A75 Premixed Combustion

The second premixed strategy explored in this study involved injecting natural gas during the intake stroke. This will allow for a more complete mixing of the fuel before injection (as compared to the partially premixed conditions above). The injection process is very similar to a gasoline DISI engine. However, with the base Cummins engine and HPDI injector, this combustion is occurring in a high compression and lean burn condition. Like traditional HPDI, the combustion will be initiated by the ignition of a diesel pilot jet injected late in the compression stroke.

While there are some practical issues (knock) in running a premixed engine at these high compression ratios, this section will investigate the PM emissions from this operating condition.

Three conditions were selected for this experiment. Mode A75 with a standard calibration other than 0% EGR to serve as a baseline, a case with 100% of the natural gas injected during the intake stroke and a case with 80% of the natural gas (by mass) in the intake stroke and 20% after the diesel pilot (similar to standard HDPI). For all cases the 50% IHR was attempted to be help constant at around 10° ATDC (However this was difficult to set exactly with due to the large quantity of premixed gas along with pilot and second injections).

In terms of engine stability, the 80% premixed condition was completely stable over the testing period. However, the 100% premixed point would gradually develop knock after around 10 minutes of run time. This would exceed cylinder pressure limits forcing the shutdown of the engine. The consistent and progressive nature of this knocking suggests that thermal stratification (hot spots) may develop, on the cylinder liner or engine head, causing the premature detonation.

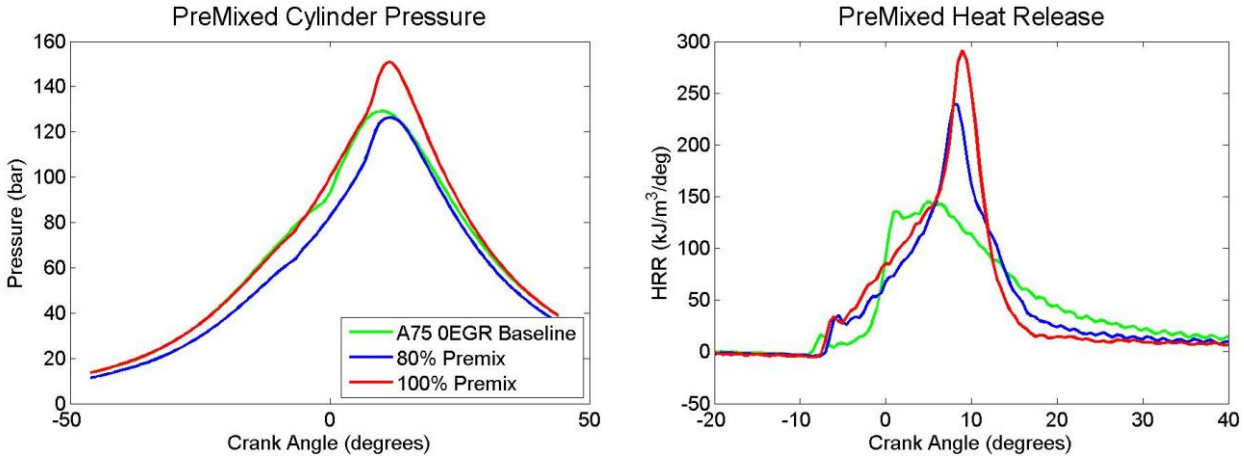

Figure 39 - Premixed In-Cylinder Pressure and Heat Release Rate

Table 13 shows the PM mass and number concentrations for these tests. The PM concentrations for the baseline condition without EGR are already quite low and the SMPS 'mass' is reported here (due to instruments sensitivity at these concentrations), however all 3 PM instruments reported the same trends.

Interestingly, the premixing does not improve the PM emissions. With 80% of the fuel premixed, the PM mass almost doubles, but has number concentrations similar to the baseline. This is most likely due to the second natural gas injection occurring after the premixed combustion has already begun. This reaction results in reduced oxidation for the second jet and poor PM emissions. With the 100% premixed condition, the emissions are slightly reduced yet the number concentration is reduced by an order of magnitude. This suggests that there are significant changes in particle morphology occurring at these conditions. (G. McTaggart-Cowan et al., 2005) found that EGR was required in order to observe reduction in PM with PSEP variations. As the PM emissions are already low at the A75 0% EGR baseline, this may be reduced the effectiveness of this technique.

PM Emissions (SMPS)	Baseline	80 %	100%
g/kW-hr	0.008	0.014	0.007
#/kW-hr	3.26×10^{13}	3.42×10^{13}	3.51×10^{12}

Table 13 - A75 Premixed PM Emissions

3.3.3.1 A75 Premixed Morphology

The premixed combustion modes resulted in changed particle morphology compared to both the standard HPDI and partially premixed modes. Figure 40 shows the 3 size distributions for these tests. As seen above, the 80% premixed mode led to increased mass and number concentrations despite the majority of the fuel being injected during the intake stroke. This may be due to unoptimized heat release and relative timings between the injections. The pressure trace shows a retarded timing and lower peak pressure than the baseline case, this is somewhat unexpected given the abruptness of the premixed combustion.

This is in contrast to the drastically reduced number concentrations when the late second gas injection is removed and all of the natural gas is injected during the intake stroke. Despite similar mass concentrations to the baseline, the particle number emissions are reduced by an order of magnitude.

The mean aggregate diameter increases with the increased levels of premixing. This is in contrast to the partially premixed conditions where the mean particles size progressively decreased as the natural gas injection was advanced. This may be caused by the increased turbulence and jet interactions when both the natural gas and diesel pilots are injected at the same time (for the partially premixed cases).

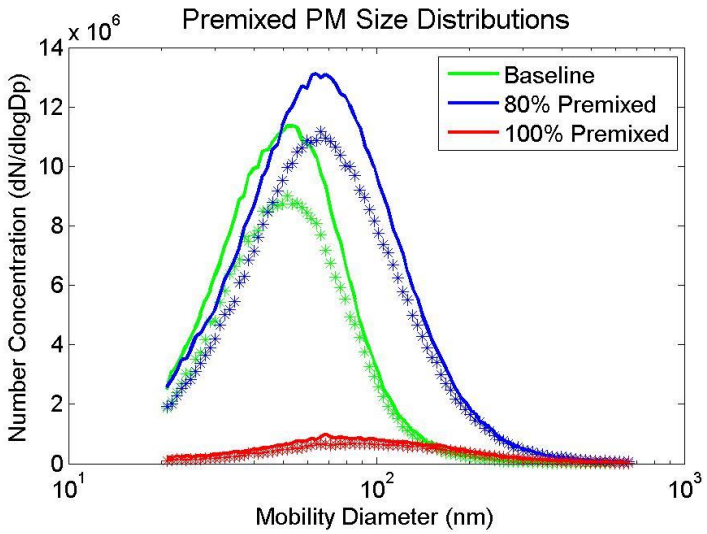

Figure 40 - A75 Premixed PM Size Distributions

The TEM images show some very interesting particles outside the range of the SMPS measurements (14-650nm). The images showed both very large (>1µm) aggregates and very small singular spherical particles (~15nm). Examples of these particles are shown in Figure 41. The prevalence of these particles increased with the amount of premixed natural gas.

Figure 42 shows the TEM size distribution histograms overlaid with the SMPS data. These non-continuous particle distributions could be caused by a combination of cycle-to-cycle to variability along with in-cylinder special variations. The premixing may cause an increased number of stratified combustion 'pockets' (compared to the diffusion flames in diesel and HPDI combustion) that produce either large or small particles.

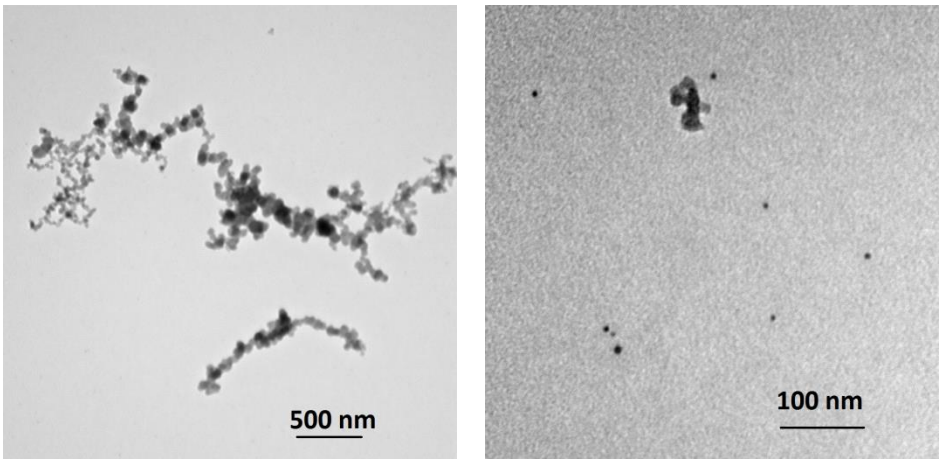

Figure 41 - 100% Premixed Unusual Particle TEM Images

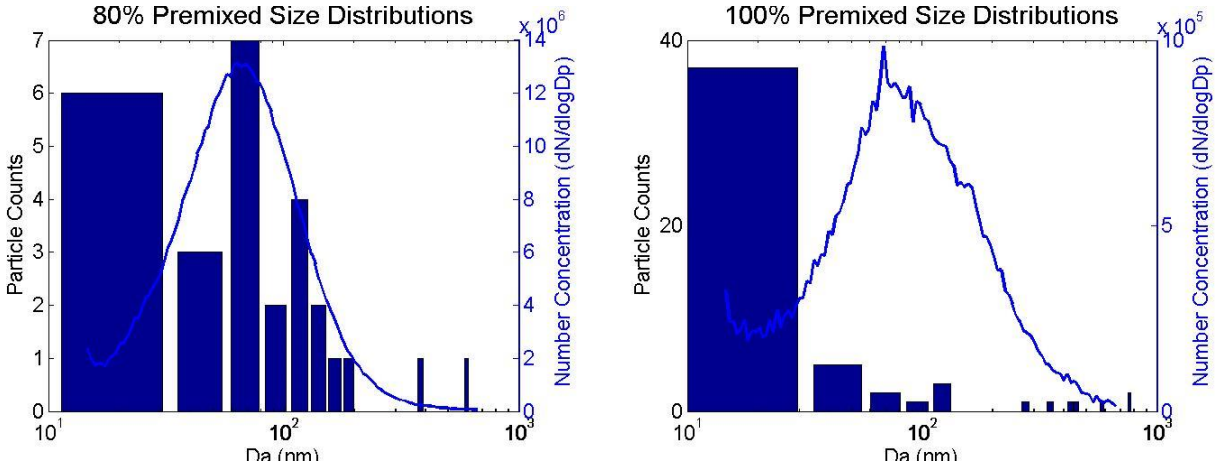

Figure 42 - Premixed SMPS and TEM Size Distribution Comparison

3.3.3.2 A75 Premixed Semi-Volatile Fraction

Like the partially premixed points, the semi-volatile fraction increased with the amount of premixed fuel injected during the intake stroke. These results for the filter analysis and SMPS/TD are shown in Table 14. Again, this is mostly caused by reduced non-volatile emissions from the reduced hot fuel rich cores in the diffusion flames and a more constant amount of burned lube oil and other semi-volatile PM formation pathways.

	Filter Analysis	SMPS Mass	SMPS Number
Premix 80	42.6%	8.9%	14.7%
Premix 100	64.2%	16.7%	23.8%

Table 14 - A75 Premixed Semi-Volatile Fraction

3.4 Variability Estimation

It is more difficult to accurately measure the PM emissions in comparison to the gaseous emissions, from an engine test cell. As such, many of the results show a higher level of variability than desired. This is especially true for day-to-day, month-to-month and year-to-year repeatability.

There are a potentially huge number of sources to this variability, but some of the most important are:

- Engine cycle-to-cycle variability
- Engine set point errors
- Dilution system variations
- Instrument accuracy

The focus of this section is the effect of engine set point errors on the emissions.

Even at steady state and decoupled air handling system on the SCRE, it is not possible to 100% correctly set every parameter on the engine. This is especially true when many of these inputs are coupled such as charge pressure, EGR and EQR on a multi-cylinder production engine with a turbocharger.

As emission levels from engines continue to be reduced, the relative importance of set point errors will grow when trying to differentiate between the emissions of different test modes.

3.4.1 Methods

This section used the previous two data sets to estimate the effect of these input errors on the measured emissions. This will be done with a Monte Carlo simulation of the data. Monte Carlo simulations rely on repeated sampling of random variables to obtain numerical approximations to a problem. For this analysis, the input errors around the set points will serve as the distributions for the sampled random variable and the empirical fits from the RSMs will link these input to predicted emissions. The distribution of the predicted emissions will then be compared to the actual measurement variability to determine the magnitude of the effect of these input errors.

The parameter variation tests serve as a starting point for response surface methods (RSM) to create empirical models linking the inputs to the emissions. Even though the test matrix was not designed specifically for RSM analysis, the wide variations allowed strong correlations to be formed. The Multimode tests show our typical set point errors over a wide range of operating conditions. All of the points in these tests have set engine calibrations for timing, pilot mass, GRP, EQR and EGR. After collecting the data, the magnitude of the deviations from the desired set point can be determined.

As described in Section 3.2.2, first order regressions were formed over the engine inputs along with a second order fit over the engine timing. This was done for the PM emissions as well as the NOx, CH_4 and CO. These empirical fits gave the partial derivatives of the emissions with respect to the input variations.

Equation 18 shows an example of the form of these equations. These will serve as the base functions for the simulation.

$$\mathrm{TEOM}\left(\frac{\mathrm{g}}{\mathrm{kWhr}}\right) = -0.334 + 0.000742 * \mathrm{Diesel} - 0.0053 * \mathrm{GRP} + 0.424 * \mathrm{EQR} + 0.0035 * \mathrm{EGR} + 0.0076 * \mathrm{GIMEP} + 0.0184 * \mathrm{Timing} - 0.000849 * \mathrm{Timing}^2 \quad (18)$$

A major assumption at this stage of the analysis is that the partial derivatives, or the emission response to the input parameters, are constant over the operating range. This was checked by entering some input parameters for modes other than B75 into the empirical functions. The predicted levels were fairly close to the measured values for many of the emissions, even though these fits have no guarantee of giving reasonable results extrapolated so far from their base values.

This gives come confidence that the input parameters have generally the same effects on the emissions, (under standard HPDI operation) over the entire operating cycle. As a note, under some non-conventional injection strategies, these effects can be markedly different.

The random variables for the simulations are determined from the error in the Multimode test points. All of the data was normalized by desired set points to provide percent difference variations. This allows the treatment of all of the data points with the empirical function. This also required the normalization of the base functions by the B75 calibration to allow its use universally.

$$\%_{diff} = 1 + \frac{input - calibration}{calibration} \quad (19)$$

Figure 43 shows some histograms showing the set point errors over the Multimode tests.

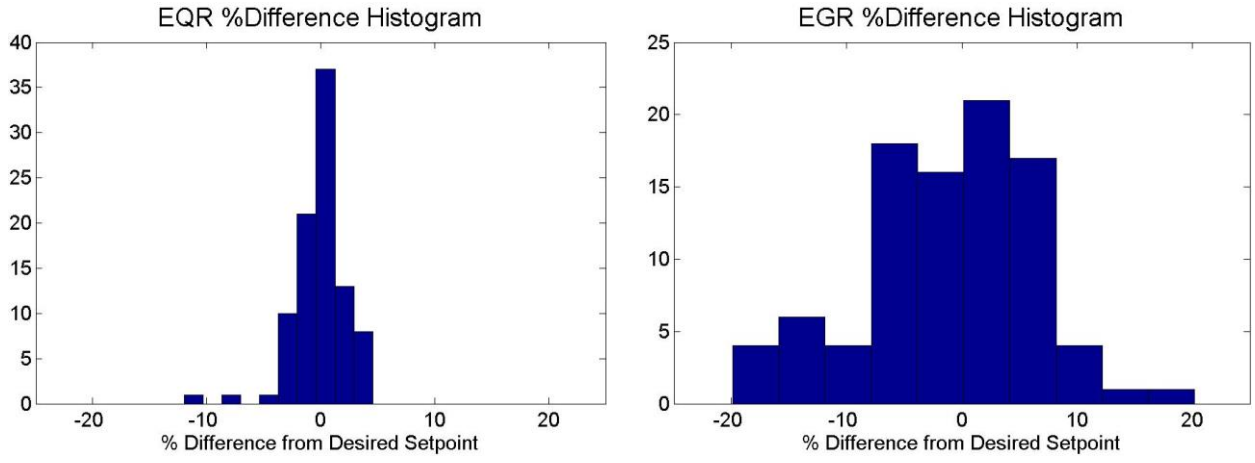

Figure 43 Input Error Histograms

The random variables are formed by calculating the standard deviations from these histograms and assuming the errors are normally distributed. Table 15 shows the coefficient of variations of the set point errors.

	Diesel	GRP	EQR	EGR	Power	Timing
Coefficient of Variation	30.6%	4.5%	2.3%	7.6%	2.3%	6.1%

Table 15 COVs for the Monte Carlo Random Variables

For each computation of the emission levels, a random variable is sampled from each input parameter distribution. Then a predicted emission value is calculated with the empirical correlation equations. This procedure is repeated 1000 times and the aggregated results give a prediction of the variability caused by the input errors.

3.4.2 Results

Figure 44 shows the predicted TEOM and NOx emission variations based on the input error variations from the multimode tests. These are then compared with the actual variations around the mean emission values at each mode in Figure 45 and Table 16. The measured emission mean values were calculated and normalized to a percent different at each of the 9 modes and then combined into a single normalized distribution.

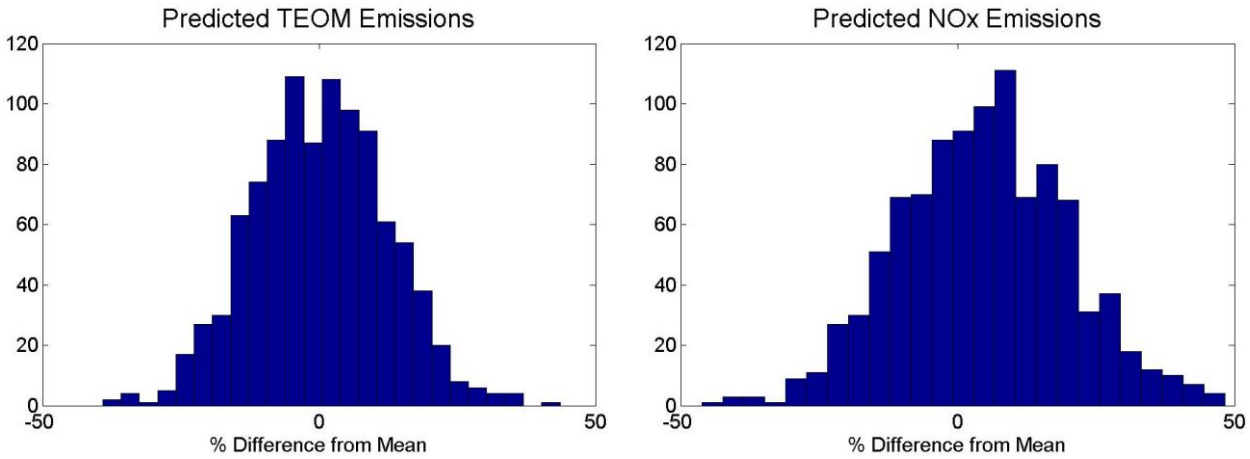

Figure 44- Predicted Emission Variability from Input Errors

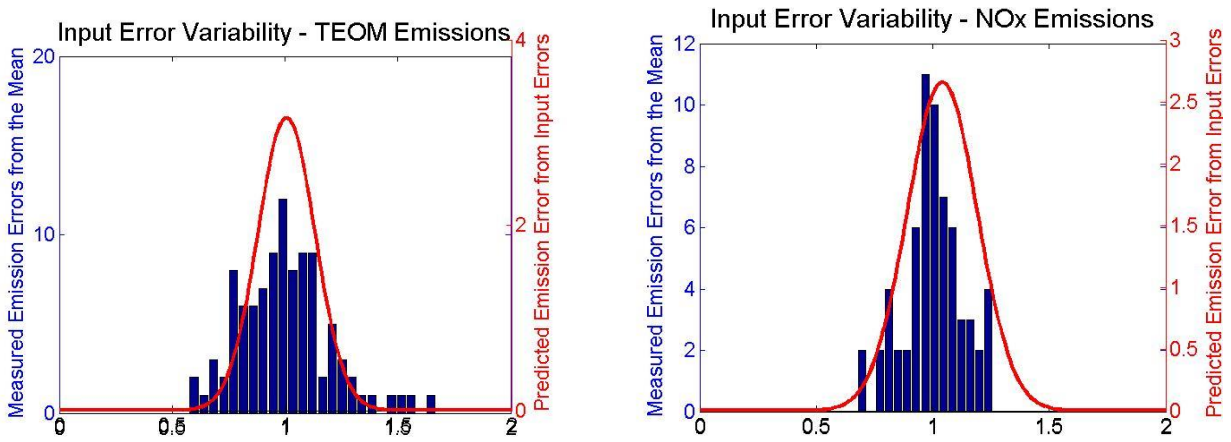

Figure 45 - Actual Emission Variations compared with Predicted Input Error Variations

RSTDs	DRX	TEOM	NOx	CO	CH4
Simulation	15.18%	12.24%	15.01%	11.03%	5.45%
Measured	35.98%	20.18%	15.92%	26.05%	13.00%

Table 16 - Simulated and Measured Variations in Emissions

3.4.3 Discussion

Differences between actual and desired engine set point have a significant effect on the engine emissions. Approximately 60% of the PM variations can be attributed to these input errors when setting the engine operating points. The relative magnitude of these variations is also similar for both the CO and CH4. According to this simulation, almost all of the variations seen in the NOx emissions can be attributed to the set point errors. This suggests that cycle-to-cycle variability and measurement uncertainties are less important for the NOx measurements.

As emissions regulations are constantly tightened, it will become more and more important to be able to resolve differences in increasingly small emission concentrations. The large magnitude of the variations caused by set point errors highlight the need for a more sophisticated testing method, as well as difficulties with transient emission control.

Fortunately, set point errors can be dealt with in post-processing. The same partial differential methods can be used to correct for any, small, set point errors from a desired point. The report in 0 applied these methods to a test evaluating the effects of a synthetic diesel pilot fuel on the PM emissions from this engine. On average, the uncertainty on the emissions measurements was reduced by 13% for traditional HPDI points. The correction was attempted on a partially premixed point but the experimental uncertainty was increased by 17%. This is because the relative effects of the input parameters on the emissions are different for the partially premixed points. Different correction derivatives would be needed to correct for these points. However the coefficients derived from this study are likely applicable for most standard conditions.

4 Conclusions

This study measured the physical and chemical characteristics of PM emissions from a heavy-duty HPDI engine over a wide range of operating conditions. Specific conditions that were explored in this study are:

4.1 Speed and Load combinations at standard engine calibrations over the majority of the engine operating range.
4.2 The Effects of EQR, EGR, GRP, Pilot quantity and Injection timing at a single speed and load combination
4.3 Gas and Diesel interactions allowing some of the fuel to premix before ignition
4.4 Statistical treatment of the engine variability with Monte Carlo simulations

The key results are summarized in Table 17. The table has grouped different operating conditions that have similar emission characteristics. The two footnote tables summarize the B75 parameter sweep and premixed combustion tests. After the table, more discussion is offered in the following sections.

		Load		
		25% Load (~5 bar GIMEP)	50% Load (~10 bar GIMEP)	75% Load (~15 bar GIMEP)
Speed	1200RPM	**Mass:** Average of **0.011g/kW-hr** Premixed A75 Table **Number: 0.88 - 1.92 - 5.13 x10^13 particles/kW-hr** over the 3 loads **Size:** Near constant particle size across the 3 loads **56.4±5.9nm** **Volatility:** The semi-volatile fraction is still mostly dominated by the engine load, with the exception of mode A75, which is similar to the 50% loads. SVOC fraction is **87%-70%-64%** across the loads **Morphology:** There is a slight negative correlation between engine speed and primary particle size. Low speed modes average **dp = 25.8nm**		
	1500RPM	**Mass: 0.009 - 0.016g/kW-hr** **Number:** Average of **1.45 x10^13** non-volatile particles/kW-hr --> up to an order of magnitude increase with externally mixed semi-volatile particles **1.13 x10^14** **Size:** Mean da: **42.7 - 45.6** nm **73-89% SVOC**	**Mass: 0.018-0.027 g/kW-hr** **Number: 8.9 - 9.23x10^13 particles/kW-hr** **Size:** Mean da: **53.3 - 59.2 nm** **50-70% SVOC**	**Mass: 0.067-0.072g/kW-hr** B75 Parameter Sweep and Neg PSEP Tables **Number: 1.70 - 1.71x10^14 particles/kW-hr** **Size:** Mean da: **81.2 - 88.7 nm** **37-39% SVOC**
	1750RPM	**Morphology:** There are large (~500nm) semi-volatile spherical splotches observed on the TEM grids at these loads.Dp = **29.7** and **25.4** for 1500 and 1750 RPM	**Morphology:** Primary particle size increases with load and decreases with speed --> dp = **23.4nm** and **21.7nm** for 1500 and 1750 RPM at 50% Load	**Morphology:** dp = **28.9nm** and **25.4nm** for 1500 and 1750 RPM at 75% Load

Mode B75 Parameter Variations

Changed the EQR, EGR, diesel pilot quantity, GRP and engine timing to the maximum levels permitted by SCRE hardware while maintaining the engine speed and load

Mass concentrations: Ranged from **0.016 g/kW-hr** at 0% EGR and early timing to **0.171 g/kW-hr** with high EQR

Number Concentrations: 0.5 - 2.5x10^14 particles/kW-hr

Size: Mean particles sizes ranged from **65-120nm**
Increasing the EQR and EGR led to larger and more numerous particles. The pilot quantity and GRP had less significant effects but also increased and decreased the mean particle size respectively

Partially Premixed Modes	
B75 Negative PSEP	A75 "fully" premixed
Mass: 0.011 g/kW-hr	**Mass:** The PM mass emissions were: Baseline **0.008 g/kW-hr** | 80% **0.014 g/kW-hr** | 100% **0.007 g/kW-hr** (SMPS masses)
Number: 3.87 x10^13 particles/kW-hr compared with 1.71 x10^14	**Number:** Baseline **3.26 x10^13** | 80% **3.42 x10^13** | 100% **3.51 x10^12** #/kW-hr
Size: Mean particle size average of **54.7nm**	**Size:** Baseline **48.2** nm | 80% **58.6** nm | 100% **81.0** nm
Volatility: Semi-volatile fraction average of **61%**	**Volatility:** Semi-volatile fraction for the premixed points 80% **42%** | 100% **64%**
Morphology: Primary particle size **23.9 nm** compared with 30.5 nm	**Morphology:** Very different PM morphology compared to other modes. Very small (~10nm) singular spherical particles along with very large (>2μm) aggregates. Increasing the amount of premixed fuel increases the number of these unusual particles. Average Dp = **23.5** and **28.1** for 80% and 100% premixed

Table 17 -Test Summary Tables

4.1 MultiMode Testing

The engine-out PM emission characteristics, from this HPDI engine, are similar to the emission trends from modern heavy duty CI diesel engines. The PM mass emissions follow NOx-PM trade-off curve, which is similar to a diesel fueled engine. On a power-specific basis, the low-load points produce higher NOx emissions while the higher load points produce higher PM concentrations.

The majority of the measured PM characteristics (mass, number, morphology and semi-volatile fraction) are generally more influenced by the engine load rather than engine speed.

The exception to this is the lowest speed points (1200 RPM), where lower mass concentrations (compared to higher speed modes at the same load) are observed. This could possibly be attributed the longer residence times leading to increased oxidation of the soot particles. Additionally, the mean particle diameters are nearly constant across loads for these low speed points (~55nm). For higher speeds, the mean particle size increases linearly with increasing load (from 40-90nm).

Other conclusions from this study are:

Number Concentrations/Size Distributions

Small <15nm nucleation mode particles are not present in the PM emissions. This may be explained by a lack of sulfur or other impurities in the fuel. Larger externally mixed, semi-volatile particles, which have grown to the same size as the non-volatile particles are present. These large SVOC particles could be

explained by lower inception rates allowing for additional particle growth when there is an approximately constant semi-volatile lube oil source across engines.

Semi-Volatile Content

The semi-volatile fraction is correlated with engine load (with the exception of mode A75) At the 3 load levels, the average semi-volatile fraction is 86%, 47% and 33% for the low, mid and high load modes respectively.

While all of the techniques used to measure the semi-volatile fraction are consistent in capturing the general trends, the absolute values of the online results disagree. This may be caused by changes in the coated particles morphology along with the spherical particle mobility assumptions causing an underestimation in the SMPS/TD measurements.

Morphology

The SMPS and TEM sample size distributions both capture a lognormal distribution for the PM aggregate sizes. The TEM images over predict the median projected aggregate diameter by 29 nm for the mid and high load modes and by 64.2 nm for the low load modes when compared to the SMPS, even though the shapes of the distributions are consistent. This could be caused by excess impaction in the TPS and a selection bias by the human operator finding larger particles.

The primary particle size varies from 22-33nm over the operating range. The primary particle size is weakly correlated with engine speed; however the other operating parameters seem to have negligible effects on the primary particle size.

The primary particle and aggregate sizes are correlated. Larger aggregates have larger primary particles. This could be caused by in-cylinder spatial variation affecting the formation, oxidation and coagulation rates for the individual particles. Normally the primary particle size is assumed to be constant for all aggregates. This could affect mass-mobility calculations for the SMPS.

4.2 Mode B75 Parameter Sweeps

Over a wide range of parameter variations, the PM mass concentrations changed monotonically and almost linearly with the input parameter changes. There were no PM valleys or non-linearities at this tested mode. This highlights the difficulty in the calibration of an engine for PM reductions; these parameter sweeps did not shift the NOx-PM trade-off curve towards the origin. Setting the parameters for minimum PM emissions (High GRP, Low EQR and 0% EGR) have large (and possibly negative) effects on the gaseous emissions and engine performance.

The effects of the input parameters were analyzed with a response surface methods sensitivity analysis. The EQR and GRP have the greatest effect on PM mass emissions with a 1% change in these inputs leading to a 3.0 and 1.4% change in PM mass respectively. Despite not being a swept parameter, the

engine power had a large influence on the PM emissions (1% change in power leading to a 2.8% change in PM mass), supporting the results from the multimode tests.

It was also found that the PM emissions are more sensitive to changes in operating conditions than gaseous emissions.

Looking at the specific effects of the parameter sweeps on the morphology of the PM; increases in the EGR and EQR lead to increases in both the number and size of the emitted particles. Changes in the pilot quantity and GRP do not show such distinct trends.

Other conclusions from this study are:

Number Concentrations / Size Distributions

Over these parameter sweeps the PM number concentrations varied from 1-5x10^7/cc and the mean particle size varied from 65-120nm.

The size distributions are qualitatively similar throughout the parameter sweeps. There are shifts in mean size and concentrations, but the distributions have similar geometric standard deviations throughout.

Semi-Volatile Content

The semi-volatile fraction was approximately constant at 25%, as measured by the DRX and TD, throughout the parameter sweeps. As seen in the Multimode tests, the semi-volatile content is dependent on load and this was held constant for this test.

Quartz filters for EC/OC analysis where taken at the 0% EGR condition. Unlike the DRX/TD measurements, these showed a 41% relative increase in semi-volatile fraction when compared to the baseline case. This mirrors diesel literature and could be somewhate attributed to the large decrease (71%) in total PM mass associated with running without EGR (greater than the other parameter sweeps). Most of this decease could be EC (with the OC emission rates from burnt lube oil remaining more constant), which would alter the semi-volatile fraction.

4.3 Partially Premixed Combustion

Two different methods of premixing the natural gas before ignition were attempted. For the partially premixed (Negative PSEP) conditions, increasing the amount of premixed fuel with high EGR and EQR lowers the PM mass concentrations by up to 85% at the expense of increased pressure rise rates, variability and CO emissions.

These large PM reductions with high levels of EGR and EQR show that the combustion behavior for the negative PSEP modes is different from traditional PSEP levels. The partial derivatives from the B75 sensitivity analysis no longer apply. This gives to opportunity to shift the NOx-PM trade-off curve downwards.

The primary particle size is reduced by 22% for the negative PSEP modes when compared to the baseline. This comes along with a 31% reduction in mean aggregate size. The shorter time of combustion at these modes along with the decreased local equivalences ratios at ignition, may cause the reductions in both metrics.

The fully premixed points did not show PM reductions despite lower local natural gas equivalence ratios at ignition. The 80% premixed points doubled the PM compared to the baseline, as the second natural gas pulse is being injected into a burnt/burning mixture which is unable to properly oxidize the fuel.

While the PM characteristics for the partially premixed points are similar to the baseline HPDI calibrations, the fully premixed modes show vastly different characteristics. The PM contains both very large aggregates (>2µm) and very small (~15nm) individual spherical particles. There are large amount of these particles at the 100% premixed mode and slightly less at the 80% premixed condition. These particles may be caused by in-cylinder spatial variations and a less robust initiation to combustion (diffusion flame ignited lean-burn premixed NG) when compared to other modes.

Other conclusions from this study are:

Mass Concentrations

Due to the different relationships between input parameters and emissions, an optimized operating condition with high EQR and EGR was developed. This mode produced acceptable NOx emissions (2.4g/kW-hr) and reduced peak pressures, increasing its viability for production engine calibrations.

Injecting natural gas during the intake stroke, thereby ensuring almost complete premixing of the fuel, did not lead to significant PM mass concentration reductions. However, this may be caused by an unoptimized engine timing calibration.

Number Concentrations/Size Distributions

The overall shape of the PM size distribution is not drastically change when the PSEP is reduced from 0.3 to -1.0ms. The mean particle size is reduced by 27nm leading to potentially more harmful particles along with a smaller reduction in number concentration relative to the mass concentration reduction.

The fully premixed modes have a broader distribution compared to the baseline HPDI case incorporating more large and small particles. The existence of these large particles mean that despite a minimal reduction in overall PM mass, there is a significant reduction in particle number (up to an order of magnitude).

Semi-Volatile Content

The negative PSEP modes had a greater semi-volatile fraction (51% relative increase) than the B75 baseline condition. Even though this mode had increased EQR and EGR when compared to the baseline, the increase in volatility can be attributed to the premixing (and decrease in the total (mostly EC) mass).

The fully premixed points showed a decrease in volatility when compared to the baseline. This is seen in both the SMPS/TD and Quartz filter measurements. This difference may be attributed to these points being run without EGR.

4.4 Variability Estimation

The sources of the measured emissions variability was analyzed using Monte Carlo simulations. These investigated the effects of set point errors on the emissions using the response surfaces developed from the input parameter sweep tests and data from the multimode tests. From this analysis, it was determined that up to 60% of the measured variability in the PM emissions can be attributed to these input errors when setting the engine operating points.

This shows the need to take care when setting engine operating modes as small differences in set point can have significant differences in emissions. This also highlights the difficulty in transient emissions testing as small set point variations (when moving between modes, variations in turbo behavior will affect to operating condition) can have large effects on the emission levels.

The empirical fits can also be used to help correct these set point errors. For the GTL test highlighted in appendix A, the variability in the measurements was reduced on average by 13% by applying the correction

5 Recommendations

5.1 PM Reductions

The data from this study suggests directions for PM reductions. With standard PSEP values and current engine hardware, input parameters will not shift the NOx-PM trade-off towards the origin. The emissions will only shift along this curve. This suggests that alternative combustion strategies such as negative PSEP, multiple injections or late-post-injection will need to be explored. A further, formalized study into input parameter variations along with PSEP could determine the change in the sensitivity of the emissions to the input parameters.

Based on the results from this single-cylinder research engine, it appears that aftertreatemt will be required to meet particle number regulations. Reductions in PM need to be framed in this context and engine calibrations need to be optimized to take advantage of the aftertreatment. This may mean increasing the NOx or PM emissions to increase engine efficiency if the aftertreatment can the handle the additional load, or calibrating the engine for different particle morphology if it aids the DPF. There needs to be a holistic approach to engine and aftertreatment tuning.

5.2 PM Measurement

No single PM measurement method will give all of the necessary information.

5.2.1 TEOM

Gravimetric filters are still the 'gold' standard for mass measurement. Luckily, the TEOM correlates will with the filters over a wide range of concentrations. The instrument is directly sensitive to particle mass, so it is mostly insensitive to PM characteristic changes. Above 0.01-0.02 g/kW-hr (~0.3µg/L), the TEOM is the most reliable instrument.

Unfortunately, the instrument is insensitive to loading conditions below this level. Given that PM emission levels at most modes are at this level, this is a serious limitation. This can be somewhat helped with longer sampling times, but at some at some point the sampling time will approach the time required for gravimetric filters.

5.2.2 DustTrak

The DustTrakDRX is sensitive and repeatable down to ambient PM concentrations and is very fast. However, it is greatly affected by particle morphology and composition. The reported mass concentrations will be greatly overestimated for modes with a large (>~70%) semi-volatile fraction. This highlights the need to use a thermodenuder upstream of the instrument. Figure 23 shows that the DustTrak has a linear correlation with gravimetric filters if the semi-volatile content is removed before

measurement. On average the instrument has a 35% underestimation compared to the filters, but the linear response means this can be corrected with the instrument's internal user calibration or with post processing if desired.

Care must be taken when comparing measurements from the DustTrak taken at different months or years. The instrument does drift and up to this point, no calibration procedure has been put in place. A monthly calibration with a reference aerosol may improve long term confidence.

5.2.3 SMPS

The SMPS provides repeatable size distributions over a wide range of concentrations. The instrument's biggest weakness is in the mass-mobility inversions required to give a final mass concentration.

The SMPS assumes that all particles are spheres. PM particles are fractal aggregates. There has been a significant amount of work relating the mass and mobility of these particles. The SMPS even has its own correction algorithm based on primary particle size. However this "black box" algorithm cuts out any particles smaller than the primary particle size. As such, the correction was not used for this study. If better accuracy is required in the absolute value of the SMPS mass measurement, a custom algorithm should be developed. This could take into account some of the morphology information from this study, and could as use additional knowledge about the semi-volatile fraction to provide a better mass estimate.

Some problems have been seen with the custom DMA and unrealistic numbers of large particles appearing at the end of scans. This is most likely due to a grounding problem on either the electrode or DMA body causing the power supply to not reach the highest voltages. If these 'particles' appear at the end of scans, the operator should ensure everything is properly grounded and watch the voltage readout over the scan.

Bibliography

Abdul-Khalek, I., & Kittelson, D. (1998). Diesel exhaust particle size: measurement issues and trends. *SAE Technical Paper*, (980525). Retrieved from http://papers.sae.org/980525

Alander, T. J. a, Leskinen, A. P., Raunemaa, T. M., & Rantanen, L. (2004). Characterization of diesel particles: effects of fuel reformulation, exhaust aftertreatment, and engine operation on particle carbon composition and volatility. *Environmental science & technology*, *38*(9), 2707–14. Retrieved from http://www.ncbi.nlm.nih.gov/pubmed/15180069

Armas, O., Ballesteros, R., & Gómez, A. (2008). The effect of diesel engine operating conditions on exhaust particle size distributions. *Proceedings of the Institution of Mechanical Engineers, Part D: Journal of Automobile Engineering*, *222*(8), 1513–1525. doi:10.1243/09544070JAUTO747

Ayres, J. G., Borm, P., Cassee, F. R., Castranova, V., Donaldson, K., Ghio, A., Harrison, R. M., et al. (2008). Evaluating the toxicity of airborne particulate matter and nanoparticles by measuring oxidative stress potential--a workshop report and consensus statement. *Inhalation toxicology*, *20*(1), 75–99. doi:10.1080/08958370701665517

Barone, T. L., Storey, J. M. E., Youngquist, A. D., & Szybist, J. P. (2012). An analysis of direct-injection spark-ignition (DISI) soot morphology. *Atmospheric Environment*, *49*, 268–274. doi:10.1016/j.atmosenv.2011.11.047

Bell, L. (2012). Tough Trucking For Natural Gas Vehicles: Can They Make It In The Long Haul? *Forbes*. Retrieved February 11, 2013, from http://www.forbes.com/sites/larrybell/2012/11/27/tough-trucking-for-natural-gas-vehicles-can-they-make-it-in-the-long-haul/

Brown, S. (2008). *High-Pressure Direct-Injection of Natural Gas with Entrained Diesel into a Compression-Ignition Engine*. *Test*. University of British Comubia.

Burnham, A., Han, J., & Clark, C. (2011). Life-cycle greenhouse gas emissions of shale gas, natural gas, coal, and petroleum. *Environmental science & technology*, *46*, 619–627. Retrieved from http://pubs.acs.org/doi/abs/10.1021/es201942m

Burtscher, H. (2005). Physical characterization of particulate emissions from diesel engines: a review. *Journal of Aerosol Science*, *36*(7), 896–932. doi:10.1016/j.jaerosci.2004.12.001

Burtscher, H., Baltensperger, U., & Bukowiecki, N. (2001). Separation of volatile and non-volatile aerosol fractions by thermodesorption: instrumental development and applications. *Journal of Aerosol*, *32*, 427–442. Retrieved from http://www.sciencedirect.com/science/article/pii/S0021850200000896

CARB. (2013). Toxic Air Contaminants Monitoring. *California Environmental Protection Agency*. Retrieved February 9, 2013, from http://www.arb.ca.gov/aaqm/toxics.htm

Desantes, J. M., Bermúdez, V., García, J. M., & Fuentes, E. (2005). Effects of current engine strategies on the exhaust aerosol particle size distribution from a Heavy-Duty Diesel Engine. *Journal of Aerosol Science*, *36*(10), 1251–1276. doi:10.1016/j.jaerosci.2005.01.002

Environmental Protection Agency. (2012). Emission Standards Reference Guide. Retrieved February 9, 2013, from http://www.epa.gov/oms/standards/heavy-duty/hdci-exhaust.htm

European Commision. (2012). Transport & Environment. Retrieved February 9, 2013, from http://ec.europa.eu/environment/air/transport/road.htm

Fino, D., & Russo, N. (2011). Characterization of Particulate Matter Emissions from a Common-Rail Diesel Engine. *Industrial & Engineering Chemistry Research*, 3004–3010. Retrieved from http://pubs.acs.org/doi/abs/10.1021/ie102094x

Flagan, R. C. (2008). Differential Mobility Analysis of Aerosols : A Tutorial. *KONA Powder and Particle*, *26*(26), 254–268.

Giechaskiel, B., Dilara, P., & Andersson, J. (2008). Particle Measurement Programme (PMP) Light-Duty Inter-Laboratory Exercise: Repeatability and Reproducibility of the Particle Number Method. *Aerosol Science and Technology*, *42*(7), 528–543. doi:10.1080/02786820802220241

Gormley, P., & Kennedy, M. (1948). Diffusion from a stream flowing through a cylindrical tube. *Proceedings of the Royal Irish Academy.*, *52*, 163–169. Retrieved from http://www.jstor.org/stable/10.2307/20488498

Hansen, A. (2005). *The Aethalometer*. Berkeley, California: Magee Scientific Company.

Harris, S. J., & Maricq, M. M. (2001). Signature size distributions for diesel and gasoline engine exhaust particulate matter. *Journal of Aerosol Science*, *32*(6), 749–764. doi:10.1016/S0021-8502(00)00111-7

Hesterberg, T. W., Long, C. M., Lapin, C. a, Hamade, A. K., & Valberg, P. a. (2010). Diesel exhaust particulate (DEP) and nanoparticle exposures: what do DEP human clinical studies tell us about potential human health hazards of nanoparticles? *Inhalation toxicology*, *22*(8), 679–94. doi:10.3109/08958371003758823

Hesterberg, T. W., Long, C. M., Sax, S. N., Lapin, C. a., McClellan, R. O., Bunn, W. B., & Valberg, P. a. (2011). Particulate Matter in New Technology Diesel Exhaust (NTDE) is Quantitatively and Qualitatively Very Different from that Found in Traditional Diesel Exhaust (TDE). *Journal of the Air & Waste Management Association*, *61*(9), 894–913. doi:10.1080/10473289.2011.599277

Heywood, J. (1988). *Internal Combustion Engine Fundamentals*. McGraw-Hill.

Johnson, T. (2008). Diesel Emission Control in Review. *SAE Technical Paper*, (2008010069), 776–790. Retrieved from http://www.new.corning.com/assets/0/507/517/589/78067417-3F69-461E-A617-473C2BB41581.pdf

Jones, H. (2004). *Source and Characterization of Particulate Matter from a Pilot-Ignited Natural Gas Fuelled Engine*. *Source*. University of British Columbia. Retrieved from https://circle-prod.library.ubc.ca/handle/2429/15549

Just, B. G. (2012). *Characterization of Ultrafine Particulate Matter from Traditional and Improved Biomass Cookstoves*. University of British Columbia.

Kelly, N., & Morgan, C. (2002). An evaluation of the tapered element oscillating microbalance method for measuring diesel particulate emissions. *Journal of the Air & Waste Management Association*, *52*(12), 1362–1377. Retrieved from http://www.tandfonline.com/doi/abs/10.1080/10473289.2002.10470875

Khalek, I. a., Bougher, T. L., Merritt, P. M., & Zielinska, B. (2011). Regulated and Unregulated Emissions from Highway Heavy-Duty Diesel Engines Complying with U.S. Environmental Protection Agency 2007 Emissions Standards. *Journal of the Air & Waste Management Association*, *61*(4), 427–442. doi:10.3155/1047-3289.61.4.427

Kittelson, D., McMurry, P., & Park, K. (2004). Structural Properties of Diesel Exhaust Particles Measured by Transmission Electron Microscopy (TEM): Relationships to Particle Mass and Mobility. *Aerosol Science & Technology*, *38*(9), 881–889. doi:10.1080/027868290505189

Kryiakis, N., Vouitsis, I., & Samaras, Z. (2002). *Study on Emission Control Technology for Heavy-Duty Vehicles* (Vol. 2002). Thessaloniki, Greece.

Kubesh, J., King, S., & Liss, W. (1992). Effect of gas composition on octane number of natural gas fuels. *SAE Technical Paper*, (922359). Retrieved from http://papers.sae.org/922359

Lähde, T., Rönkkö, T., Happonen, M., Söderström, C., Virtanen, A., Solla, A., Kytö, M., et al. (2011). Effect of fuel injection pressure on a heavy-duty diesel engine nonvolatile particle emission. *Environmental Science & Technology*, *45*(6), 2504–9. doi:10.1021/es103431p

Lapuerta, M., Martos, F. J., & Herreros, J. M. (2007). Effect of engine operating conditions on the size of primary particles composing diesel soot agglomerates. *Journal of Aerosol Science*, *38*(4), 455–466. doi:10.1016/j.jaerosci.2007.02.001

Lapuerta, M., Oliva, F., Agudelo, J. R., & Boehman, A. L. (2012). Effect of fuel on the soot nanostructure and consequences on loading and regeneration of diesel particulate filters. *Combustion and Flame*, *159*(2), 844–853. doi:10.1016/j.combustflame.2011.09.003

Leidenberger, U., Mühlbauer, W., Lorenz, S., Lehmann, S., & Brüggemann, D. (2012). Experimental Studies on the Influence of Diesel Engine Operating Parameters on Properties of Emitted Soot Particles. *Combustion Science and Technology*, *184*(1), 1–15. doi:10.1080/00102202.2011.611551

Lev-On, M., LeTavec, C., Uihlein, J., Alleman, T. L., Lawson, D. R., Vertin, K., Thompson, G. J., et al. (2002). Chemical Speciation of Exhaust Emissions from Trucks and Buses Fueled on Ultra-Low Sulfur Diesel and CNG. *SAE Technical Paper*, (724), 01–0432. Retrieved from http://subscriptions.sae.org/content/2002-01-0432/

Lu, T., Cheung, C. S., & Huang, Z. (2012). Effects of engine operating conditions on the size and nanostructure of diesel particles. *Journal of Aerosol Science*, *47*, 27–38. doi:10.1016/j.jaerosci.2011.12.004

Majewski, W. (2012). DieselNet Technology Guide. *DieselNet.com*. Retrieved February 9, 2013, from http://www.dieselnet.com/tg.php

Maricq, M. M. (2013). Monitoring Motor Vehicle PM Emissions: An Evaluation of Three Portable Low-Cost Aerosol Instruments. *Aerosol Science and Technology*, (February), 130206084502004. doi:10.1080/02786826.2013.773394

Maricq, M. M., & Xu, N. (2004). The effective density and fractal dimension of soot particles from premixed flames and motor vehicle exhaust. *Journal of Aerosol Science*, *35*(10), 1251–1274. doi:10.1016/j.jaerosci.2004.05.002

Mathis, U., Kaegi, R., Mohr, M., & Zenobi, R. (2004). TEM analysis of volatile nanoparticles from particle trap equipped diesel and direct-injection spark-ignition vehicles. *Atmospheric Environment*, *38*(26), 4347–4355. doi:10.1016/j.atmosenv.2004.04.016

McDow, S., & Huntzicker, J. (1990). Vapor adsorption artifact in the sampling of organic aerosol: Face velocity effects. *Atmospheric Environment*, *24*(10), 2563–2571.

McTaggart-Cowan, G., Bushe, W., & Rogak, S. (2005). PM and NOx reduction by injection parameter alterations in a direct injected, pilot ignited, heavy duty natural gas engine with EGR at various operating conditions. *SAE transactions*, (724). Retrieved from http://cat.inist.fr/?aModele=afficheN&cpsidt=17553822

McTaggart-Cowan, G. P. (2006). *Pollutant Formation in a Gaseous-Fuelled, Direct Injection Engine*. *Direct*. University of British Columbia. Retrieved from http://scholar.google.com/scholar?hl=en&btnG=Search&q=intitle:P+O+L+L+U+T+A+N+T+FORMATION+IN+A+GASEOUS-FUELLED+,#0

MECA. (2009). *Retrofitting Emission Controls for Diesel-Powered Vehicles*. Retrieved from http://www.meca.org/galleries/default-file/MECA diesel retrofit white paper 1009.pdf

Mohr, M., & Lehmann, U. (2003). Comparison study of particle measurement systems for future type approval application. *EMPA Report*, *41*(202779). Retrieved from http://www.sootgenerator.com/documents/empa_mohr.pdf

Myers, R., Montgomery, D., & Anderson-Cook, C. (2009). *Response Surface Methodology* (3rd ed.). New Jersey: John Wiley & Sons.

Natural Gas Vehicle Global. (2012). Current Natural Gas Vehicle Statistics. *Natural Gas Vehicle Knowledge Base*. Retrieved February 11, 2013, from http://www.iangv.org/current-ngv-stats/

Neer, a, & Koylu, U. (2006). Effect of operating conditions on the size, morphology, and concentration of submicrometer particulates emitted from a diesel engine. *Combustion and Flame*, *146*(1-2), 142–154. doi:10.1016/j.combustflame.2006.04.003

Oberdörster, G. (2000). Pulmonary Effects of Inhaled Ultrafine Particles. *International Archives of Occupational and Environmental Health*, *74*, 1–8. Retrieved from http://www.springerlink.com/index/FVM951M11WWCV5JT.pdf

Oberdörster, Günter, Stone, V., & Donaldson, K. (2007). Toxicology of nanoparticles: A historical perspective. *Nanotoxicology*, *1*(1), 2–25. doi:10.1080/17435390701314761

Park, S. H., & Rogak, S. N. (2003). A One-Dimensional Model for Coagulation , Sintering and Surface Growth of Aerosol Agglomerates. *Aerosol Science & Technology*, (1993), 947–960. doi:10.1080/02786820390230398

Patashnick, H., & Rupprecht, E. (1991). Continuous PM-10 Measurements using the Tapered Element Oscillating Microbalance. *Journal of the Air & Waste M*, *41*(8), 1079–1083. Retrieved from http://www.tandfonline.com/doi/abs/10.1080/10473289.1991.10466903

Patychuk, B. D., & Rogak, S. N. (2012). Particulate Matter Emissions from a Natural Gas Fueled High Pressure Direct Injection Engine tested over the SCRE 9 Mode Test Cycle. *Proceedings of the Combustion Institute Canadian Section Spring Technical Meeting*.

Ristovski, Z. D., Miljevic, B., Surawski, N. C., Morawska, L., Fong, K. M., Goh, F., & Yang, I. a. (2012). Respiratory Health Rffects of Diesel Particulate Matter. *Respirology*, *17*, 201–12. doi:10.1111/j.1440-1843.2011.02109.x

Rogak, S., Flagan, R., & Nguyen, H. (1993). The Mobility and Structure of Aerosol Agglomerates. *Aerosol Science and Technology*, *18*(1), 25–47. Retrieved from http://www.tandfonline.com/doi/abs/10.1080/02786829308959582

Rogak, S. N., & Flagan, R. C. (1992). Coagulation of aerosol agglomerates in the transition regime. *Journal of Colloid and Interface Science*, *151*(1), 203–224. doi:10.1016/0021-9797(92)90252-H

Seigneur, C. (2009). Current Understanding of Ultrafine Particulate Matter Emitted from Mobile Sources. *Journal of the Air & Waste Management Association*, *59*(1), 3–17. doi:10.3155/1047-3289.59.1.3

Shi, J. P., Mark, D., & Harrison, R. M. (2000). Characterization of Particles from a Current Technology Heavy-Duty Diesel Engine. *Environmental Science & Technology*, *34*(5), 748–755. doi:10.1021/es990530z

Silverman, D. T., Samanic, C. M., Lubin, J. H., Blair, A. E., Stewart, P. a, Vermeulen, R., Coble, J. B., et al. (2012). The Diesel Exhaust in Miners study: a nested case-control study of lung cancer and diesel exhaust. *Journal of the National Cancer Institute*, *104*(11), 855–68. doi:10.1093/jnci/djs034

Stevens, P. (2012). The “Shale Gas Revolution”: Developments and Changes. *chathamhouse.org*, (August). Retrieved from http://www.chathamhouse.org/sites/default/files/public/Research/Energy, Environment and Development/bp0812_stevens.pdf

U.S.-Department-of-Energy. (2012). *Clean Cities Alternative Fuel Price Report*.

Valavanidis, A. (2008). Airborne particulate matter and human health: toxicological assessment and importance of size and composition of particles for oxidative damage and carcinogenic. *Journal of Environmental Science and Health*, (February 2013), 37–41. Retrieved from http://www.tandfonline.com/doi/abs/10.1080/10590500802494538

Wang, S. C., & Flagan, R. C. (1990). Scanning electrical mobility spectrometer. *Aerosol Science and Technology*, *13*(2), 230–240. Retrieved from http://www.tandfonline.com/doi/abs/10.1080/02786829008959441

Wehner, B., & Philippin, S. (2002). Design and calibration of a thermodenuder with an improved heating unit to measure the size-dependent volatile fraction of aerosol particles. *Journal of aerosol science*, *33*, 1087–1093. Retrieved from http://www.sciencedirect.com/science/article/pii/S0021850202000563

Appendix A: Synthetic Diesel PM Reduction and Input Error Corrections

Summary

Testing was done to evaluate the effects that synthetic diesel and the aromatic content of the pilot have on the PM emissions of the SCRE.

The PM emissions were reduced on average by 25% (DRX) / 17% (TEOM) with the synthetic diesel at 3 different Mode B75 injection strategies. This is a greater percentage than is contributed by the diesel pilot by itself. This suggests that the aromatic rings in the diesel fuel provided soot formation sites for the natural gas to form PM.

The error correction adjusts the emission levels for any input errors in the engine set point. This was the first application of the empirical input error correction to a testing block. On average, for standard HPDI combustion, this algorithm reduces the uncertainty in the measurements. However, it can increase the uncertainty for negative PSEP points as the input parameters affect the emissions differently for this combustion regime.

Introduction

This report outlines the testing done to compare GTL derived synthetic diesel with the standard ULSD used for the HPDI pilot in the SCRE. This testing was done with synthetic diesel provided by Rentech (http://www.rentechinc.com/) which is derived from Natural Gas and the Fischer Tropsch process. Additionally, this report will use the empirical correlations derived from the Mode 4 Parameter Sweep testing to improve the resolution of our emission measurements.

Soot Formation

Traditional diesel fuel is a complex mixture of many different hydrocarbons. Some percentages of these hydrocarbons are aromatic rings such as benzene or naphthalene.

Particulate Matter is formed in cylinder when hydrocarbon radicals from fuel decomposition react with each other and begin to start to form benzene/aromatic rings. These initial benzene rings eventually grow into soot precursors and primary soot particles. The process of decomposition and formation takes time and can limit the total soot production rates.

Conversely, any aromatic rings, already found in the fuel do not have to decompose and reform to create a benzene ring. This removes this rate limiting step and leads to much higher soot formation rates.

Synthetic Diesel Fuel

Synthetic Diesel is refined from Natural Gas by Gas-to-Liquid processes. As the result of this process, the fuel has essentially no aromatic compounds and likewise a very high cetane number. Table 18 shows the properties of our synthetic diesel fuel (As provided by the manufacturer) with typical ULSD.

	Synthetic Diesel	Ultra Low Sulfur Diesel
Cetane	>70	40-45
Density	0.77	0.87
Aromatic Content	<0.5%	<35%

Table 18 - Fuel Properties Comparison

As there are almost no aromatics in the synthetic diesel, the soot formation rates due to the diesel pilot should be reduced, ultimately leading to lower engine out PM emissions.

Methods

Testing Methods

The synthetic diesel testing took place over 5 days from October 12-18, 2012. Baseline diesel tests occurred on the first and last day, synthetic diesel was tested on the third and the middle days were used to clean out the fuel system and switch the fuels.

To switch between the 2 fuels, all of the fuel lines were drained as much as possible, before being blown out by compressed air. Additionally, the fuel filters were removed for the synthetic diesel testing as they represented a large fuel volume and we only had a limited quantity of the synthetic diesel.

The 2 fuels are different colors and during testing it appeared that we managed to completely flush the system of the standard diesel. However, at the end of the day, when the fuel pumps were turned off, some standard diesel flowed back into the reservoir. Overall, I believe we were injecting >95% pure synthetic diesel for our testing.

The results are the combination of 4 repeats of the baseline conditions along with 3 repeats of the synthetic diesel. 3 injection variations of mode B75 (HPDI Baseline, 0 EGR, Neg PSEP High EQR/EGR) as well as some low load points were tested.

Empirical Correction

These results will also show the use of an input error correction algorithm designed to increase the resolution of our measurements. As we try to measure lower and lower emission levels from the engine,

a more sophisticated way of setting the engine or treatment of data may be required for increased accuracy and noise reduction.

As described in early reports on the Mode 4 Parameter Study, first order regressions were formed over the engine inputs along with a second order fit over the engine timing. This was done for the PM emissions as well as the NOx, CH4 and CO. These empirical fits gave the partical derivatives of the emissions with respect to the input variations. Equation 1 shows an example of the form of these equations. These will serve as the base functions for the simulation.

$$TEOM\left(\frac{g}{kWhr}\right) = -0.334 + 0.000742 * Diesel - 0.0053 * GRP + 0.424 * EQR + 0.0035 * EGR + 0.0076 * GIMEP + 0.0184 * Timing - 0.000849 * Timing^2$$

Equation 20 Empirical TEOM Response

These equations were then normalized to estimate percentage changes in emissions due to percent differences in input parameters. The input errors in each of the measured operating points are then calculated and the emissions changed accordingly.

Results

Reductions

The following results focus on the heavily sooting mode B75 points. Figure 46 shows the NOx – PM trade off curve for these 3 injection strategies. The upper points represent the standard engine calibration. The lower left points are the negative PSEP points and the ones in the lower right are 0% EGR points. The blue points are with standard ULSD whereas the red are with the synthetic diesel. The points with a filled circle have had the error correction applied.

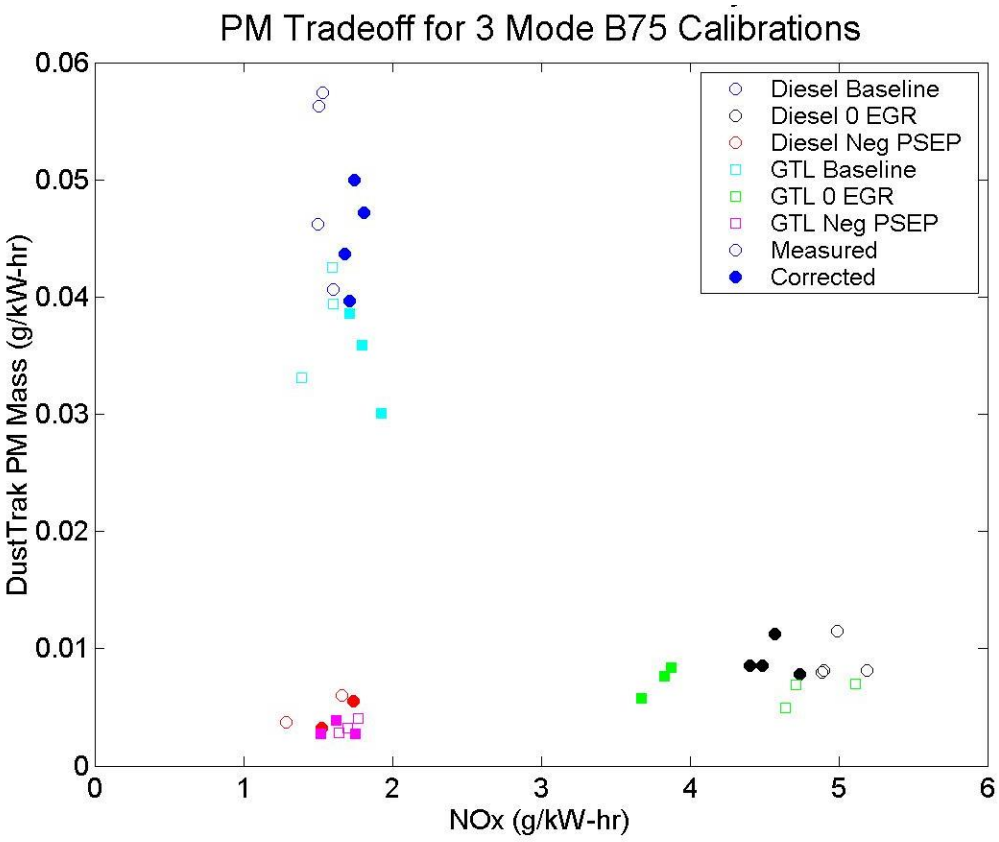

Figure 46 - NOx - PM Tradeoff with Diesel/GTL and Corrections

On this overview plot, it can be seen that the synthetic diesel reduced the PM at every condition as well as the NOx for the 0% EGR case.

The emission reductions are shown graphically in Figure 47 as measured by the DustTrak and as percent reductions in Table 19 with both DustTrak and TEOM measurements. Overall, there is a large reduction in the PM, 25% by the DustTrak and 17% by the TEOM. This is especially interesting as the diesel pilot only provides ~5% of the energy to the system and the aromatics are only 25% of the diesel. This shows that soot interactions between the diesel and natural gas are very important. Although the total amount of soot from the diesel is small, it provides additional soot formation pathways for the natural gas radicals, increasing the final soot emissions.

	DustTrak	TEOM
Baseline	23.4	19.9
0% EGR	29.6	17.5
Neg PSEP	31.4	13.4

Table 19 - Percent Reduction in DustTrak PM with Synthetic Diesel

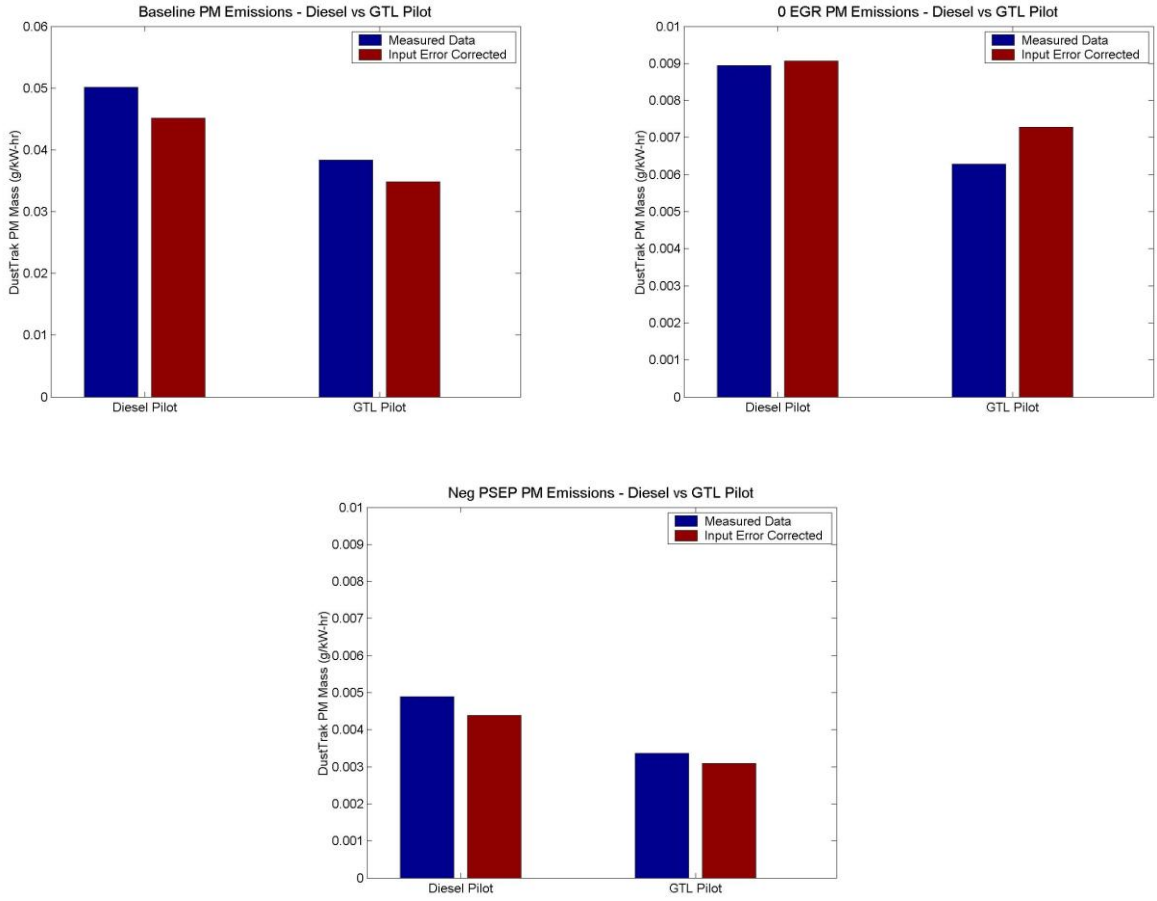

Figure 47 - DustTrak PM Emission for the 3 B75 Injection Strategies

High Speed Data (HRR and Cylinder Pressure)

The higher cetane number of the GTL may be influencing the combustion behaviour, resulting in the reduced emissions. Figure 48 shows the averaged heat release rates for the 3 tests conditions.

For the two points with standard (0.3ms) PSEP, there is a reduced quantity of energy released in the pilot injection and thus a larger amount of energy released from the natural gas (to maintain the power). Despite this reduction in pilot energy, there is no change in the cycle to cycle variability for the two fuels. (COVs of the peak pressure were 0.9/0.7% for the baseline and 0.6/0.6% for the 0 EGR; Diesel and GTL respectively)

For these test points, the pilot start of injection was between 22 and 23° BTDC. There does not appear to be a large difference in ignition delay.

The differences are less apparent for the negative PSEP point as the natural gas is partially premixed and combusts alongside the igniting diesel pilot. This overwhelms any small changes in pilot energy released between the two fuels. On average, the diesel PSOI was 1.3° later than the GTL and this is seen in both the HRR and pressure curves.

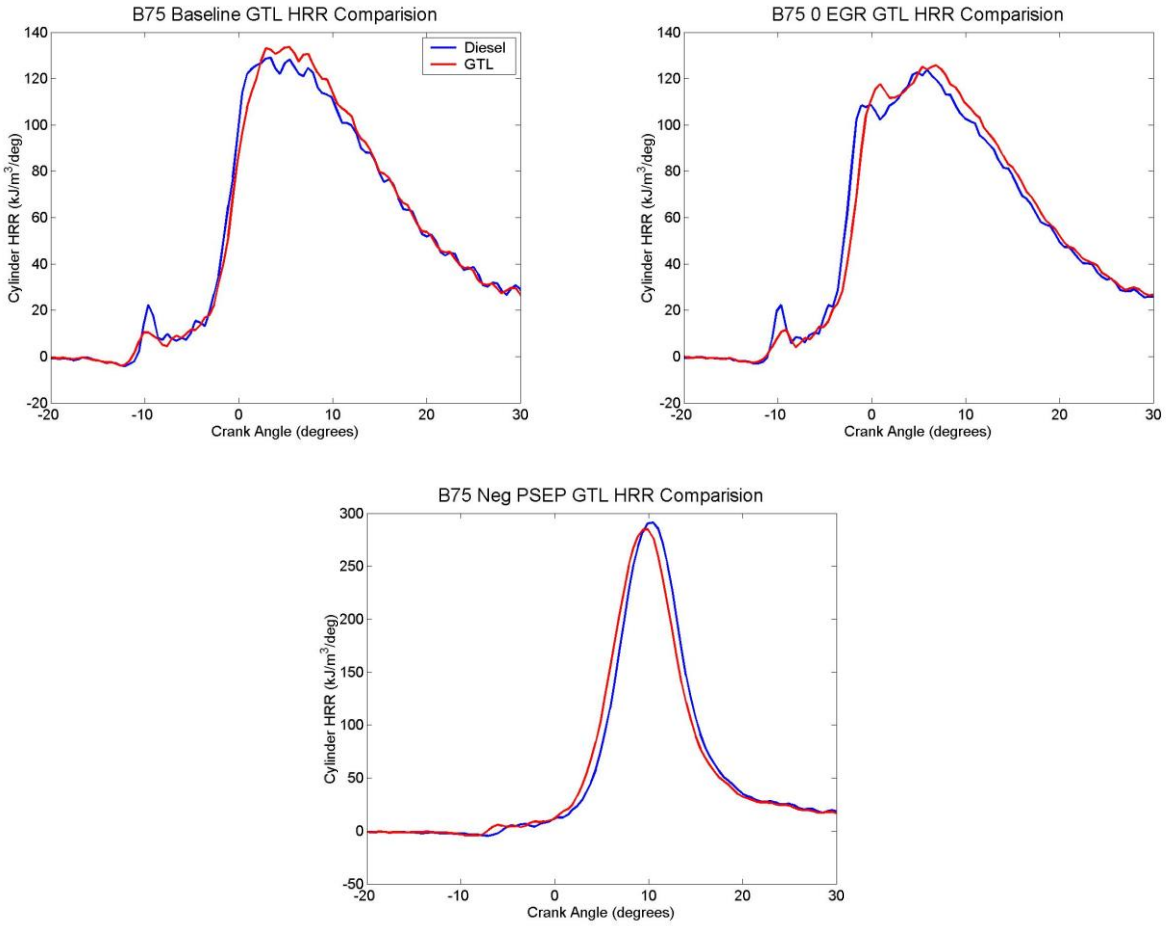

Figure 48 - Heat Release Rates for the two Pilot Fuels

Figure 49 shows the pressure curves for the 3 test conditions. There are no major differences between the two pilot fuels. Natural gas provides ~95% of the energy/pressure changes.

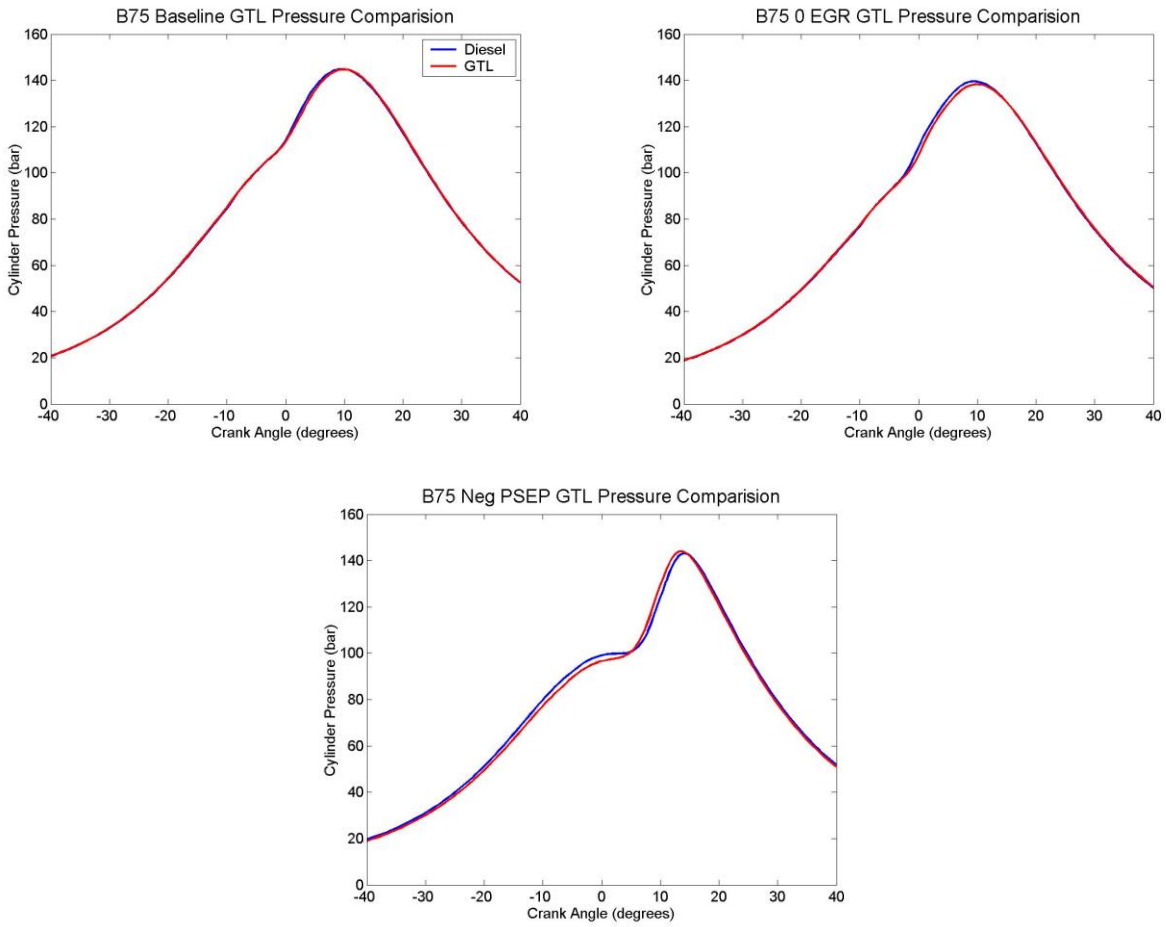

Figure 49 - Incylinder Pressure for the 2 Pilot Fuels

Pilot Mass Comparison

As the density of the GTL is less than the standard diesel, the PM reductions could be attributed to a lower pilot quantity. Figure 50 shows the delivered diesel injection mass vs the commanded pulse width.

There is no clear trend or difference between the two fuels. The injected mass is almost constant across commanded PPW; this is somewhat troubling. This testing was performed with a AJ36 injector, which has had diesel control issues in the past. The pilot quantity question is inconclusive in this testing.

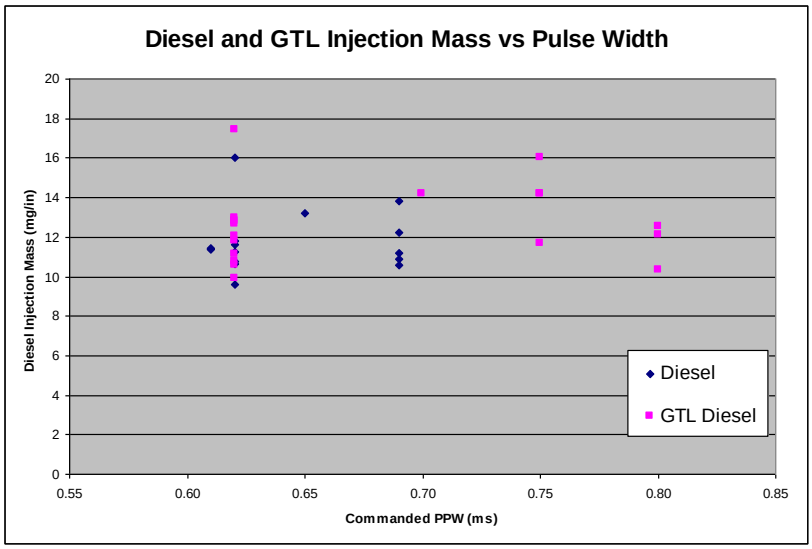

Figure 50 - Diesel and GTL Pilot Quantities

Error Corrections

The input error correction changes not only the absolute value of the emissions, but also the uncertainty involved. For the standard HPDI injection strategies, the uncertainty of the measurement is generally reduced after applying the correction. This holds for the other emissions not shown here (TEOM, CH4, CO). For the negative PSEP conditions, the uncertainty is generally increased. This quantitatively indicates that the effects of the input parameters have on the emissions are different than for standard HPDI combustion. These uncertainties are shown in Table 20.

	Synthetic Diesel		ULSD	
Baseline	PM	NOx	PM	NOx
Average COV	12.55	7.84	16.12	3.09
Corrected COV	12.57	5.84	9.86	3.29
Percent Reduction	-0.2	25.5	38.8	-6.5
0% EGR				
Average COV	18.16	5.22	19.09	2.81
Corrected COV	18.36	2.8	16.35	3.13
Percent Reduction	-1.1	46.4	14.4	-11.4
Neg PSEP				
Average COV	18.64	3.67	33.13	17.98
Corrected COV	21.07	7.17	36.16	9.09
Percent Reduction	-13.0	-95.4	-9.1	49.4

Table 20 - Measurement Uncertainties with the Error Correction

Conclusions

Testing was done to evaluate the effects that synthetic diesel and the aromatic content of the pilot have on the PM emissions of the SCRE. This was a fairly preliminary test with this fuel, as well as the first application of the empirical input error correction.

The PM emissions were reduced on average by 25% (DRX) / 17% (TEOM) with the synthetic diesel at 3 different mode B75 injection strategies. This is much greater reduction in total PM than would be provided solely from the diesel pilot.

This suggests that the aromatic rings in the diesel fuel provided soot formation sites for the natural gas to form PM. Eliminating this soot formation pathway appears to have a significant effect on the final emissions.

The quantity of energy provided by the diesel pilot is also reduced with the GTL fuel. This shifts the ratio between pilot and natural gas energies and will also lead to a reduced PM emissions.

The relative importance of these 2 effects is unclear. These results suggest that further testing of the synthetic diesel may be warranted.

The error correction adjusts the emission levels for any input errors in the engine set point. These are based on linear correlations from the Mode 4 input parameter variations tests. The corrections change not only the absolute levels of the uncertainty. On average, for standard HPDI combustion, this algorithm reduces the uncertainty in the measurements. However, it can increase the uncertainty for negative PSEP points as the input parameters affect the emissions differently for this combustion regime.

Appendix B - Matlab Processing Code

The following appendix contains the Matlab processing code for both the SCRE engine results as well as the TEM image morphology processing. Both these codes were developed by Hugo Tjong. The first script will import the excel data sheets produced by the SCRE emission software into excel all and allow the user to sort modes by flags such as EQR, EGR etc.

The TEM code provides a graphic user interface to help with particle sizing and measurements from the images produced from the microscope.

```
%% About The Script

% I.  Overview
%    The Script was created to find all the data that fall into the
%    categogy that requested by user (datespan and engine mode) from all
%    the excel files in the input folder.
%
% II. How to run the script
%    1. The script can be started by typing its name in the command window.
%    2. Input the engine mode number at the first input box.
%    3. Input the start of the date for the engine test's time span on the
%       second input box
%    4. Input the end of the date for the engine test's time span on the
%       third input box
%    5. Please change value of the 4th input box to y if a new excel file has
%       been added or the input directory has been changed.
%    6. Input the intended name for the output file in the last input box.
%    7. Input the input file directory. Remember that the directory has to
%       be in a stucture of year folder, month folder, and day folder
%    8. Click on 'ok' button
%    9. Wait until the program finish and the output file can be found in
%       the Output box.
%
% III.How the Script Works
%    1. The script started with asking inputs from the user.
%    2. The file index is loaded to the memory with excelfileindex function.
%    3. The script will search the data base for files with data that match
%       the user input specification.
%    4. The excel files that matche the criteria are loaded to the memory
%       one by one.
%    5. The script will find all the columns with specified engine mode and
take
%       all the column out.
%    6. All the collums is combined into 'numdataout' variable (for numeric
%       data). The text data is combined in 'txtdataout' variable
%    7. The output data are writen to the output files
%    8. The output file header was taken from an excel file that has the
%       longest row due to the header variation.
%
% IV. Excel time format
%    The time format for the excel files is specified in the 'exdtfm'
%    variable. The value needs to be changed if the excel file use a time
%    format other than dd/mm/yyy.
```

```
%    The excel time format can create a lot of problem if its unconsistent
%    between the inputs files. This restriction exist due to the way Matlab
%    reads the date value from the excel as string. The date value need to
%    be converted to Matlab numerical date format before cn be manipulated.
%    To do this the time format needs to be specify.
%    There is a solution for this. A time format can be provided in a cell
%    inside each excel file and the script can read the cell and use it as
%    the time format indicator. This solution need a modificarion in the
%    script and the excell files.
%
% V.  How to Modify The Script to Adapt Different Excel Data Format
%    There are several area of Script that can be modify to match a simple
%    structure change in the excel data format. (for matching the time
%    format please res the previous section)
%
%    The test id row can be change by modifying the 'IDrow' value. This
%    value does not correspond with the excel row. The row value is the row
%    value of the imported text data in the matlab. The value is different
%    due to the matlab removing all the empty row in the beginning of the
%    excel file. The numerical data imported has even a bigger diference.
%    Please check the imported data stucture first before modifying these
%    value by running the 'excellimport' function alone:
%       [datanum datatxt]=excellimport(filename,sheetnumber)
%    The date row and the time row should be modified in the same way.
%
%    If the test ID format is changed then the keyword also has to be
%    change. These keyword can be found in the 'enginetestfilter.m'
%    (core section) and 'excelfileindex.m' (line 27 and 30).
%    Right now the script uses 'M#-'keyword to search the engine mode value
%    and 'epeat' for the reapeatability mode.


%% clean up
clear all
clc

mainfolder=cd;
addpath(mainfolder);
global inputfiledirectory
%% User input

if exist('defaultsetting.mat','file')==2

load('defaultsetting.mat','inputfiledirectory','Startdate','Enddate','Seconda
rykey');
else
    inputfiledirectory=cd;
    Startdate='01-01-2010';
    Enddate='31-12-2011';
    Secondarykey='-0EGR';
end

dlg_title='User Input';
promt={'Enter mode (repeatability=15):','Start date (dd-mm-yyyy):', ...
    'End date (dd-mm-yyyy)','Renew database(y/n):','Output filename:', ...
```

```
    'Input Folder Directory\n(e.g. C:\InputFolder)','Secondary Search Type
(0:OFF; 1:Keep Maching Result; 2: Remove Matching Result)','Secondary Search
Keyword'}; %User input questions
num_lines=1;
def={'',Startdate,Enddate,'n','Filtered data',inputfiledirectory,'0'
,Secondarykey}; %default value for user input
usrinput=inputdlg(promt,dlg_title,num_lines,def); %user input execution
startprocess=now;
clear def dlg_title num_lines

%% Other input

%matlab input matrix coodinate
IDrow=24;
Timerow=23;
Daterow=26;

%excel date format
global exdtfm
exdtfm='dd/mm/yyyy'; %date excel format

%% Preprocessing

Startdate=char(usrinput(2,1));
Enddate=char(usrinput(3,1));
inputfiledirectory=char(usrinput(6,1));
save('defaultsetting.mat','inputfiledirectory','Startdate','Enddate','Seconda
rykey');

outoutfilename=char(usrinput(5,1)); %filename output

[filelist,modedatelist,numofrow,mastertitle,FastMlist,Fastcsvlist,...
    Slowlist]=excelfileindex(char(usrinput(4,1))); %loading index file

matstartdate=datenum(usrinput(2,1),'dd-mm-yyyy'); %converting start date to
matlab format
matenddate=datenum(usrinput(3,1),'dd-mm-yyyy'); %converting end date to
matlab format

Emode=str2double(usrinput(1,1)); %assigning mode to special variable
Secondarytype=str2double(usrinput(7,1)); %assigning Secondary Search Type to
special variable
Secondarykey=char(usrinput(8,1)); %assigning secondary search keyword to
special variable

[frow,~]=find(modedatelist(:,Emode)==1 & modedatelist(:,16)<=matenddate & ...
    modedatelist(:,16)>=matstartdate); %finding the files containing data
that match the criteria

if isempty(frow)==1
    error('No Match'); %error control
end

NumOfFile=size(frow,1); %number of files that match the criteria
```

```
matchnumofrow=max(numofrow(frow,1));  %finding the maximum number of data row

numdataout=zeros(matchnumofrow,1); %numerical data container preparation

clear usrinput promt Startdate Enddate

%% header loading(processing the text header for output file
%   (taken from the files that have all the rows)

cd (char(mastertitle(1,2)));
[~,txtdataout]=excellimport(char(mastertitle(1,1)),2);
cd (mainfolder);
[txtnumofrow,txtnumcol]=size(txtdataout);
if txtnumofrow<max(numofrow)
    txtdataout=[txtdataout;cell(max(numofrow)-txtnumofrow,txtnumcol)];
end
txtdataout(txtnumofrow+1,1)={'© Hugo Tjong 2011'};
txtdataout(:,2:txtnumcol)=[];
[txtnumofrow,~]=size(txtdataout);

%% Core

for f=1:NumOfFile

    fprintf(1,['Loading Data ' num2str(f*100/NumOfFile) '%%']);

    cd (char(filelist(frow(f,1),2)));
    filename=char(filelist(frow(f,1),1)); %loading the name of the file
    [datanum datatxt]=excellimport(filename,2); %loading execl file
    cd (mainfolder)

    if Emode==15 %creating the search criterion
        passcode='epeat';
    else
        passcode=['M' int2str(Emode) '-'];
    end

    [~,matchcol]=find(cellfun('isempty',(strfind(datatxt(IDrow,:), ...
        passcode)))==0); %fiding column matching the mode criteria

    if isnan(datanum(23,1))==1
        [baris,~]=size(datanum);
        smpsdiameterbar=datanum(216:baris,1);
        datanum(:,1)=[];
    end

    nummatchcol=matchcol-ones(size(matchcol)); %converiting to numerical data
column

    matchdata=datanum(:,nummatchcol); %taking out the matching data

    [trow,tcol]=size(matchdata); %matching the array size with the main array
container
    if trow<matchnumofrow
```

```
        matchdata=[matchdata;zeros((matchnumofrow-trow),tcol)];
    end

    numdataout=[numdataout,matchdata]; %combining the numerical output data

    matchtxtdata=datatxt(:,matchcol); %same with above but for text data
    [trow,tcol]=size(matchtxtdata);
    if trow<txtnumofrow
        matchtxtdata=[matchtxtdata;cell(txtnumofrow-trow,tcol)];
    end
    txtdataout=[txtdataout,matchtxtdata];
    clc
end

if isempty(numdataout)==1 %error control
    error('No Match');
end
%% Secondary Search

if Secondarytype==1
    [~,matchcol]=find(cellfun('isempty',(strfind(txtdataout(IDrow,:), ...
        Secondarykey)))==0); %fiding column matching the secondary key
criteria


    matchtxtdataout=txtdataout(:,matchcol);
    matchnumdataout=numdataout(:,matchcol);

    txtdataout(:,2:size(txtdataout,2))=[];
    numdataout(:,2:size(numdataout,2))=[];

    txtdataout=[txtdataout,matchtxtdataout];
    numdataout=[numdataout,matchnumdataout];

elseif Secondarytype==2
    [~,matchcol]=find(cellfun('isempty',(strfind(txtdataout(IDrow,:), ...
        Secondarykey)))==0); %fiding column matching the secondary key
criteria


    txtdataout(:,matchcol)=[];
    numdataout(:,matchcol)=[];

end


%% putting the test id, date and time to the output
numdataout(:,1)=[];
testid=txtdataout(IDrow,:);
datetest=txtdataout(Daterow,:);
[~,numcol]=size(numdataout);

timevalue=cell(1,numcol);
```

```
    for n=1:numcol
        timevalue(1,n)={datestr(numdataout(Timerow,n))};
    end

%% Output Variable

if Secondarytype==1

elseif Secondarytype==2
    Secondarykey=['Sans' Secondarykey];

else
    Secondarykey='';

end

nd=['numdataout' int2str(Emode)  Secondarykey];
eval([nd '=numdataout;']);
td=['txtdataout' int2str(Emode)  Secondarykey];
eval([td '=txtdataout;']);
ti=['testid' int2str(Emode)  Secondarykey];
eval([ti '=testid;']);
dt=['datetest' int2str(Emode)  Secondarykey];
eval([dt '=datetest;']);
tt=['timevalue' int2str(Emode)  Secondarykey];
eval([tt '=timevalue;']);

 %% Saving result

if exist('Output','dir')~=7 %checking wheter the Output folder available
    mkdir('Output')
end

mainfolder=cd;

cd Output

%saving matlab output file

if exist([char(outoutfilename) '.mat'],'file')==2 %checking wheter the Output
folder available
    save([char(outoutfilename) '.mat'],nd,td,ti, ...
    dt,tt','-append');
else
    save([char(outoutfilename) '.mat'],nd,td,ti, ...
    dt,tt');
end



%writing excel file
xlswrite(char(outoutfilename),txtdataout,['M' int2str(Emode) ' ' Secondarykey
]);
```

```
xlswrite(char(outoutfilename),numdataout,['M' int2str(Emode) ' ' Secondarykey
],'B3');
xlswrite(char(outoutfilename),testid,['M' int2str(Emode) ' ' Secondarykey
],'A24');
xlswrite(char(outoutfilename),datetest,['M' int2str(Emode) ' ' Secondarykey
],'A26');
xlswrite(char(outoutfilename),timevalue,['M' int2str(Emode) ' ' Secondarykey
],'B25');

cd (mainfolder)

fprintf(1,['Finished in ' num2str((now-startprocess)/1.157407407403888e-05) '
s']);

clear matchnumdataout matchtxtdataout Secondarykey Secondarytype txtdataout
numdataout testid datetest timevalue nd td ti dt tt startprocess
inputfiledirectory Daterow IDrow Timerow mainfolder ...
    passcode txtnumcol trow tcol outoutfilename numofrow nummatchcol ...
    numcol n modedatelist matstartdate matenddate matchtxtdata matchcol ...
    mastertitle frow filename filelist f datanum datatxt Emode NumOfFile ...
    matchnumofrow txtnumofrow matchdata FastMlist Fastcsvlist Slowlist % ©
Hugo Tjong 2011


function[filelist,modedatelist,numofrow,mastertitle,FastMlist,Fastcsvlist,Slo
wlist]=excelfileindex(renew)
% load or create the fileindex for every .xls file in the folder
% It will return the list of .xls files along with the date and modes
% of the file

 global exdtfm inputfiledirectory
 mainfolder=cd;
 addpath(mainfolder);

if exist('fileindex.mat','file')==2 && renew=='n' %checking wheter the index
file available


load('fileindex.mat','filelist','modedatelist','numofrow','mastertitle','Fast
Mlist','Fastcsvlist','Slowlist'); %loading the index file

else %if the index file is not available

    %% creating file and directory list
    fprintf(1,'indexing file');

    filelist=cell(1,2);
    FastMlist=cell(1,2);
    Fastcsvlist=cell(1,2);
    Slowlist=cell(1,2);

    cd (inputfiledirectory);
    templistoffile=dir;
    temprow=(find(cell2mat({templistoffile(:).isdir})==1))';
```

```
    temprow(1:2,:)=[];
    [q,~]=size(temprow);
    yearfolderlist=cell(q,1);
    for k=1:q
        yearfolderlist(k,1)={(templistoffile(temprow(k,1)).name)};
    end
    clear k templistoffile temprow

    for k=1:q
        cd (char(yearfolderlist(k,1)));
        templistoffile=dir;
        temprow=(find(cell2mat({templistoffile(:).isdir})==1))';
        temprow(1:2,:)=[];
        [w,~]=size(temprow);
        monthfolderlist=cell(w,1);
        for l=1:w
            monthfolderlist(l,1)={(templistoffile(temprow(l,1)).name)};
        end
        clear l templistoffile temprow

        for l=1:w
            cd (char(monthfolderlist(l,1)));
            templistoffile=dir;
            temprow=(find(cell2mat({templistoffile(:).isdir})==1))';
            temprow(1:2,:)=[];
            [e,~]=size(temprow);
            dayfolderlist=cell(e,1);
            for m=1:e
                dayfolderlist(m,1)={(templistoffile(temprow(m,1)).name)};
            end
            clear m templistoffile temprow

            for m=1:e
                cd (char(dayfolderlist(m,1)));

                tempexcellfilelist=struct2cell(dir('*SCRE*.xls*')); %create a
list of *.xls file with its properties
                tempFastMfilelist=struct2cell(dir('*FastM*.xls*'));
                tempFastcsvfilelist=struct2cell(dir('*Fast*.csv'));
                tempSlowcsvfilelist=struct2cell(dir('*Slow*.csv'));

                tempnumofile=size((tempexcellfilelist),2);
                tempnumoFastM=size((tempFastMfilelist),2);
                tempnumoFastcsv=size((tempFastcsvfilelist),2);
                tempnumoSlow=size((tempSlowcsvfilelist),2);

                tempfilelist=cell(tempnumofile,2);
                tempFastMlist=cell(tempnumoFastM,2);
                tempFastcsvlist=cell(tempnumoFastcsv,2);
                tempSlowlist=cell(tempnumoSlow,2);

                tempfilelist(:,1)=(tempexcellfilelist(1,:))'; %creating list
of .excell filename
                tempFastMlist(:,1)=(tempFastMfilelist(1,:))';
                tempFastcsvlist(:,1)=(tempFastcsvfilelist(1,:))';
```

```
                tempSlowlist(:,1)=(tempSlowcsvfilelist(1,:))';

                for n=1:tempnumofile
                    tempfilelist(n,2)={cd};
                end

                for n=1:tempnumoFastM
                    tempFastMlist(n,2)={cd};
                end

                for n=1:tempnumoFastcsv
                    tempFastcsvlist(n,2)={cd};
                end

                for n=1:tempnumoSlow
                    tempSlowlist(n,2)={cd};
                end

                filelist=[filelist;tempfilelist];
                FastMlist=[FastMlist;tempFastMlist];
                Fastcsvlist=[Fastcsvlist;tempFastcsvlist];
                Slowlist=[Slowlist;tempSlowlist];

                cd ..
            end
            cd ..
        end
        cd ..
    end
    cd (mainfolder)
    filelist(1,:)=[];
    FastMlist(1,:)=[];
    Fastcsvlist(1,:)=[];
    Slowlist(1,:)=[];

 clear k l m w dayfolderlist yearfolderlist monthfolderlist  e n q
tempexcellfilelist tempfilelist tempnumofile tempFastMlist tempFastcsvlist
tempSlowlist tempnumoFastM tempnumoFastcsv tempnumoSlow
    %%

    [numofile,~]=size(filelist);
    modedatelist=zeros(numofile,16);
    numofrow=zeros(numofile,1);


    for i=1:numofile
        cd (char(filelist(i,2)));
        [num,txt]=excellimport(char(filelist(i,1)),2); %loading the .xls file
        cd (mainfolder)
        modedatelist(i,16)=datenum(char(txt(26,2)),exdtfm); %taking out the
id row
        for k=1:14  %creating list of mode available in the file
            modedatelist(i,k)=any(cell2mat(strfind(txt(24,:),['M' int2str(k)
'-'])));
```

```
        end
        modedatelist(i,15)=any(cell2mat(strfind(txt(24,:),'epeat'))); %for
repeatability mode
        [trow,~]=size(num);
        [txtrow,~]=size(txt);
        numofrow(i,1)=trow; %counting number of row in the num file
        numoftxtrow(i,1)=txtrow; %counting number of row in the txt file

    end

    [srow,~]=find(numoftxtrow==max(numoftxtrow)); %finding file to be use as
the template

    mastertitle=(filelist(srow(1,1),:));


save('fileindex.mat','filelist','modedatelist','numofrow','mastertitle','Fast
Mlist','Fastcsvlist','Slowlist'); %saving the file index variable for later
use
    clc
end



function[datanum datatxt]=excellimport(filename,sheetnumber)
%Importing data from .xls file
%
[~,sheets,~] = xlsfinfo(filename); %finding info about the excel file
sheetname=char(sheets(1,sheetnumber)); % choosing the second sheet
[datanum datatxt]=xlsread(filename,sheetname); %loading the data
```

TEM Processing Code

```
%
% Version: 24072012 by HugoTjong2012

%% Housekeeping

close all
clear all

global mainfolder processed_img Im_Dir report_txt report_num FileName
report_txt=cell(1,1);

Extra_function=0; % 0: No extra function 1: with extra function


report_title={'Image_ID','Primary Width (nm)','Primary Length (nm)',...
    'Primary Area Based on LW average(nm^2)','Particle Width (nm)',...
    'Particle Length (nm)','Particle Area (nm^2)',...
    'Primary Particle_Count','Particle Perimeter (nm)',...
    'Particle Type','Image_ref_number','Radius of Gyration'};
%% Default Value

if exist('default_dpda_setting.mat','file')==2
    load('default_dpda_setting.mat','Im_Dir','mainfolder');
else
    mainfolder=cd;
    addpath(mainfolder);
    Im_Dir=cd;
end

%% Getting image file location and name

[Img_files,Im_Dir] = uigetfile({'*.tif','TEM image (*.tif)'},...
    'Select Images',Im_Dir,'MultiSelect', 'on');

if iscell(Img_files)==1 % Handling for 1 image selection
    Img_files=Img_files';
elseif isempty(Img_files)==1
    error('no image was selected');
end

if exist('default_dpda_setting.mat','file')==2
    save('default_dpda_setting.mat','Im_Dir','-append');
else
    save('default_dpda_setting.mat','Im_Dir','mainfolder');
end


%% Image Processing

global Crop_image Binary_Image_3 %Manual_Edge Filtered_Image_2
FinalImposedImage
```

```
[num_img,~]=size(Img_files);

particle_count=0;
tot_primary=0;
for k=1:num_img

    cd(Im_Dir);

    if num_img==1
        FileName=char(Img_files);
    else
        FileName=char(Img_files(k,1));
    end

    processed_img=imread(FileName);

    cd(mainfolder)

    pixsize=TEM_pix_size();

    imshow(processed_img);

    dlg_title='Number of Particle';
    promt={'Please input number of particle to be analized:'};
    num_lines=1;
    def={'1'};  %default value for user input
    n_particle=str2double(cell2mat(inputdlg(promt,dlg_title,num_lines,def)));
%user input execution
    close all
    clear num_lines dlg_title promt def

    for l=1:n_particle

        particle_count=particle_count+1;

        %% Cropping image

        uiwait(msgbox('Please crop the image to the particle as close as
possible. Double click when finish.',...
            ['Process Stage: Crooping Image' num2str(l)...
            '/' num2str(n_particle)],'help'));

        Crop_image = imcrop(processed_img);

        %% Particle type selection

        choise=questdlg('Selec Particle Type:',...
                'Particle Type','Aggregate',...
                'Aggregate (dp measurement only)','Other','Aggregate');

        if strcmp(choise,'Aggregate')
            Particle_Type=1;
```

```
        elseif strcmp(choise,'Aggregate (dp measurement only)')
            Particle_Type=2;
        elseif strcmp(choise,'Other')
            Particle_Type=3;
        end

        %% Saving Crop  image

        close (gcf);
        clear choise

        cd (Im_Dir)

        if exist('Output','dir')~=7 %checking wheter the Output folder
available
            mkdir('Output')
        end

        cd('Output')

        imwrite(Crop_image,[FileName '_CropImage_' num2str(l) '.tif'])


        %% Image refindment

        if Particle_Type==1
            Discard=Refine_image(l);
            if Discard==1
                Particle_Type=2;
            end
        end


        %% Particle sizing (dp for aggregate; particle size for others)

        imshow(Crop_image);
        hold on

        if Particle_Type<3

            dlg_title='Number of Primary Particle';
            promt={'Please input the number of primary particle to be
analyzed'};
            num_lines=1;
            def={'1'};  %default value for user input

num_primary=str2double(cell2mat(inputdlg(promt,dlg_title,num_lines,def)));
%user input execution
            clear def
            title_measurement='primary particle';
        else
            num_primary=1;
            title_measurement='particle';
        end
```

```
        clear num_lines dlg_title promt def

        length=zeros(num_primary,1);
        width=zeros(num_primary,1);

        for m=1:num_primary

            uiwait(msgbox(['Please select two points on the image that
coresponds to the length of the ' title_measurement ],...
            ['Process Stage: Length of' title_measurement ' ' num2str(m)...
            '/' num2str(num_primary)],'help'));

            [x, y] = ginput(2);

            length(m,1) = pixsize*sqrt((x(2)-x(1))^2+(y(2) - y(1))^2);
            line ([x(1),x(2)],[y(1),y(2)], 'linewidth', 3);

            uiwait(msgbox(['Please select two points on the image that
coresponds to the width of the ' title_measurement ],...
            ['Process Stage: Width of' title_measurement ' ' num2str(m)...
            '/' num2str(num_primary)],'help'));

            [a, b] = ginput(2);

            width(m,1)=pixsize*sqrt((a(2)-a(1))^2+(b(2) - b(1))^2);
            line ([a(1),a(2)],[b(1),b(2)],'Color', 'r', 'linewidth', 3);

        end
        clear a b x y
        cd (Im_Dir)
        cd ('Output')

        saveas(gcf,[FileName '_Primary_L_W_' num2str(l) '.tif'])
        close all
        cd (mainfolder)



        if Particle_Type==1

        %% Calculating Aggregate Area
        % to determine the total area of the agglomerate

        area_pixelcount=nnz(Binary_Image_3);
        Aggregate_Area=area_pixelcount*pixsize^2;

        %% Calculating Aggregate Perimeter
        % to determine an estimate of the perimeter of the particle

        Aggregate_perimeter=Perimeter_Length(pixsize,area_pixelcount);

        %% Calculating Aggregate Length and Width
```

```
        %to determine the length and width of the agglomerate

        [A_length, A_width] = Aggregate_Dimension (pixsize,l);

        %% Calculating Radius of Gyration

        [ Radius_Gyration ] = Gyration( pixsize );

        %% Extra function

        if Extra_function==1
            [DDC PCF RADIUS col
row_extra]=extra_function(area_pixelcount,pixsize,l);
        end

        clear area_pixelcount
        end

        %% recording report
        tot_primary=tot_primary+1;

        if Particle_Type==2
            Aggregate_Area=NaN;
            Aggregate_perimeter=NaN;
            A_width=NaN;
            A_length=NaN;
            Radius_Gyration=NaN;

        end

        if Particle_Type<3
            if num_primary>1
                report_num(tot_primary:tot_primary+num_primary-1,2)=length;
                report_num(tot_primary:tot_primary+num_primary-1,1)=width;
                report_num(tot_primary:tot_primary+num_primary-
1,3)=(((width+length)./2).^2).*(pi()/4);
                report_num(tot_primary:tot_primary+num_primary-
1,9)=Particle_Type;
                report_num(tot_primary:tot_primary+num_primary-
1,7)=num_primary;
                report_num(tot_primary:tot_primary+num_primary-
1,6)=Aggregate_Area;
                report_num(tot_primary:tot_primary+num_primary-
1,8)=Aggregate_perimeter;
                report_num(tot_primary:tot_primary+num_primary-1,4)=A_width;
                report_num(tot_primary:tot_primary+num_primary-1,5)=A_length;
                report_num(tot_primary:tot_primary+num_primary-1,10)=l;
                report_num(tot_primary:tot_primary+num_primary-
1,11)=Radius_Gyration;
                report_txt(tot_primary:tot_primary+num_primary-
1,1)={FileName};
            else
                report_num(tot_primary,2)=length;
                report_num(tot_primary,1)=width;
                report_num(tot_primary,3)=(pi()/4)*(mean([width,length]))^2;
```

```
                report_num(tot_primary,9)=Particle_Type;
                report_num(tot_primary,7)=num_primary;
                report_num(tot_primary,6)=Aggregate_Area;
                report_num(tot_primary,8)=Aggregate_perimeter;
                report_num(tot_primary,4)=A_width;
                report_num(tot_primary,5)=A_length;
                report_num(tot_primary,10)=1;
                report_num(tot_primary,11)=Radius_Gyration;
                report_txt(tot_primary,1)={FileName};
            end
            tot_primary=tot_primary+num_primary-1;
        else
            report_num(tot_primary,1)=NaN;
            report_num(tot_primary,2)=NaN;
            report_num(tot_primary,3)=NaN;
            report_num(tot_primary,5)=length;
            report_num(tot_primary,4)=width;
            report_num(tot_primary,6)=NaN;
            report_num(tot_primary,8)=NaN;
            report_num(tot_primary,9)=Particle_Type;
            report_num(tot_primary,7)=0;
            report_num(tot_primary,10)=1;
            report_num(tot_primary,11)=NaN;
            report_txt(tot_primary,1)={FileName};

        end

        %% Autobackup

        cd(Im_Dir)
        cd('Output')
        if exist('Report_dpda.mat','file')==2
            save('Report_dpda.mat','report_num','report_txt','-append');
        else
            save('Report_dpda.mat','report_num','report_txt','report_title');
        end

        cd(mainfolder)

        clear length width A_length A_width
    end


end

    %% Writing Excel Report

    cd(Im_Dir)
    cd('Output')

    if exist('Final_dpda_Report.xls','file')==2
        [datanum ~]=excellimport('Final_dpda_Report.xls',4);
        starting_row=size(datanum,1)+2;
```

```
xlswrite('Final_dpda_Report.xls',report_txt,'Jet_Engine_Emission_Data',['A'
num2str(starting_row)]);

xlswrite('Final_dpda_Report.xls',report_num,'Jet_Engine_Emission_Data',['B'
num2str(starting_row)]);
    else

xlswrite('Final_dpda_Report.xls',report_title,'Jet_Engine_Emission_Data','A1'
);

xlswrite('Final_dpda_Report.xls',report_txt,'Jet_Engine_Emission_Data','A2');

xlswrite('Final_dpda_Report.xls',report_num,'Jet_Engine_Emission_Data','B2');
    end

    cd(mainfolder)

clear k l mainfolder n_particle num_image num_primary particle_count...
    pixsize starting_row title_measurement tot_primary width processed_img

function [ A_length, A_width ] = Aggregate_Dimension( pixsize,particle_number
)
%Aggregate_Dimension etermines the length & width of the agglomerate, and
%provides a rotated image of the particle with length and width axis
%   Based on function_length_width3 (Arka) with memory saving improvement
%   @Hugo2012
%
%   ---LENGTH---
%   ---ALGORITHM---
%   Given the agglomerate's fourth edge image, E4, the algorithm finds the
%   y and x indices of the white pixels (value = 1) in the arrays of ROW and
%   COL, respectively. Then, it computes the euclidean distance between every
%   single white pixel with reference to every other white pixel, and
%   selects the greatest distance, which yields the length of the
%   agglomerate.  It is important to note that for speed, the distances are
%   computed in a vectorized form, such that each 'DISTANCE' array represents
%   the distances of the considered white pixel with reference to all other
%   pixels.  The maximum of the 'DISTANCE' array is chosen as the
%   'greatest_distance', and then compared to the length.  Once the length is
%   found, the position of the two pixels is recorded via x1_l_bot, etc...
%
%   ---WIDTH---
%   ---ALGORITHM---
%   this algorithm calculates the width by rotating the image by 'theta'
degrees
%   counterclockwise, until the length axis is parallel with the y-axis.
%   Then the width corresponds to the location of the greatest x indices of a
%   white pixel minus the location of the smallest x indices of a white
pixel.

global mainfolder Im_Dir Manual_Edge FileName

[ROW1, COL1] = find (Manual_Edge);
area_edge_particle = nnz(Manual_Edge);
length = 0;
```

```
%% Lenght Calculation

% to compute the length in vector form, and record the position of the two
% pixels that specify the length.  Since the 'find' function searches
% column-by-column, in the order of increasing x, then increasing y, the
% pixel specified by 'pos1' will always have a greater y-indices than the
% pixel specified by pos2.  This helps determine theta, later on in the
% program.

for pos1 = 1:1:area_edge_particle
    DISTANCE = ( (COL1 - COL1(pos1)).^2 + (ROW1 - ROW1(pos1)).^2 ).^.5;
    [greatest_distance, pos2] = max(DISTANCE);
    if greatest_distance >= length
        length = greatest_distance;
        x1_l_bot = COL1(pos1);
        y1_l_bot = ROW1(pos1);
        x2_l_top = COL1(pos2);
        y2_l_top = ROW1(pos2);
    end
end
A_length=length*pixsize;
clear COL1 ROW1 DISTANCE area_edge_particle

%% Width Calculation

% to mark the pixels that specify the length.  It is important to note that
% an error may arise during the rotation of the image, because some pixels
% are obscured, or even deleted via the rotation process.  In order to
% prevent this, the pixel left-adjacent to the true length-defining pixels
% are also marked with a value of '2', or '3'.

Temp_Manual_Edge = Manual_Edge;
Temp_Manual_Edge (y1_l_bot, x1_l_bot:(x1_l_bot+2)) = 2;
Temp_Manual_Edge (y1_l_bot, x1_l_bot+1) = 2;
Temp_Manual_Edge (y2_l_top, x2_l_top) = 3;
Temp_Manual_Edge (y2_l_top, x2_l_top+1) = 3;

% to determine theta, the problem becomes a system of 2 equations with 2
% unknown, with 2 differing situations.
if x1_l_bot == x2_l_top
    theta = 0;
end
if x1_l_bot < x2_l_top
    theta = abs(atan( (x2_l_top - x1_l_bot) / (y1_l_bot - y2_l_top) ) * 180 /
pi);
end
if x1_l_bot > x2_l_top
    theta = abs (180 - (atan( (x1_l_bot - x2_l_top) / (y1_l_bot - y2_l_top) )
* 180 / pi));
end


% to rotate the image counterclockwise, until the length axis is vertical
Rotated_Manual_Edge = imrotate (Temp_Manual_Edge, theta);
```

```
clear Temp_Manual_Edge theta

% to find the maximum and minimum x values to calculate the width
[ROW2, COL2] = find (Rotated_Manual_Edge > 0);
[x1_w_rit, i]  = max(COL2);
y1_w_rit = ROW2(i);
[x2_w_lef, i] = min(COL2);
y2_w_lef = ROW2(i);

width = x1_w_rit - x2_w_lef;

A_width=width*pixsize;

clear ROW2 COL2

%% PLOT LENGTH AND WIDTH AXIS ALONG ROT
% ---ALGORITHM---
% To draw the perpendicular length axis, the indices of the length-defining
% pixels are needed.  These are located by finding the pixels that were
% originally marked with values of '2' and '3'.  However, due to the fact
% that during rotation, some pixels are lost, it may be better to find the
% maximum and minimum y values instead.

[ROW3, COL3] = find (Rotated_Manual_Edge == 2);
if Rotated_Manual_Edge (ROW3(1), COL3(1)) == 2
    x1_l_bot_rot = COL3(1);
    y1_l_bot_rot = ROW3(1);
end

[ROW4, COL4] = find (Rotated_Manual_Edge == 3);
if Rotated_Manual_Edge (ROW4(1), COL4(1)) == 3
    x2_l_top_rot = COL4(1);
    y2_l_top_rot = ROW4(1);
end

% to plot and save ROT with length and width, where the length is the blue
vertical
% line and the width is the red horizontal line.  Note that they are
% perpendicular.

imshow(Rotated_Manual_Edge)
hold on
line ([x1_l_bot_rot, x2_l_top_rot], [y1_l_bot_rot, y2_l_top_rot],
'linewidth', 3);
line ([x1_w_rit, x2_w_lef], [y2_w_lef, y2_w_lef],'Color', 'r', 'linewidth',
3);
line ([x1_w_rit, x1_w_rit], [y1_w_rit, y2_w_lef],'Color', 'r', 'linewidth',
3);

cd(Im_Dir)
cd('Output')

saveas(gcf,[FileName '_Aggregate_L_W_' num2str(particle_number) '.tif'])
```

```
close all
cd (mainfolder)


end



function [AREA_R_WHOLE] = function_area_r (slope, X, Y)
%accept length, original distance transform, X, Y
%
%obtain max value from  distance transform of max possible
%create a new image, of X = 2* length, Y = same
%at the centre of this image, make = 1
%do a distance transform on this
%divide that entire distance transf by the max value from original
%then go up to r = slope of original

%do area calculations
AREA_CIRCLE = 0;
AREA_R_WHOLE = 0;
row = 0;

% to create a the biggest possible distance transform (one corner to the
% other)
BW1 = zeros(Y, X);
y1 = uint16(Y/2);
x1 = uint16(X/2);
BW1(y1,x1) = 1;
BW2 = bwdist(BW1);

% find the maximum distance in BW2
for col = 1:1:Y
    MAX(col) = max(BW2(col,:));
end
maximum = max(MAX);

% to create the largest pseudo-grayscale image which encompasses the
% largest possible r
X2 = uint16(4 * maximum(1));
Y2 = uint16(4 * maximum(1));
BW3 = zeros(Y2, X2);
y2 = uint16(Y2 / 2);
x2 = uint16(X2 / 2);
BW3(y2, x2) = 1;
BW4 = bwdist(BW3);
BW5 = BW4 ./ maximum;

% to create threshold proportional to radius, create the black circle and
% caclulate/store the data
for r = 1:1:slope
    row = row + 1;
    thresh = r / slope;
    BW6 = im2bw(BW5, thresh);
    AREA_CIRCLE(row, 1) = r;
```

```
    [ AREA_CIRCLE(row, 2) ] = function_area_total (~BW6);
end

% calculate AREA_RING
%  nfigure, imshow(BW6), title ('BW6');
AREA_R_WHOLE(1:row, 1) = AREA_CIRCLE(:, 1);
AREA_R_WHOLE(1, 2) = AREA_CIRCLE(1, 2) - 1;
AREA_R_WHOLE(2:row, 2) = AREA_CIRCLE(2:row, 2) - AREA_CIRCLE(1:(row-1), 2);
% figure, plot (AREA_CIRCLE(:, 1), AREA_CIRCLE(:, 2)), xlabel('radius'),
ylabel('total area');
% figure, plot (AREA_R_WHOLE(:, 1), AREA_R_WHOLE(:, 2)), xlabel('radius'),
ylabel('ring area');


function [AREA_R_WHOLE] = function_area_r_whole (tr_coefficient, X, Y)
% this function calculates the area of a black ring of an outer radius r, and
% thickness of dr = 1, and returns it in matrix form, with increasing r.

% ---ALGORITHM---
% To obtain area_r_whole, first a psuedo-grayscale image of identical
% height and width is created, similar to that in function_tr_coefficient.

% Second, a pseudo-grayscale image of the distance transform with height
% and width equal to 4 times the maximum euclidean distance in BW2 is
% created.
% The reason for this is as follows: for the density density correlation,
% large values of r are needed to cover the particle, therefore, large
% values for area_r_whole are also necessary for the density density
% correlation.  The maximum value of r coincides with r = tr_coefficient,
since the
% threshold value cannot be greater than 1.  With BW2, the pixel of
% value = 1 will be located at the farthest corner from the centre.  This
% means that as r approaches the value of tr_coefficient, the area of the
circle is
% lost as it exceeds the dimensions of BW2, and thus making the processes
% inaccurate.  Therefore, a pseudo-grayscale image with dimensions large
% enough to contain the black circle in BW6 is necessary. Logic dictates
% that r will at most be equal to the length of the particle, which could
% at most be equal to 2 times the maximum distance in BW2.  Therefore, an
% image that could contain a black circle of diameter equal to 4 times the
% maximum would guarentee to be large enough for r = tr_coefficient.

% Third, for an increasing r, the 'im2bw' function is used to generate
% circular binary images of radius r.  The area is counted and recorded.

% Fourth, area_r_whole is calculated for r by subtracting the area of
% (r-1) from the circular area of r, thus producing the area of r - (r-1).
% This represents a black ring of outer radius r, and inner radius (r-1).

% Note: the discreteness of the circles affects the values.  It can be
% considered to simply calculate the ideal area using pi*(r^2 - (r-1)^2),
% which would be much faster; however, it was decided that consistency
% throughout the entire calculation process was more important.

% It is important to note the logical flaw in this program:  that the
```

```
% agglomerate's length is often greater than the tr_coefficient, yet r can
only be
% measured up to r = tr_coefficient.  And given the linear relationship
between
% threshold value and radius, r = tr_coefficient refers to a black circle
with a
% radius of r.  Nevertheless, the whole image of BW2, if turned into a
% pseudo-grayscale image and then binary image via the 'im2bw' function,
% becomes entirely black - clearly creating a circle of radius much greater
% than r = tr_coefficient.  At the moment, it is assumed that this leads to
% slightly greater values of the density density correlation for large r,
% though the effect would seem to be minimal, since the pair correlation
% function validifies the results of function_density_density_correlation.

% to initialize variables
row = 0;

% to create a the biggest possible distance transform (one corner to the
% other)
BW1 = zeros(Y, X);
y1 = uint16(Y/2);
x1 = uint16(X/2);
BW1(y1,x1) = 1;
BW2 = bwdist(BW1);

% find the maximum distance in BW2
for col = 1:1:Y
    MAX(col) = max(BW2(col,:));
end
maximum = max(MAX);

% to create the largest pseudo-grayscale image which encompasses the
% largest possible r
X2 = uint16(4 * maximum(1));
Y2 = uint16(4 * maximum(1));
BW3 = zeros(Y2, X2);
y2 = uint16(Y2 / 2);
x2 = uint16(X2 / 2);
BW3(y2, x2) = 1;
BW4 = bwdist(BW3);
BW5 = BW4 ./ maximum;

% to create threshold proportional to radius, create the black circle and
% caclulate/store the data
for r = 1:1:tr_coefficient
    row = row + 1;
    thresh = r / tr_coefficient;
    BW6 = im2bw(BW5, thresh);
    AREA_CIRCLE(row, 1) = r;
    [ AREA_CIRCLE(row, 2) ] = nnz (~BW6);
end

% to calculate AREA_R_WHOLE
AREA_R_WHOLE(1:row, 1) = AREA_CIRCLE(:, 1);
AREA_R_WHOLE(1, 2) = AREA_CIRCLE(1, 2) - 1;
AREA_R_WHOLE(2:row, 2) = AREA_CIRCLE(2:row, 2) - AREA_CIRCLE(1:(row-1), 2);
```

```
% End of function_area_r_whole


 function [DDC, row] = function_density_density_correlation4 ( X, Y,
tr_coefficient, area_agglomerate, AREA_R_WHOLE, file, scale_factor)
% this function determines the density density correlation and provides its
% graph, and the same graph on a loglog scale.
% * consider putting the function into different parts!

% ---ALGORITHM---
% To obtain the density density correlation, the function was broken down
% into stages.  First, the maximum value of the BW5 distance transform was
% obtained, in order to create pseudo-grayscale images.

% Second, the indices of all white pixels (value = 1) were found using the
% 'find' function, and stored in the ROW and COL arrays.

% Third, a sample of the white pixels are considered for the density
% density correlation, regulated by the variable, 'density'.  According to
% the 'density', every 200th pixel is sampled for the density density
% correlation.  This greatly improves the operation time, and is still
% considered a good representation of the entire collection of white
% pixels. For each pixel of consideration, a pseudo-grayscale distance
% transform is created, represented by BW6.  BW6 and BW3, the binary image
% of the agglomerate, are multiplied element-by-element, to create BW7, the
% distance transform of only the agglomerate. For each of these
% "agglomerate distance transforms", the area_r has been defined as the
% area of the agglomerate that has been overlaid by the black circle
% created by the 'im2bw' function.  In other words, area_r is the
% difference between the area of BW3 and the area of BW8.  AREA_R is the
% sum of the area_r's for all of the pixels considered.  difference
% between the original area of the agglomerate and the new binary image.

% Fourth, AREA_R_PARTICLE is the area of the 'ring' of a given r, and
% calculated by subtracting the element of AREA_R by its previous element,
% thus the area of circles, r - (r-1).  For the case of r = 1, the area of
% r = 0 is defined as 1, being the pixel of consideration.

% Fifth, the density density correlation is calculated by dividing
% AREA_R_PARTICLE by AREA_R_WHOLE, element-by-element, and then further
% dividing by the total sample of pixels.
global Binary_Image_3
% to initialize variables
DDC = 0;
AREA_R = 0;
AREA_R(1, 2) = 0;
density = 200;

% to find the maximum value given the height and width of the image, in
% which to create pseudo-grayscale images
BW4 = zeros(Y, X);
y1 = uint16(Y/2);
```

```
x1 = uint16(X/2);
BW4(y1,x1) = 1;
BW5 = bwdist(BW4);
for col = 1:1:Y
    MAX(col) = max(BW5(col,:));
end
maximum = max(MAX);

% to find the indices of all white pixels, representing the agglomerate
[ROW, COL] = find (Binary_Image_3);

% to determine AREA_R, the number of pixels of radius r, and
% that reside within the boundary that is the agglomerate.  Note that this
% is the area of the 'circle', and not the 'ring'
for k = 1:density:area_agglomerate
    BW4 = zeros(Y, X);
    BW4(ROW(k), COL(k)) = 1;
    BW5 = bwdist(BW4, 'euclidean');
    BW6 = BW5 ./ maximum;
    BW7 = Binary_Image_3 .* BW6;
    row = 0;
    for r = 1:1:tr_coefficient
        row = row + 1;
        thresh = r / tr_coefficient;
        BW8 = im2bw (BW7, thresh);
        [area_remainder] = nnz (BW8);
        area_r = area_agglomerate - area_remainder;
        AREA_R(row, 1) = r;
        AREA_R(row, 2) = AREA_R(row, 2) + area_r;
    end
end

% to find AREA_R_PARTICLE, the number of pixels of outer radius r, and
% thickness dr = 1, that reside within the boundary that is the
% agglomerate.  Note that this is the area of the 'ring'
AREA_R_PARTICLE(1,1)=0;
AREA_R_PARTICLE(1,2) = AREA_R(1) - 1;
AREA_R_PARTICLE(2:row, 2) = AREA_R(2:row, 2) - AREA_R(1:(row-1), 2);

% to find DDC, the density density correlation
DDC(1:row, 1) = AREA_R(1:row, 1) .* scale_factor;
DDC(1:row, 2) = AREA_R_PARTICLE(1:row, 2) ./ AREA_R_WHOLE(1:row, 2);
DDC(1:row, 2) = DDC(1:row, 2) ./ (area_agglomerate/density);

% to calculate the density density correlation, we define the value of C(r)
% to be equal to the difference in areas between the sum of the areas of r
% and the sum of the areas of (r-1), and then the whole thing divided by
% the number of pixels considered.  In this case, the area.
filename = 'Density Density Correlation Function.jpeg';
path = strcat(file, filename);
figure, plot (DDC(1:row, 1), DDC(1:row, 2)), xlabel ('radius'),
ylabel('C(r)');
saveas(gcf, path);

% change log-log plot
filename = 'Density Density Correlation Function loglog.jpeg';
```

```
path = strcat(file, filename);
figure, loglog (DDC(1:row, 1), DDC(1:row, 2)), xlabel ('radius'),
ylabel('C(r)');
saveas(gcf, path);


% End of function_density_density_correlation4

 function [tr_coefficient] = function_tr_coefficient (X, Y)
% this function determines the tr_coefficient of the relationship between
threshold
% value and the radius of the circle, thus allowing one to control the
% radius of a circle by controlling the threshold value.
% this function was previously known as "function_slope2"

% ---ALGORITHM---
% To obtain the tr_coefficient, first, a black image (pixel values = 0) of
identical
% height and width is created, and the central pixel is made white (value =
% 1).

% Second, a distance transform, BW5, is performed on the black image,
% BW4.  For each pixel in BW4, the distance transform assigns a number
% equal to the euclidean distance between that pixel and the nearest
% nonzero pixel in BW4.  In this case, it is the central white pixel.
% Therefore, a series of concentric circles of increasing pixel value from
% the centre of BW5 is created, which is precisely similar to the
% increasing radius of a circle.  In other words, given that the centre of
% the circle in BW5 is the location of the white pixel in BW4, as one
% increases the radial distance from the centre, one encounters increasing
% pixel values, and an increasing brightness.  The origin has a value of 0,
% while the farthest pixel from the centre has the greatest value in the
% data matrix of BW5.

% Third, in order to use the 'im2bw' function that turns an image into a
% binary image given a threshold value of [0,1], the image must be in
% grayscale format.  Grayscale format is where all intensity values of an
% image range from 0 to 1, where 0 represents the minimum value and 1
% represents the maximum value of the previous image, respectively. By
% finding the maximum value of BW5, and dividing this data matrix
% element-by-element, one can create a pseudo-grayscale image, which is
% still accepted by the 'im2bw' function.  This pseudo-grayscale image is
% represented by BW6.

% Fourth, given a known threshold value, the 'im2bw' function converts all
% pixels below the threshold value to black pixels, and those above, white.
% Since BW6 is a psuedo-grayscale image representing the distance
% transform, as the threshold value increases, the area of the circle
% increases according to pi*r^2.  Therefore, one can also graph how the
% radius of the black circle increases with the threshold value.  In the
% program, as the threshold value is increased, the area of the black
% circle is counted, the radius is calculated, and recorded in array
% format.
```

```
% Fifth, given the many points of threshold value and radius, the
tr_coefficient is
% calculated via delta y / delta x.  In this case, the points sampled are
% the first and final points of the array.

% to place a white pixel in the middle of an image that is identical in
% height and width to the image being processed
BW4 = zeros(Y, X);
y1 = uint16(Y / 2);
x1 = uint16(X / 2);
BW4(y1, x1) = 1;

% to create the distance transform of BW4
BW5 = bwdist(BW4, 'euclidean');

% to create a pseudo-grayscale image of BW5
for col = 1:1:Y
    MAX(col) = max(BW5(col,:));
end
maximum = max(MAX);
BW6 = BW5 ./ maximum;

% to calculate and record the increasing radius, given the increasing
% threshold value
THRESH = 0;
RAD = 0;
row = 0;

for thresh = 0.001:0.001:.5
    row = row + 1;
    BW7 = im2bw(BW6, thresh);
    area = nnz(~BW7);
    r = sqrt (area/pi);
    THRESH(row) = thresh;
    RAD(row) = r;
end

% to calculate the tr_coefficient via (delta)y / (delta)x
row = row - 1;
tr_coefficient = (RAD(row) - RAD(2)) / (THRESH(row) - THRESH(2));
% fprintf ('\ntr_coefficient = %g\n\n', tr_coefficient);

% End of function_tr_coefficient

 function [ Radius_Gyration ] = Gyration( pixsize )
%Gyration calculates radius of gyration by assuming ever pixel as an area
%of pixsize^2
%   [ Radius_Gyration ] = Gyration( pixsize )
%   Radius_Gyration: radius of gyration
%   pixsize: 1 pixel length= ... nm

global Binary_Image_3

Total_area=nnz(Binary_Image_3)*pixsize^2;
```

```
[xpos ypos]=find(Binary_Image_3);
n_pix=size(xpos,1);
Centroid.x=sum(xpos)/n_pix;
Centroid.y=sum(ypos)/n_pix;

Ar2=zeros(n_pix,1);

for k=1:n_pix;
    Ar2(k,1)=(((xpos(k,1)-Centroid.x)*pixsize)^2+((ypos(k,1)-
Centroid.y)*pixsize)^2)*pixsize^2;
end



Radius_Gyration=(sum(Ar2)/Total_area)^0.5;


end


function [ out ] = isnotequal( A,B )
%UNTITLED2 Summary of this function goes here
%   Detailed explanation goes here
stat=isequal(A,B);

if stat==1
    out=0;
else
    out=1;
end


function [ perimeter ] = Perimeter_Length( pixsize,area_pixelcount )
%Perimeter_Length calculates the lengt of aggregate perimeter
%   Written based on function_perimeter3 (Arka)
%   In the binary image, an edge is defined as the side of a white pixel
%   (value = 1) that is adjacent to a black pixel (value = 0).  First, the
%   program uses the 'find' function to list all of the y-indices in the
%   'ROW' array, and all of the x-indices in the 'COL' array.  This allows
%   one to process only the white pixels, byassing the need to search for the
%   white pixels, and greatly increasing the speed of the function.  Then for
%   each white pixel, the program accumulates a count of how many edges
%   throughout the particle within a 4-neighborhood (up, left, right, down).

global Binary_Image_3

[row, col]=find(Binary_Image_3);
perimeter_pixelcount=0;

for k = 1:1:area_pixelcount
    if (Binary_Image_3(row(k)-1, col(k)) == 0)
        perimeter_pixelcount = perimeter_pixelcount + 1;
    elseif (Binary_Image_3(row(k), col(k)+1) == 0)
        perimeter_pixelcount = perimeter_pixelcount + 1;
```

```
    elseif (Binary_Image_3(row(k), col(k)-1) == 0)
        perimeter_pixelcount = perimeter_pixelcount + 1;
    elseif (Binary_Image_3(row(k)+1, col(k)) == 0)
        perimeter_pixelcount = perimeter_pixelcount + 1;
    end
end

perimeter=perimeter_pixelcount * pixsize;

end


function [Discard] = Refine_image( particle_number )
%Refine_image crops TEM image to the particle serounding and improve the
%image quality
%   Version: 17072012

global mainfolder Im_Dir FileName
global Crop_image Filtered_Image_2 Binary_Image_3 Manual_Edge
FinalImposedImage

Discard=0;

%% "average" filter

h = fspecial('average');
Filtered_Image_1 = imfilter(Crop_image, h);

clear h

%% median filter2
% using the median filter2 function, examine a neighborhood WxW matrix,
% take and make the centre of that matrix the median of the original
% neighborhood.  Specialized for "salt and pepper" noise.

W = 5;
Filtered_Image_2 = medfilt2(Filtered_Image_1 , [W W]);


pass=0;
adj=0;
while pass==0;
    %% Binary image via threshold value

    level = graythresh(Filtered_Image_2);

    imshow(Filtered_Image_2);
    dlg_title='Manual Threshold Control';
    promt={['Please input the adjustment for threshold level (' num2str(0-
level) ' to ' num2str(1-level) '):']};
    num_lines=1;
    def={num2str(adj)};  %default value for user input
    adj=str2num(cell2mat(inputdlg(promt,dlg_title,num_lines,def)));
%#ok<ST2NM> %user input execution
```

```
    level = level+adj;

    Binary_Image_1 = im2bw(Filtered_Image_1,level);

    %% Binary image via Dilation
    % to reduce initial noise and fill initial gaps
    SE1 = strel('square',1);
    Binary_Image_2 = imdilate(~Binary_Image_1,SE1);


    temp_image=imimposemin(Filtered_Image_2,Binary_Image_2);
    imshow(temp_image);

    choise=questdlg('Do you want to change the threshold level?',...
        'Manual Threshold Control','Change the threshold level',...
        'Keep the threshold level','Discard The Image','Change the threshold
level');

    if  strcmp(choise,'Keep the threshold level')==1
        pass=1;
    elseif strcmp(choise,'Discard The Image')==1
        pass=1; Discard=1;
    end

end

if Discard==1
else
%% Binary image via SELECTION
% to further reduce the noise, and solve the area calculation problems of
% multiple particle images

uiwait(msgbox('Please select which particle(s) wished to be analyzed.\nDouble
click, or right click, or shift-click on the desired particle.\nNote that
only one particle may be selected per analysis!',...
    'Process Stage: Manual Artifact Removal','help'));

Binary_Image_3 = bwselect(Binary_Image_2,8);

clear Filtered_Image_1 Binary_Image_1 Binary_Image_2


%% Imposed Image
% to get particle, with no background, thus eliminating the semi-large
% carbon frames in the background
% impose the inverse of Binary_Image_3 on Filtered_Image_2

Imposed_Image=imimposemin(Filtered_Image_2, ~Binary_Image_3);

%% Edge Image via Sobel
% Use Sobel's Method as a built-in edge detection function for particle's
% outline.  Can consider using other methods (Roberts, Canny, etc)
```

```
Edge_Image = edge(Imposed_Image,'sobel');

%% Dilated Edge Image
% to strengthen the particle's outline, use dilation

SE2 = strel('disk',1);
Dilated_Edge_Image = imdilate(Edge_Image,SE2);

clear Edge_Image SE2

%% Manual Edge Image
% to get rid of large spots that are not part of the image obvious to the
% human eye.  May consider automating this process later on for cleaner
% images


pass=0;
while pass==0;

    uiwait(msgbox('Please LEFT click on the pixels that are clearly not part
of the outline.  Push ENTER when finish.',...
        'Process Stage: Manual Edge','help'));

    temp_Edge=bwselect(Dilated_Edge_Image,4);
    close all
    Manual_Edge=Dilated_Edge_Image-temp_Edge;

    imshow(Manual_Edge)

    choise=questdlg('Do you want to repeat the Manual Edge process?',...
        'Manual Edge Clarification','Yes',...
        'No','Yes');
    close all
    if  strcmp(choise,'No')==1
        pass=1;
    end

end


clear temp_Edge Dilated_Edge

FinalImposedImage=imimposemin(Crop_image, Manual_Edge);

%% Saving Images
cd (Im_Dir)

if exist('Output','dir')~=7 %checking wheter the Output folder available
    mkdir('Output')
end

cd('Output')
```

```
imwrite(Filtered_Image_2,[FileName '_Filtered_Image_'
num2str(particle_number) '.tif'])
imwrite(Binary_Image_3,[FileName '_Binary_Image_' num2str(particle_number)
'.tif'])
imwrite(Manual_Edge,[FileName '_Edge_Image_' num2str(particle_number)
'.tif'])
imwrite(FinalImposedImage,[FileName '_Imposed_Image_'
num2str(particle_number) '.tif'])


end
cd(mainfolder);


end


function [ PixSiZe ] = TEM_pix_size()
%Finding TEM Magnification
%   Searching TEM image for bar lenght and it's coresponding size
%   To use this function, put the TEM image on global variable
'processed_img'

global processed_img mainfolder

cd(mainfolder);

xs=811; ys=1108; % Coordinate of the magnification data in the image

if exist('TEMfont.mat','file')==2 % Loading TEM font data
    load('TEMfont.mat');
else
    error('Cannot find the character recognition font')
end

blank=ones(12,5); % blank font
blank=blank.*255;

numdigit=1;

%% Recognizing character
while isnotequal(processed_img(ys:ys+11,xs-2:xs+11-2),kali)

    if processed_img(ys:ys+11,xs:xs+7)==nol
        digit(1,numdigit)=0;
        xs=xs+13;
    elseif processed_img(ys:ys+11,xs:xs+7)==satu
        digit(1,numdigit)=1;
        xs=xs+13;
    elseif processed_img(ys:ys+11,xs:xs+7)==two
        digit(1,numdigit)=2; %#ok<*AGROW>
        xs=xs+13;
```

```
    elseif processed_img(ys:ys+11,xs:xs+7)==three
        digit(1,numdigit)=3;
        xs=xs+13;
    elseif processed_img(ys:ys+11,xs:xs+7)==four
        digit(1,numdigit)=4;
        xs=xs+13;
    elseif processed_img(ys:ys+11,xs:xs+7)==five
        digit(1,numdigit)=5;
        xs=xs+13;
    elseif processed_img(ys:ys+11,xs:xs+7)==six
        digit(1,numdigit)=6;
        xs=xs+13;
    elseif processed_img(ys:ys+11,xs:xs+7)==seven
        digit(1,numdigit)=7;
        xs=xs+13;
    elseif processed_img(ys:ys+11,xs:xs+7)==eight
        digit(1,numdigit)=8;
        xs=xs+13;
    elseif processed_img(ys:ys+11,xs:xs+7)==nine
        digit(1,numdigit)=9;
        xs=xs+13;
    elseif processed_img(ys:ys+11,xs-2:xs+11-2)==kali
        break

    end
    numdigit=numdigit+1;

end

numdigit=numdigit-1;
tempval=0;
%% Calculation
for i=1:numdigit
    tempval=tempval+digit(1,i)*(10^(numdigit-i)); %Calculating the
magnification
end

PixSiZe = 213524*tempval^(-1.001); % Equation to calculate the pixel size
```

Appendix C: Sunset Laboratory EC/OC analysis results

A summary of the method used by Sunset Laboratory is detailed below; full details of NIOSH Method 5040 are detailed by Schlecht and O'Connor (2003).

Part A
In a completely oxygen-free helium atmosphere, the sample is heated in four increasing temperature steps to remove all organic carbon on the filter. The transition from the third temperature to the fourth (from 500 °C to 700 °C) will quickly decompose inorganic carbonates, producing a sharp, characteristic peak. During this first phase there are usually some organic compounds that are pyrolitically converted to elemental carbon. As much as 30% of the organics may be pyrolitically converted to elemental carbon. This pyrolitic conversion is continuously monitored by measuring the transmission of a laser through the filter. As the organic compounds are vaporized, they are immediately oxidized to carbon dioxide in an oxidizer oven which follows the sample oven. The flow of helium, containing the carbon dioxide, then goes to a methanator oven where the CO2 is reduced to methane. The methane, then, is detected by a flame ionization detector (FID).

Part B
After the sample oven is cooled to 525 °C, the pure helium eluent is switched to a 2% oxygen / helium mixture in the sample oven. Then the sample oven temperature is stepped up to 850 °C. During this phase, both the original elemental carbon and that produced by the pyrolysis of organics during the first phase (Part A) are oxidized to carbon dioxide due to the presence of oxygen in the eluent. The carbon dioxide, as in Part A, is then converted to methane and detected by the FID. As previously stated, the darkness of the filter is continuously monitored throughout all stages of the analysis.

Part C
After all carbon has been oxidized from the sample, a known volume and concentration of methane is injected into the sample oven. Thus, each sample is calibrated to a known quantity of carbon. This also provides a means of checking the operation of the instrument. Based on the FID response and laser transmission data, the quantities of organic and elemental carbon are calculated for the sample. (Sunset Laboratory 2010)

The results of this analysis are shown below.

Sample ID	OC(ug/sq cm)	OC unc	EC(ug/sq cm	EC unc	CC(ug/sq cm	CC unc	TC(ug/sq c	TC unc	EC/TC ratio
Mode B50-1	26.95	1.55	9.65	0.68	0.00	0.20	36.60	2.13	0.264
Mode B50-2	16.87	1.04	7.72	0.59	0.00	0.20	24.58	1.53	0.314
Mode B75-1	30.09	1.70	36.74	2.04	0.00	0.20	66.83	3.64	0.550
Mode B75-2	21.90	1.29	31.70	1.78	0.00	0.20	53.59	2.98	0.591
Mode A50-1	16.12	1.01	4.45	0.42	0.00	0.20	20.57	1.33	0.216
Mode A50-2	18.15	1.11	4.22	0.41	0.00	0.20	22.37	1.42	0.189
Mode A75-1	21.45	1.27	7.29	0.56	0.00	0.20	28.74	1.74	0.254
Mode A75-2	15.25	0.96	4.94	0.45	0.00	0.20	20.19	1.31	0.245
Mode A25-1	20.13	1.21	3.80	0.39	0.00	0.20	23.93	1.50	0.159
Mode B25-1	34.30	1.92	2.68	0.33	0.00	0.20	36.99	2.15	0.072
Mode C25-1	29.06	1.65	1.84	0.29	0.00	0.20	30.91	1.85	0.060
Mode C75-1	24.78	1.44	29.93	1.70	0.00	0.20	54.71	3.04	0.547
Mode C75-2	24.69	1.43	30.23	1.71	0.00	0.20	54.91	3.05	0.550
Mode C50-1	25.66	1.48	11.94	0.80	0.00	0.20	37.60	2.18	0.318
B75-NEG-1-1	11.74	0.79	6.81	0.54	0.00	0.20	18.55	1.23	0.367
B75-NEG-1-2	11.88	0.79	5.54	0.48	0.00	0.20	17.42	1.17	0.318
B75-OEGR-1	17.30	1.07	10.45	0.72	0.00	0.20	27.75	1.69	0.376
B75-OEGR-2	15.57	0.98	10.02	0.70	0.00	0.20	25.59	1.58	0.392
Premix 80-1	11.93	0.80	6.25	0.51	0.00	0.20	18.18	1.21	0.344
Premix 80-1	14.77	0.94	18.55	1.13	0.00	0.20	33.33	1.97	0.557
Premix 100-1	11.08	0.75	4.05	0.40	0.00	0.20	15.13	1.06	0.268
Premix 100-2	10.27	0.71	3.05	0.35	0.00	0.20	13.32	0.97	0.229
Blank 1	0.17	0.21	0.00	0.20	0.00	0.20	0.17	0.31	0.000
Blank 2	0.14	0.21	0.00	0.20	0.00	0.20	0.14	0.31	0.000
	0.16								
instrument blank	-0.04	0.20	0.00	0.20	0.00	0.20	-0.04	0.30	0.000
sucrose standard 35.04ug	35.39	1.97	0.00	0.20	0.00	0.20	35.39	2.07	0.000

Sample ID	OC (ug/sq cm)		Difference	Ratio	OC unc	EC (ug/sq cm)	EC unc	CC (ug/sq cm)	CC unc	TC (ug/sq cm)	TC unc	EC/TC ratio	OC/TC rati
B25-1-F	19.58	19.35	10.42	0.46	1.18	1.83	0.29	0.00	-	21.41	1.37	0.09	0.85
B25-1-B	9.16	8.93			0.66	0.07	0.20	0.00	-	9.23	0.76	0.01	0.00
B25-2-F	20.16	19.92	10.65	0.47	1.21	1.63	0.28	0.00	-	21.79	1.39	0.07	0.87
B25-2-B	9.51	9.27			0.68	0.07	0.20	0.00	-	9.58	0.78	0.01	0.00
B50-1-F	14.50	14.27	8.28	0.42	0.93	10.77	0.74	0.00	-	25.27	1.56	0.43	0.43
B50-1-B	6.22	5.98			0.51	0.07	0.20	0.00	-	6.28	0.61	0.01	0.00
B50-2-F	15.62	15.38	9.47	0.38	0.98	10.88	0.74	0.00	-	26.49	1.62	0.41	0.47
B50-2-B	6.14	5.91			0.51	0.05	0.20	0.00	-	6.20	0.61	0.01	0.00
B75-1-F	11.50	11.27			0.78	21.70	1.28	0.00	-	33.20	1.96	0.65	0.00
B75-1-F Duplicate	11.63	11.40	9.17	0.20	0.78	22.26	1.31	0.00	-	33.89	1.99	0.66	0.29
B75-1-B	2.46	2.23			0.32	0.00	0.20	0.00	-	2.46	0.42	0.00	0.00
B75-2-F	16.37	16.14	13.66	0.15	1.02	24.26	1.41	0.00	-	40.63	2.33	0.60	0.36
B75-2-B	2.72	2.48			0.34	0.00	0.20	0.00	-	2.72	0.44	0.00	0.00
B75-LPI-1-F	15.10	14.86			0.95	22.57	1.33	0.00	-	37.66	2.18	0.60	0.00
B75-LPI-1-F Duplicate	14.72	14.48	11.34	0.22	0.94	21.40	1.27	0.00	-	36.12	2.11	0.59	0.35
B75-LPI-1-B	3.38	3.14			0.37	0.00	0.20	0.00	-	3.38	0.47	0.00	0.00
TB-1	0.23				0.21	0.00	0.20	0.00	-	0.23	0.31	0.00	0.00

Sample Calculation for the backup filter correction

Calculation will look at the high load condition

From the second test:

B75-1-F = 11.40 ug/cm^2 OC | 21.70 ug/cm^2 EC

B75-2-B = 2.23 ug/cm^2 OC | 0 ug/cm^2 EC

The SVOC from particles, rather than VOC is:

$\text{OCFront filter} - \text{OCBackup filter} = \text{Particulate OC}$ → 11.63-2.46 = 9.17

And the ratio between the Particulate OC = 11.4/2.23 = 19%

The assumption made in correcting the first round of filter measurements is that this ratio of SVOC to VOC is constant at each load.

This means that the correction from mode B75 is applied to modes B75 and C75 (This is the same for the 50 and 25% load conditions)

From the first test

B75-1-F = 29.94 ug/cm^2 OC | 36.74 ug/cm^2 EC

The corrected OC on the front filter is then

$$m'_{OC,Front} = m_{OC,Front} - \left(\frac{m_{OC,Front}}{f}\right) = 29.94 - \frac{29.94}{0.19} = 24.25$$

And then the corrected volatile fraction is

$$SVOC\ \% = \frac{m'_{OC,Front}}{m'_{OC,Front} + m_{EC,Front}} = \frac{24.25}{24.25 + 36.74} = 35.7\%$$

Appendix D: Raw Data Tables

The following tables show raw engine and emission data for this study:

Appendix D.1 contains the multimode, and premixed combustion modes

Appendix D.2 contains the B75 parameter sweeps.

For the multimode, files are named by the mode, the repeat number and if the SMPS was denuded

For example B50-2-D, is the second repeat at mode B50 with the TD in front of the SMPS

For the parameter sweeps, the name contains the varied parameters as well as the 50% IHR timing

For example, B75-15-MG-INJ-23-MPa-10 is a mode with 15mg/in diesel pilot, with a 23 MPa GRP and 10deg ATDC 50% IHR

Appendix D.1 Multimode Data

Test ID	A25-1'	A25-1-D'	A25-1-B'	A25-1-B-D'	A50-1'	A50-1-D'	A50-2'	A50-2-D'
Engine speed (rpm)	1243	1244	1241	1242	1214	1214	1255	1255
Diesel Rail Pressure (Mpa)	17.88	17.97	18.22	18.25	22.82	22.67	22.64	22.65
CNG downstream pressure (MPa)	16.52	16.43	16.41	16.43	21.43	21.48	21.33	21.34
Manifold air temperature (°C)	38.42	38.23	38.18	37.92	35.69	36.48	40.92	40.86
Surge tank pressure (kPag)	11.96	11.81	11.61	11.62	77.58	77.78	83.40	83.31
Exhaust pressure (before BP valve) (kPag)	15.20	14.99	14.86	14.77	81.09	81.15	86.56	86.49
CNG flow (kg/hr)	2.08	2.07	2.07	2.10	4.34	4.38	4.57	4.65
Diesel flow (kg/hr)	0.29	0.29	0.28	0.26	0.36	0.36	0.36	0.36
Air flow (kg/hr)	82.01	82.40	82.58	82.68	127.46	127.18	131.50	131.58
Peak cylinder pressure (bar)	48.20	48.66	48.88	48.88	85.91	85.40	83.96	83.81
Gross IMEP (bar)	5.02	5.12	5.08	5.08	10.74	10.76	10.61	10.67
50% IHR	14.03	13.85	13.73	13.73	13.52	13.75	14.62	14.65
90% IHR	27.95	28.95	27.45	27.45	35.95	35.95	36.45	36.95
PSOI set [deg]	-18.00	-18.00	-18.00	-18.00	-17.00	-17.00	-17.00	-17.00
PPW [ms]	0.64	0.64	0.64	0.64	0.70	0.70	0.62	0.62
GSOI set [deg]	-5.77	-5.76	-5.78	-5.78	-6.07	-6.07	-6.31	-6.31
GPW [ms]	1.17	1.19	1.19	1.19	1.31	1.31	1.32	1.32
Disel injection mass (mg/inj)	7.84	7.87	7.60	7.00	9.81	10.01	9.56	9.59
CNG injection mass (mg/inj.)	55.76	55.37	55.65	56.36	119.24	120.13	121.32	123.49
Equivalence ratio - total	0.48	0.48	0.48	0.48	0.62	0.63	0.63	0.64
EGR Flow Rate (%)	18.68	18.10	17.52	17.18	16.63	16.90	18.08	17.91
Carbon balance ratio	0.98	1.00	0.99	0.99	1.01	1.01	0.98	0.97
CO (g/kW-hr)	2.64	2.43	2.33	2.23	0.73	0.71	1.15	1.10
CO2 (kg/kW-hr)	0.50	0.50	0.50	0.50	0.49	0.49	0.49	0.49
NOx (g/kW-hr)	1.99	2.06	2.19	2.25	1.77	1.70	1.51	1.52
O2 (kg/kW-hr)	0.78	0.77	0.78	0.78	0.42	0.41	0.42	0.42
CH4 (g/kW-hr)	1.81	1.60	1.50	1.44	0.64	0.61	0.72	0.67
nmHC (g/kW-hr,C1)	0.88	0.91	0.91	1.04	0.46	0.43	0.45	0.44
tHC (g/kW-hr,C1)	2.69	2.50	2.42	2.48	1.10	1.04	1.16	1.11
PM TEOM (g/kW-hr)	0.009	0.009	0.009	0.010	0.010	0.009	0.011	0.011
PM DustTrak (g/kW-hr)	0.005	0.005	0.005	0.005	0.004	0.004	0.003	0.003
Total Number Concentration (#/kWhr)	1.08E+13	7.47E+12	9.98E+12	6.93E+12	1.66E+13	1.56E+13	2.28E+13	2.18E+13
Total Mass Concentration (g/kWhr)	0.014	0.010	0.013	0.010	0.012	0.011	0.012	0.012
Particles Size Geo. Mean(nm)	62.56	63.24	60.37	64.72	50.55	51.62	47.67	49.06

Test ID	A75-1'	A75-1-D'	A75-2'	A75-2-D'	B25-1'	B25-1-D'	B25-1-B'	B25-1-B-D'
Engine speed (rpm)	1216	1216	1236	1235	1498	1497	1498	1498
Diesel Rail Pressure (Mpa)	26.14	26.10	25.91	25.81	21.00	20.82	20.88	20.96
CNG downstream pressure (MPa)	24.84	24.84	24.57	24.60	19.38	19.40	19.33	19.36
Manifold air temperature (°C)	38.18	38.46	40.18	40.20	38.22	38.36	38.66	38.98
Surge tank pressure (kPag)	158.74	158.79	167.25	167.19	16.19	16.31	16.23	15.85
Exhaust pressure (before BP valve) (kPag)	161.53	161.46	169.50	169.47	20.03	20.11	20.00	19.66
CNG flow (kg/hr)	6.83	6.88	7.28	7.31	2.76	2.76	2.70	2.74
Diesel flow (kg/hr)	0.27	0.29	0.32	0.38	0.30	0.30	0.30	0.30
Air flow (kg/hr)	186.34	186.58	197.89	198.00	96.48	96.28	95.87	94.91
Peak cylinder pressure (bar)	118.84	117.61	120.22	120.44	55.64	55.26	55.54	53.66
Gross IMEP (bar)	16.16	16.24	16.47	16.59	5.79	5.66	5.66	5.58
50% IHR	15.24	15.58	15.79	15.82	11.52	11.41	11.31	11.94
90% IHR	38.45	38.95	40.45	40.45	31.95	31.45	31.95	31.95
PSOI set [deg]	-14.00	-14.00	-14.00	-14.00	-25.00	-25.00	-25.00	-25.00
PPW [ms]	0.66	0.66	0.60	0.60	0.64	0.64	0.64	0.64
GSOI set [deg]	-6.27	-6.26	-6.59	-6.59	-10.26	-10.27	-10.26	-10.26
GPW [ms]	1.70	1.70	1.75	1.75	1.06	1.06	1.06	1.06
Disel injection mass (mg/inj)	7.46	8.06	8.58	10.23	6.63	6.58	6.65	6.58
CNG injection mass (mg/inj.)	187.33	188.59	196.31	197.14	61.36	61.35	60.17	60.89
Equivalence ratio - total	0.65	0.65	0.65	0.66	0.53	0.53	0.53	0.54
EGR Flow Rate (%)	15.52	15.46	13.84	13.67	18.91	18.90	18.99	19.55
Carbon balance ratio	1.01	0.99	0.99	0.98	1.00	1.00	1.00	1.00
CO (g/kW-hr)	1.45	1.36	2.35	2.23	1.72	1.74	1.77	1.85
CO2 (kg/kW-hr)	0.49	0.48	0.49	0.49	0.47	0.49	0.48	0.49
NOx (g/kW-hr)	1.66	1.65	1.70	1.72	1.77	1.82	1.80	1.73
O2 (kg/kW-hr)	0.38	0.38	0.40	0.39	0.59	0.61	0.61	0.60
CH4 (g/kW-hr)	0.53	0.53	0.49	0.48	1.17	1.19	1.22	1.26
nmHC (g/kW-hr,C1)	0.29	0.28	0.22	0.21	0.83	0.86	0.90	0.85
tHC (g/kW-hr,C1)	0.83	0.81	0.71	0.69	2.01	2.06	2.13	2.10
PM TEOM (g/kW-hr)	0.012	0.009	0.020	0.019	0.015	0.016	0.016	0.015
PM DustTrak (g/kW-hr)	0.005	0.005	0.007	0.007	0.004	0.004	0.004	0.004
Total Number Concentration (#/kWhr)	4.5E+13	3.54E+13	6.8E+13	5.7E+13	1.13E+14	9.89E+12	9.03E+13	3.77E+13
Total Mass Concentration (g/kWhr)	0.024	0.019	0.040	0.034	0.021	0.007	0.021	0.313
Particles Size Geo. Mean(nm)	54.24	53.40	59.62	60.18	41.36	49.87	45.06	49.95

Test ID	B50-1'	B50-1-D'	B50-2'	B50-2-D'	B75-1'	B75-1-D'	B75-2'	B75-2-D'
Engine speed (rpm)	1495	1496	1502	1503	1475	1476	1483	1484
Diesel Rail Pressure (Mpa)	25.68	25.50	25.61	25.57	27.02	27.10	26.09	26.21
CNG downstream pressure (MPa)	24.49	24.53	24.37	24.31	25.72	25.84	24.93	25.12
Manifold air temperature (°C)	38.64	38.98	40.64	40.60	39.76	40.34	42.74	42.76
Surge tank pressure (kPag)	107.3	107.48	105.6	105.5	174.62	174.16	176.54	176.39
Exhaust pressure (before BP valve) (kPag)	111.5	111.63	110.0	109.8	178.38	177.80	180.68	180.53
CNG flow (kg/hr)	5.67	5.66	5.57	5.54	8.54	8.51	8.41	8.47
Diesel flow (kg/hr)	0.49	0.43	0.54	0.53	0.40	0.56	0.34	0.47
Air flow (kg/hr)	170.5	170.32	168.2	168.3	225.48	223.37	222.45	222.38
Peak cylinder pressure (bar)	104.3	104.27	101.8	101.3	144.43	145.80	140.40	140.34
Gross IMEP (bar)	11.43	11.44	11.01	11.06	16.65	16.42	16.14	15.92
50% IHR	10.67	10.65	10.71	10.93	10.79	10.05	11.18	10.91
90% IHR	37.95	37.95	37.95	37.95	38.95	37.95	38.95	38.45
PSOI set [deg]	-24.0	-24.00	-24.0	-24.00	-23.00	-23.00	-23.00	-23.00
PPW [ms]	0.63	0.63	0.63	0.63	0.61	0.61	0.61	0.61
GSOI set [deg]	-12	-12.06	-12.0	-12.01	-14.95	-14.94	-14.90	-14.90
GPW [ms]	1.15	1.15	1.13	1.13	1.67	1.67	1.70	1.70
Disel injection mass (mg/inj)	10.87	9.63	12.03	11.65	9.11	12.64	7.60	10.55
CNG injection mass (mg/inj.)	126.3	126.07	123.6	122.7	193.06	192.13	189.01	190.16
Equivalence ratio - total	0.61	0.60	0.61	0.61	0.67	0.69	0.67	0.68
EGR Flow Rate (%)	18.97	19.11	19.48	19.50	17.82	18.33	19.55	19.57
Carbon balance ratio	0.98	1.00	0.96	0.97	0.99	0.97	0.99	0.97
CO (g/kW-hr)	2.04	2.26	2.75	2.73	7.13	7.16	7.88	7.87
CO2 (kg/kW-hr)	0.47	0.48	0.48	0.47	0.47	0.48	0.48	0.48
NOx (g/kW-hr)	1.64	1.59	1.50	1.49	1.66	1.60	1.37	1.40
O2 (kg/kW-hr)	0.46	0.45	0.47	0.48	0.35	0.35	0.36	0.36
CH4 (g/kW-hr)	0.83	0.83	0.91	0.90	0.74	0.78	0.85	0.86
nmHC (g/kW-hr,C1)	0.50	0.50	0.44	0.43	0.29	0.29	0.27	0.27
tHC (g/kW-hr,C1)	1.34	1.33	1.35	1.33	1.03	1.07	1.12	1.13
PM TEOM (g/kW-hr)	0.023	0.026	0.029	0.029	0.073	0.069	0.080	0.080
PM DustTrak (g/kW-hr)	0.006	0.007	0.007	0.007	0.030	0.028	0.031	0.030
Total Number Concentration (#/kWhr)	8.7E+13	8.0E+13	1.0E+14	8.8E+13	1.83E+14	1.61E+14	1.92E+14	1.71E+14
Total Mass Concentration (g/kWhr)	0.038	0.035	0.056	0.048	0.249	0.211	0.281	0.252
Particles Size Geo. Mean(nm)	58.41	57.02	60.36	61.27	85.80	86.05	88.46	89.03

Test ID	B75-0EGR-1'	B75-0EGR-1-D'	1.0-EQR-0.72-EGR-25-1'	1.0-EQR-0.72-EGR-25-1-D'	B75-0-EGR-2'	B75-0-EGR-2-D'	1.0-EQR-0.72-EGR-25-2'	1.0-EQR-0.72-EGR-25-2-D'
Engine speed (rpm)	1488	1487	1483	1483	146	146	1461	1462
Diesel Rail Pressure (Mpa)	26.33	26.36	26.07	26.15	25.9	25.9	25.73	25.74
CNG downstream pressure (MPa)	25.22	25.25	25.32	25.35	25.3	25.4	25.11	25.11
Manifold air temperature (°C)	30.50	30.55	39.86	40.38	26.4	27.6	38.23	39.61
Surge tank pressure (kPag)	148	149	147	144	143	143	147	147
Exhaust pressure (before BP valve) (kPag)	155	157	153	148	112	110	153	153
CNG flow (kg/hr)	8.59	8.54	8.23	8.21	8.62	8.63	8.14	8.13
Diesel flow (kg/hr)	0.38	0.37	0.52	0.45	0.33	0.32	0.35	0.36
Air flow (kg/hr)	249	249	191	193	247	247	185	184
Peak cylinder pressure (bar)	134	134	146	149	134	134	132	126
Gross IMEP (bar)	16.45	16.45	16.66	16.65	16.7	16.7	16.47	16.28
50% IHR	11.32	11.32	10.01	9.43	11.2	11.2	12.34	13.17
90% IHR	38.95	38.95	33.45	33.45	39.4	39.9	32.95	33.95
PSOI set [deg]	-22.0	-22.0	-21	-21.0	-22	-22	-21.0	-21.0
PPW [ms]	0.58	0.58	0.67	0.67	0.62	0.62	0.63	0.63
GSOI set [deg]	-14.14	-14.15	-23.9	-23.94	-13	-13	-24.24	-24.25
GPW [ms]	1.75	1.75	1.69	1.69	1.73	1.73	1.73	1.73
Disel injection mass (mg/inj)	8.51	8.31	11.59	10.00	7.50	7.25	7.89	8.14
CNG injection mass (mg/inj.)	192	191	185	184	196	196	186	185
Equivalence ratio - total	0.61	0.61	0.77	0.76	0.61	0.61	0.78	0.78
EGR Flow Rate (%)	0.21	0.20	23.28	20.75	0.18	0.18	24.69	24.74
Carbon balance ratio	0.99	0.99	0.98	0.98	0.97	0.96	0.99	0.98
CO (g/kW-hr)	3.76	3.74	8.21	6.39	3.82	4.12	8.36	8.41
CO2 (kg/kW-hr)	0.48	0.48	0.46	0.46	0.47	0.47	0.46	0.46
NOx (g/kW-hr)	4.47	4.51	2.27	3.29	4.67	4.66	1.64	1.57
O2 (kg/kW-hr)	0.46	0.46	0.21	0.22	0.47	0.47	0.21	0.20
CH4 (g/kW-hr)	0.34	0.35	0.52	0.40	0.42	0.43	0.88	0.83
nmHC (g/kW-hr,C1)	0.16	0.16	0.21	0.20	0.28	0.26	0.34	0.31
tHC (g/kW-hr,C1)	0.51	0.50	0.73	0.60	0.70	0.69	1.22	1.14
PM TEOM (g/kW-hr)	0.023	0.021	0.015	0.011	0.018	0.018	0.010	0.009
PM DustTrak (g/kW-hr)	0.005	0.005	0.007	0.006	0.006	0.006	0.006	0.005
Total Number Concentration (#/kWhr)	8.46E+13	7.33E+13	5.2E+13	3.71E+13	7E+13	7E+13	3.51E+13	3.07E+13
Total Mass Concentration (g/kWhr)	0.043	0.039	0.036	0.026	0.036	0.039	0.024	0.020
Particles Size Geo. Mean(nm)	62.37	63.83	57.08	56.69	61.9	63.2	51.87	52.99

Test ID	B75-NEG-1.0-EQR-0.72-EGR-25-2'	B75-NEG-1.0-EQR-0.72-EGR-25-2-D'	C25-1'	C25-1-D'	C25-1-B'	C25-1-B-D'	C50-1'	C50-1-D'
Engine speed (rpm)	1461	1462	1748	1747	1747	1746	1744	1745
Diesel Rail Pressure (Mpa)	25.73	25.74	20.88	20.91	20.87	20.93	26.30	26.12
CNG downstream pressure (MPa)	25.11	25.11	19.21	19.14	19.22	19.11	25.35	25.23
Manifold air temperature (°C)	38.23	39.61	36.79	36.69	36.47	36.32	34.95	36.39
Surge tank pressure (kPag)	146.8	147.0	13.78	13.17	13.39	13.39	72.47	72.58
Exhaust pressure (before BP valve) (kPag)	152.7	152.5	36.62	36.06	36.44	36.43	77.17	76.97
CNG flow (kg/hr)	8.14	8.13	2.84	2.75	2.97	2.85	5.19	5.17
Diesel flow (kg/hr)	0.35	0.36	0.44	0.43	0.43	0.38	0.55	0.54
Air flow (kg/hr)	184.5	183.6	112.6	111.5	111.8	112.0	162.3	161.2
Peak cylinder pressure (bar)	132.1	125.6	55.26	55.65	55.79	55.27	94.99	94.10
Gross IMEP (bar)	16.47	16.28	5.01	5.14	5.28	5.16	9.13	9.04
50% IHR	12.34	13.17	9.46	9.51	9.73	9.65	7.35	7.61
90% IHR	32.95	33.95	33.95	34.95	36.45	34.45	37.95	37.45
PSOI set [deg]	-21.00	-21.00	-31.00	-31.00	-31.00	-31.00	-30.00	-30.00
PPW [ms]	0.63	0.63	0.63	0.63	0.63	0.63	0.61	0.61
GSOI set [deg]	-24.24	-24.25	-13.90	-13.92	-13.92	-13.92	-16.29	-16.29
GPW [ms]	1.73	1.73	1.02	1.02	1.04	1.04	0.96	0.96
Disel injection mass (mg/inj)	7.89	8.14	8.48	8.14	8.13	7.19	10.44	10.38
CNG injection mass (mg/inj.)	185.7	185.4	54.08	52.54	56.68	54.38	99.27	98.76
Equivalence ratio - total	0.78	0.78	0.49	0.48	0.51	0.48	0.59	0.60
EGR Flow Rate (%)	24.69	24.74	14.61	14.67	14.71	14.68	20.03	20.47
Carbon balance ratio	0.99	0.98	0.95	0.97	0.95	0.99	0.98	0.98
CO (g/kW-hr)	8.36	8.41	1.96	1.90	1.82	1.89	2.93	2.85
CO2 (kg/kW-hr)	0.46	0.46	0.48	0.46	0.48	0.48	0.48	0.47
NOx (g/kW-hr)	1.64	1.57	2.38	2.29	2.20	2.26	1.80	1.74
O2 (kg/kW-hr)	0.21	0.20	0.78	0.76	0.71	0.74	0.48	0.49
CH4 (g/kW-hr)	0.88	0.83	1.30	1.25	1.18	1.22	1.13	1.17
nmHC (g/kW-hr,C1)	0.34	0.31	0.85	0.83	0.82	0.85	0.57	0.59
tHC (g/kW-hr,C1)	1.22	1.14	2.15	2.08	2.01	2.08	1.69	1.76
PM TEOM (g/kW-hr)	0.010	0.009	0.010	0.008	0.010	0.011	0.018	0.018
PM DustTrak (g/kW-hr)	0.006	0.005	0.002	0.001	0.001	0.001	0.004	0.004
Total Number Concentration (#/kWhr)	3.51E+13	3.07E+13	2.25E+13	8.64E+12	3.19E+13	9.60E+12	1.01E+14	8.42E+13
Total Mass Concentration (g/kWhr)	0.024	0.020	0.007	0.003	0.008	0.004	0.032	0.026
Particles Size Geo. Mean(nm)	51.87	52.99	45.19	39.84	47.07	38.60	53.24	52.73

Test ID	C75-1'	C75-1-D'	C75-2'	C75-2-D'	C75-2B'	C75-2B-D'
Engine speed (rpm)	1754	1756	1747	1746	1766	1766
Diesel Rail Pressure (Mpa)	26.80	26.85	26.72	26.63	26.20	26.42
CNG downstream pressure (MPa)	24.10	24.02	25.70	25.65	25.22	25.25
Manifold air temperature (°C)	39.05	39.60	39.25	39.62	34.49	35.89
Surge tank pressure (kPag)	142.75	143.48	148.91	148.40	141.27	141.42
Exhaust pressure (before BP valve) (kPag)	147.67	148.52	153.39	152.91	147.56	147.26
CNG flow (kg/hr)	8.07	7.96	8.55	8.59	8.46	8.44
Diesel flow (kg/hr)	0.72	0.56	0.38	0.59	0.49	0.48
Air flow (kg/hr)	229.85	228.08	236.43	235.95	234.43	234.12
Peak cylinder pressure (bar)	128.66	125.58	133.97	134.19	133.40	134.13
Gross IMEP (bar)	13.78	13.20	14.14	14.06	13.99	13.97
50% IHR	9.74	9.87	9.13	8.95	8.70	8.44
90% IHR	39.95	39.95	39.95	39.45	38.45	38.45
PSOI set [deg]	-29.00	-29.00	-29.00	-29.00	-30.00	-30.00
PPW [ms]	0.59	0.59	0.58	0.58	0.58	0.58
GSOI set [deg]	-18.60	-18.57	-18.73	-18.73	-19.62	-19.62
GPW [ms]	1.47	1.50	1.37	1.39	1.37	1.37
Disel injection mass (mg/inj)	13.70	10.69	7.18	11.35	9.20	9.10
CNG injection mass (mg/inj.)	153.26	151.03	163.15	163.87	159.65	159.29
Equivalence ratio - total	0.64	0.63	0.64	0.66	0.65	0.64
EGR Flow Rate (%)	19.81	20.42	18.83	18.88	19.12	18.90
Carbon balance ratio	0.93	0.97	0.99	0.96	0.98	0.98
CO (g/kW-hr)	5.28	6.12	6.45	7.44	6.00	5.87
CO2 (kg/kW-hr)	0.45	0.47	0.47	0.48	0.47	0.47
NOx (g/kW-hr)	1.47	1.41	1.75	1.66	1.68	1.76
O2 (kg/kW-hr)	0.42	0.43	0.41	0.40	0.40	0.39
CH4 (g/kW-hr)	0.98	1.08	0.98	1.00	0.99	0.97
nmHC (g/kW-hr,C1)	0.37	0.39	0.34	0.33	0.35	0.32
tHC (g/kW-hr,C1)	1.35	1.47	1.32	1.33	1.34	1.29
PM TEOM (g/kW-hr)	0.061	0.071	0.062	0.074	0.062	0.074
PM DustTrak (g/kW-hr)	0.019	0.023	0.018	0.025	0.015	0.014
Total Number Concentration (#/kWhr)	1.83E+14	1.9E+14	1.9E+12	2.14E+12	1.66E+14	1.44E+14
Total Mass Concentration (g/kWhr)	0.175	0.217	0.001	0.001	0.180	0.155
Particles Size Geo. Mean(nm)	77.85	84.01	67.79	68.41	81.15	81.73

Test ID	A50-EGI-Baseline'	A50-EGI-Baseline-D'	EGI-A50-B-05-060-480-156-080-18'	EGI-A50-B-05-060-480-156-080-18-D'	EGI-A50-B-05-00-480-185-062-18'	EGI-A50-B-05-00-480-185-062-18-D'
Engine speed (rpm)	1210	1210	1215	1214	1213	1195
Diesel Rail Pressure (Mpa)	25.64	25.61	25.68	25.52	25.48	25.36
CNG downstream pressure (MPa)	24.59	24.56	24.45	24.39	24.46	23.53
Manifold air temperature (°C)	28.52	29.07	30.46	30.75	30.93	30.80
Surge tank pressure (kPag)	120.11	120.66	91.04	90.94	126.53	122.74
Exhaust pressure (before BP valve) (kPag)	107.31	107.81	89.64	89.73	106.22	103.83
CNG flow (kg/hr)	6.32	6.28	6.03	6.00	6.20	6.19
Diesel flow (kg/hr)	0.39	0.38	0.40	0.40	0.43	0.44
Air flow (kg/hr)	185.40	185.73	150.54	150.25	179.15	175.99
Peak cylinder pressure (bar)	129.99	129.37	121.20	118.98	154.31	148.61
Gross IMEP (bar)	15.33	15.28	14.72	14.62	15.65	15.67
50% IHR	9.65	9.61	9.97	10.17	8.09	8.92
90% IHR	35.95	35.95	29.45	29.45	21.95	23.45
PSOI set [deg]	-18.00	-18.00	-18.00	-18.00	-18.00	-18.00
PPW [ms]	0.61	0.61	0.61	0.61	0.61	0.61
GSOI set [deg]	-10.67	-10.67	-5.25	-5.25	-5.25	-5.25
GPW [ms]	1.58	1.58	0.60	0.60	0.00	0.00
2GSOI set [deg]	0.00	0.00	480.00	480.00	480.00	480.00
2GPW [ms]	0.00	0.00	1.40	1.40	1.83	1.83
Disel injection mass (mg/inj)	10.71	10.61	10.84	10.95	11.77	12.25
CNG injection mass (mg/inj.)	174.12	173.12	165.43	164.72	170.45	172.65
Equivalence ratio - total	0.61	0.61	0.72	0.72	0.63	0.64
EGR Flow Rate (%)	0.19	0.18	0.16	0.16	0.18	0.19
Carbon balance ratio	0.98	0.98	0.97	0.97	0.97	0.96
CO (g/kW-hr)	1.65	1.54	2.88	2.93	1.38	1.37
CO2 (kg/kW-hr)	0.48	0.48	0.46	0.46	0.45	0.45
NOx (g/kW-hr)	6.24	6.30	10.43	10.55	15.77	15.72
O2 (kg/kW-hr)	0.45	0.46	0.30	0.30	0.43	0.43
CH4 (g/kW-hr)	0.30	0.31	3.08	3.10	2.87	2.82
nmHC (g/kW-hr,C1)	0.19	0.19	0.53	0.53	0.48	0.46
tHC (g/kW-hr,C1)	0.49	0.49	3.61	3.63	3.35	3.28
PM TEOM (g/kW-hr)	0.007	0.008	0.010	0.010	0.007	0.005
PM DustTrak (g/kW-hr)	0.002	0.002	0.005	0.006	0.005	0.006
Total Number Concentration (#/kWhr)	3.26E+13	2.59E+13	1.97E+13	1.77E+13	3.14E+12	1.96E+12
Total Mass Concentration (g/kWhr)	0.010	0.008	0.019	0.017	0.010	0.003
Particles Size Geo. Mean(nm)	48.23	49.17	58.59	60.08	80.97	63.64

Test ID	EGI-A50-B-05-00-480-185-062-18-D-3'	EGI-A50-B-05-060-480-156-080-18-2'	EGI-A50-B-05-060-480-156-080-18-2-D'	EGI-A50-B-05-00-480-185-062-18-C'	EGI-A50-B-05-00-480-185-062-18-C-D'
Engine speed (rpm)	1212	1215	1215	1207	1210
Diesel Rail Pressure (Mpa)	25.46	25.22	25.15	25.22	25.50
CNG downstream pressure (MPa)	24.56	24.40	24.41	24.35	24.48
Manifold air temperature (°C)	31.66	31.80	32.11	32.96	33.44
Surge tank pressure (kPag)	125.59	89.42	89.51	126.93	127.75
Exhaust pressure (before BP valve) (kPag)	104.59	87.33	87.71	105.00	106.14
CNG flow (kg/hr)	6.16	6.52	6.50	6.18	6.19
Diesel flow (kg/hr)	0.38	0.28	0.50	0.26	0.26
Air flow (kg/hr)	178.83	146.62	146.30	178.03	180.19
Peak cylinder pressure (bar)	154.24	141.52	139.88	151.77	154.63
Gross IMEP (bar)	15.56	15.36	15.36	15.54	15.61
50% IHR	7.95	7.60	8.03	8.41	8.22
90% IHR	22.45	29.95	30.45	22.95	22.45
PSOI set [deg]	-18.00	-18.00	-18.00	-18.00	-18.00
PPW [ms]	0.61	0.61	0.61	0.61	0.61
GSOI set [deg]	-5.25	-5.25	-5.25	-5.25	-5.25
GPW [ms]	0.00	0.60	0.60	0.00	0.00
2GSOI set [deg]	480.00	480.00	480.00	480.00	480.00
2GPW [ms]	1.83	1.45	1.45	1.82	1.82
Disel injection mass (mg/inj)	10.40	7.73	13.70	7.07	7.16
CNG injection mass (mg/inj.)	169.41	179.06	178.49	170.67	170.48
Equivalence ratio - total	0.62	0.79	0.81	0.61	0.61
EGR Flow Rate (%)	0.19	0.15	0.15	0.18	0.19
Carbon balance ratio	0.97	1.00	0.96	1.00	0.99
CO (g/kW-hr)	1.42	6.58	6.21	1.37	1.48
CO2 (kg/kW-hr)	0.45	0.48	0.48	0.45	0.45
NOx (g/kW-hr)	16.06	11.69	11.71	15.97	15.70
O2 (kg/kW-hr)	0.44	0.20	0.21	0.43	0.45
CH4 (g/kW-hr)	3.11	2.14	2.16	3.09	3.40
nmHC (g/kW-hr,C1)	0.51	0.38	0.38	0.48	0.54
tHC (g/kW-hr,C1)	3.61	2.52	2.54	3.57	3.94
PM TEOM (g/kW-hr)	0.006	0.019	0.018	0.007	0.007
PM DustTrak (g/kW-hr)	0.005	0.012	0.012	0.006	0.005
Total Number Concentration (#/kWhr)	2.64E+12	4.87E+13	3.93E+13	3.88E+12	2.76E+12
Total Mass Concentration (g/kWhr)	0.009	0.049	0.044	0.011	0.010
Particles Size Geo. Mean(nm)	88.28	65.07	66.88	79.07	88.36

Appendix D.2 Input Parameter Sweeps

Test ID	B75-10T-Baseline'	B75-10T-Baseline-D'	B75-15T-Baseline'	B75-15T-Baseline-D'	B75-05T-Baseline'	B75-05T-Baseline-D'	B75-15MG-ING-23MPA'	B75-15MG-ING-23MPA-D'
Engine speed (rpm)	1487	1487	1481	1483	1482	1482	1471	1472
Diesel Rail Pressure (Mpa)	25.94	25.89	25.87	25.89	25.81	25.80	23.56	23.53
CNG downstream pressure (MPa)	25.04	25.05	24.57	25.15	23.90	23.56	22.92	22.87
Manifold air temperature (°C)	38.99	40.88	43.43	42.31	43.75	43.83	36.11	37.54
Surge tank pressure (kPag)	221.3	221.61	222.46	222.1	223.22	222.55	186.38	186.12
Exhaust pressure (before BP valve) (kPag)	227.9	227.89	228.65	228.6	228.42	228.24	190.84	190.83
CNG flow (kg/hr)	9.26	9.27	9.05	9.47	8.76	8.55	8.11	8.10
Diesel flow (kg/hr)	0.40	0.42	0.45	0.41	0.49	0.50	0.63	0.63
Air flow (kg/hr)	249.3	247.83	245.08	246.0	248.67	246.77	222.56	222.50
Peak cylinder pressure (bar)	154.9	154.63	129.99	131.7	178.56	176.11	148.31	147.72
Gross IMEP (bar)	16.48	16.44	15.97	16.49	16.30	15.82	16.51	16.41
50% IHR	10.12	10.16	15.55	15.50	4.31	4.31	9.41	9.33
90% IHR	36.95	36.95	41.45	41.95	30.95	30.95	34.95	34.95
PSOI set [deg]	-25	-25	-20	-20	-31	-31	-28	-28
PPW [ms]	0.55	0.55	0.55	0.55	0.55	0.55	0.9	0.9
GSOI set [deg]	-17.4	-17.42	-12.45	-12.4	-23.44	-23.44	-17.41	-17.40
GPW [ms]	2.2	2.2	2.15	2.15	2.45	2.45	1.97	1.97
Disel injection mass (mg/inj)	8.93	9.35	10.15	9.27	10.96	11.32	14.32	14.28
CNG injection mass (mg/inj.)	207.4	207.91	203.74	212.8	197.08	192.40	183.83	183.52
Equivalence ratio - total	0.66	0.66	0.66	0.68	0.63	0.62	0.66	0.66
EGR Flow Rate (%)	18.59	18.39	18.74	18.60	17.21	17.34	19.12	18.43
Carbon balance ratio	0.97	0.97	0.97	0.97	0.97	0.97	0.97	0.97
CO (g/kW-hr)	7.48	7.79	5.79	6.99	5.41	5.07	8.46	8.49
CO2 (kg/kW-hr)	0.51	0.51	0.52	0.52	0.49	0.50	0.46	0.46
NOx (g/kW-hr)	1.98	1.95	1.12	1.07	4.81	4.86	1.80	1.86
O2 (kg/kW-hr)	0.42	0.41	0.42	0.38	0.45	0.47	0.37	0.38
CH4 (g/kW-hr)	0.71	0.67	0.54	0.54	0.68	0.72	0.70	0.69
nmHC (g/kW-hr,C1)	0.59	0.57	0.55	0.54	0.60	0.62	0.49	0.49
tHC (g/kW-hr,C1)	1.30	1.23	1.09	1.08	1.28	1.34	1.20	1.18
PM TEOM (g/kW-hr)	0.109	0.113	0.095	0.106	0.066	0.068	0.107	0.104
PM DustTrak (g/kW-hr)	0.079	0.055	0.062	0.048	0.041	0.029	0.066	0.054
Total Number Concentration (#/kWhr)	1.6E+14	1.42E+14	1.55E+14	1.4E+14	1.48E+14	1.05E+14	1.98E+14	1.72E+14
Total Mass Concentration (g/kWhr)	0.148	0.130	0.112	0.106	0.110	0.072	0.350	0.309

Test ID	B75-15MG-ING-23MPA-15'	ING-23MPA-15-D'	B75-15MG-ING-23MPA-5'	B75-15MG-ING-23MPA-5-D'	B75-1100-RPM-10'	B75-1100-RPM-10-D'	B75-1100-RPM-15'	B75-1100-RPM-15-D'	B75-1100-RPM-5'
Engine speed (rpm)	1466	1467	1491	1490	1114	1114	1112	1111	1078
Diesel Rail Pressure (Mpa)	23.6	23.5	23.5	23.5	26.0	25.9	25.9	25.9	25.4
CNG downstream pressure (MPa)	22.9	22.9	23.0	22.9	25.3	25.3	25.3	25.3	24.9
Manifold air temperature (°C)	40.2	40.4	36.5	37.9	30.2	30.6	32.2	32.2	26.7
Surge tank pressure (kPag)	197.1	197.3	167	169.4	140.2	140	144.9	144	138.5
Exhaust pressure (before BP valve) (kPag)	203.2	202.9	171	173.8	143.9	144	149.0	148	143.1
CNG flow (kg/hr)	8.47	8.45	7.81	7.83	6.11	6.09	6.23	6.25	5.88
Diesel flow (kg/hr)	0.59	0.59	0.66	0.67	0.45	0.43	0.40	0.43	0.30
Air flow (kg/hr)	232.1	233.1	214	213.9	171.8	171	170.2	170	157.2
Peak cylinder pressure (bar)	127.9	127.7	160	162.4	138.8	138	121.3	120	163.5
Gross IMEP (bar)	16.7	16.6	16.0	16.0	16.4	16.4	16.5	16.5	16.7
50% IHR	15.0	15.0	4.1	4.2	10.6	10.5	14.8	14.9	5.4
90% IHR	40.5	40.5	29.5	29.5	33.5	33.0	36.0	36.0	28.0
PSOI set [deg]	-23	-23	-33	-33	-15	-15	-11	-11	-19
PPW [ms]	0.9	0.9	0.92	0.92	0.62	0.62	0.62	0.62	0.55
GSOI set [deg]	-12.4	-12.4	-22.1	-22.1	-8.9	-8.9	-4.9	-4.9	-13.5
GPW [ms]	2.03	2.03	1.88	1.88	1.66	1.66	1.71	1.71	1.66
Disel injection mass (mg/inj)	13.3	13.4	14.7	14.9	13.3	13.0	11.9	12.9	9.1
CNG injection mass (mg/inj.)	192.6	191.9	174	175.2	183.0	182	186.8	187	181.6
Equivalence ratio - total	0.66	0.65	0.67	0.67	0.64	0.64	0.66	0.66	0.66
EGR Flow Rate (%)	17.8	17.4	17.7	18.2	16.7	16.7	18.2	17.9	20.1
Carbon balance ratio	0.97	0.97	0.98	0.97	1.00	1.01	1.00	1.00	0.99
CO (g/kW-hr)	6.54	6.18	7.18	7.64	3.55	3.50	1.62	1.64	3.14
CO2 (kg/kW-hr)	0.48	0.48	0.46	0.46	0.48	0.48	0.49	0.49	0.46
NOx (g/kW-hr)	1.10	1.12	3.79	3.52	2.42	2.42	1.71	1.75	3.39
O2 (kg/kW-hr)	0.38	0.39	0.35	0.35	0.37	0.37	0.35	0.35	0.33
CH4 (g/kW-hr)	0.52	0.50	0.70	0.71	0.43	0.44	0.41	0.41	0.38
nmHC (g/kW-hr,C1)	0.43	0.42	0.45	0.43	0.59	0.57	0.50	0.49	0.59
tHC (g/kW-hr,C1)	0.95	0.92	1.15	1.14	1.02	1.01	0.91	0.90	0.97
PM TEOM (g/kW-hr)	0.088	0.089	0.05	0.057	0.025	0.02	0.018	0.01	0.025
PM DustTrak (g/kW-hr)	0.061	0.049	0.02	0.020	0.028	0.02	0.023	0.01	0.027
Total Number Concentration (#/kWhr)	1.78E+14	1.61E+14	1.6E+14	1.25E+14	7.08E+13	5.8E+13	4.07E+13	3.3E+13	5.26E+13
Total Mass Concentration (g/kWhr)	0.271	0.241	0.24	0.136	0.067	0.05	0.037	0.03	0.047

Test ID	B75-055-EQR-10-D'	B75-055-EQR-15'	B75-055-EQR-15-D'	B75-055-EQR-05'	B75-055-EQR-05-D'	B75-065-EQR-10'	B75-065-EQR-10-D'	B75-065-EQR-5'
Engine speed (rpm)	1473	1469	1469	1478	1478	1482	1482	1483
Diesel Rail Pressure (Mpa)	26.2	26.2	26.2	26.2	26.2	25.4	25.4	25.4
CNG downstream pressure (MPa)	25.7	25.6	25.5	25.4	25.3	24.7	24.7	24.7
Manifold air temperature (°C)	34.3	35.0	35.3	35.1	34.8	29.4	32.1	32.2
Surge tank pressure (kPag)	212.3	212.1	212.5	198.8	198.9	161.6	162.0	163.9
Exhaust pressure (before BP valve) (kPag)	216.4	216.4	216.0	202.6	202.5	165.8	166.1	167.3
CNG flow (kg/hr)	8.09	8.44	8.30	8.01	7.99	8.61	8.63	8.56
Diesel flow (kg/hr)	0.85	0.82	0.58	0.59	0.59	0.53	0.52	0.48
Air flow (kg/hr)	252.1	252.1	252.2	242.3	242.0	217.6	216.1	221.9
Peak cylinder pressure (bar)	164.8	137.8	137.1	178.4	178.1	145.8	145.0	165.5
Gross IMEP (bar)	16.5	16.6	16.4	16.4	16.3	16.4	16.2	16.5
50% IHR	8.8	14.6	14.5	4.8	4.6	9.5	9.5	5.1
90% IHR	35.0	40.5	40.0	31.0	30.5	37.5	37.5	34.0
PSOI set [deg]	-25	-20	-20	-29	-29	-25	-25	-29
PPW [ms]	0.67	0.67	0.67	0.67	0.67	0.65	0.65	0.65
GSOI set [deg]	-16.4	-11.5	-11.4	-20.4	-20.4	-16.6	-16.6	-20.5
GPW [ms]	1.6	1.7	1.7	1.67	1.67	1.83	1.83	1.85
Disel injection mass (mg/inj)	19.2	18.7	13.1	13.4	13.2	12.0	11.7	10.9
CNG injection mass (mg/inj.)	183.1	191.6	188.4	180.7	180.2	193.8	194.2	192.4
Equivalence ratio - total	0.60	0.62	0.59	0.60	0.60	0.71	0.72	0.69
EGR Flow Rate (%)	20.6	20.4	20.4	19.7	19.6	20.1	20.3	17.9
Carbon balance ratio	0.95	0.95	0.98	0.97	0.97	0.98	0.98	0.99
CO (g/kW-hr)	3.76	4.10	3.57	4.20	4.33	12.59	13.31	10.64
CO2 (kg/kW-hr)	0.47	0.49	0.48	0.46	0.46	0.48	0.48	0.47
NOx (g/kW-hr)	2.15	1.19	1.18	3.45	3.45	1.55	1.41	2.96
O2 (kg/kW-hr)	0.51	0.48	0.50	0.47	0.48	0.32	0.31	0.33
CH4 (g/kW-hr)	0.97	0.87	0.87	0.98	0.99	0.79	0.80	0.71
nmHC (g/kW-hr,C1)	0.39	0.36	0.35	0.38	0.39	0.41	0.41	0.38
tHC (g/kW-hr,C1)	1.36	1.23	1.22	1.36	1.38	1.20	1.21	1.10
PM TEOM (g/kW-hr)	0.056	0.071	0.054	0.039	0.040	0.092	0.138	0.083
PM DustTrak (g/kW-hr)	0.038	0.079	0.045	0.034	0.025	0.121	0.099	0.056
Total Number Concentration (#/kWhr)	1.21E+14	1.53E+14	1.29E+14	1.16E+14	1.03E+14	2.16E+14	1.94E+14	1.69E+14
Total Mass Concentration (g/kWhr)	0.135	0.184	0.135	0.092	0.080	0.607	0.479	0.221

Test ID	B75-065-EQR-5-D'	B75-065-EQR-15'	B75-065-EQR-15-D'	B75-070-EQR-10'	B75-070-EQR-10-D'	B75-23-MPa-10'	B75-23-MPa-10-D'	B75-23-MPa-05'
Engine speed (rpm)	1483	1477	1476	1479	1479	1477	1477	1475
Diesel Rail Pressure (Mpa)	25.4	25.3	25.3	25.3	25.3	23.6	23.7	23.6
CNG downstream pressure (MPa)	24.7	24.7	24.9	24.0	23.7	22.9	23.0	22.8
Manifold air temperature (°C)	31.9	33.4	33.7	35.6	36.3	29.4	30.6	33.6
Surge tank pressure (kPag)	164.3	176.2	176.6	160.7	159.6	174.9	175.1	190.3
Exhaust pressure (before BP valve) (kPag)	167.6	179.7	180.0	164.5	163.6	179.3	179.2	194.4
CNG flow (kg/hr)	8.57	8.94	9.12	8.89	8.73	8.57	8.64	8.81
Diesel flow (kg/hr)	0.51	0.79	0.79	0.53	0.55	0.43	0.44	0.42
Air flow (kg/hr)	222.0	228.7	228.7	209.5	206.4	232.2	231.3	235.8
Peak cylinder pressure (bar)	165.9	129.0	130.3	142.4	140.9	149.3	148.8	132.4
Gross IMEP (bar)	16.5	16.6	16.8	16.4	16.3	16.5	16.3	16.5
50% IHR	5.1	14.4	14.4	10.4	10.4	9.9	10.0	14.9
90% IHR	34.0	41.5	41.5	39.5	40.0	38.0	38.5	42.5
PSOI set [deg]	-29	-21	-21	-25	-25	-26	-26	-22
PPW [ms]	0.65	0.65	0.65	0.65	0.65	0.65	0.65	0.65
GSOI set [deg]	-20.5	-12.6	-12.6	-16.6	-16.6	-17.6	-17.6	-13.6
GPW [ms]	1.85	1.9	1.9	2	2	2.05	2.05	2.08
Disel injection mass (mg/inj)	11.4	17.8	17.9	12.0	12.3	9.6	10.0	9.4
CNG injection mass (mg/inj.)	192.5	201.7	206.0	200.3	196.7	193.4	194.9	199.1
Equivalence ratio - total	0.69	0.72	0.73	0.76	0.76	0.66	0.66	0.66
EGR Flow Rate (%)	17.5	18.9	18.8	21.2	21.7	18.2	18.1	20.3
Carbon balance ratio	0.98	0.95	0.95	0.96	0.96	0.98	0.98	0.98
CO (g/kW-hr)	10.21	9.52	10.51	16.57	15.95	8.03	8.61	6.28
CO2 (kg/kW-hr)	0.47	0.49	0.50	0.48	0.47	0.48	0.48	0.49
NOx (g/kW-hr)	3.05	1.06	1.06	1.05	0.99	1.85	1.84	0.96
O2 (kg/kW-hr)	0.34	0.34	0.32	0.26	0.27	0.39	0.39	0.39
CH4 (g/kW-hr)	0.69	0.65	0.65	0.88	0.90	0.75	0.75	0.68
nmHC (g/kW-hr,C1)	0.38	0.37	0.36	0.42	0.44	0.41	0.38	0.35
tHC (g/kW-hr,C1)	1.06	1.02	1.01	1.30	1.33	1.16	1.14	1.03
PM TEOM (g/kW-hr)	0.077	0.107	0.131	0.171	0.231	0.107	0.104	0.008
PM DustTrak (g/kW-hr)	0.043	0.096	0.097	0.172	0.167	0.078	0.062	0.068
SMPS Number Concentration (#/kWhr)	1.53E+14	2.08E+14	1.95E+14	2.88E+14	2.49E+14	1.82E+14	1.69E+14	1.82E+14
SMPS Mass Concentration (g/kWhr)	0.197	0.341	0.366	1.032	0.950	0.287	0.271	0.227

Test ID	B75-23-MPa-05-D'	B75-23-MPa-15'	B75-23-MPa-15-D'	B75-28-MPa-10'	B75-28-MPa-10-D'	B75-28-MPa-05'	B75-28-MPa-05-D'	B75-28-MPa-15'
Engine speed (rpm)	1476	1475	1475	1478	1477	1481	1481	1475
Diesel Rail Pressure (Mpa)	23.7	23.6	23.6	28.8	28.8	28.8	28.7	28.8
CNG downstream pressure (MPa)	22.9	22.9	22.8	28.1	28.0	28.0	28.2	27.2
Manifold air temperature (°C)	34.8	34.1	33.6	33.2	34.0	33.8	33.6	35.4
Surge tank pressure (kPag)	190.6	192.7	192.8	180.9	181.0	179.5	179.9	190.5
Exhaust pressure (before BP valve) (kPag)	194.8	196.5	196.4	185.2	185.2	183.1	183.6	194.4
CNG flow (kg/hr)	8.85	8.86	8.84	8.38	8.42	8.29	8.36	8.69
Diesel flow (kg/hr)	0.42	0.40	0.40	0.48	0.49	-0.09	0.46	0.42
Air flow (kg/hr)	235.6	242.6	243.3	226.3	225.9	228.6	229.4	239.7
Peak cylinder pressure (bar)	131.9	133.4	133.5	149.0	148.9	173.4	174.4	129.4
Gross IMEP (bar)	16.5	16.6	16.6	16.3	16.4	16.6	16.4	16.7
50% IHR	14.9	14.9	14.9	10.0	10.0	4.7	4.3	14.7
90% IHR	43.0	43.0	42.5	36.5	36.5	32.5	31.5	40.0
PSOI set [deg]	-22	-22	-22	-22	-22	-27	-27	-18
PPW [ms]	0.65	0.65	0.65	0.58	0.58	0.58	0.58	0.52
GSOI set [deg]	-13.6	-13.6	-13.6	-14.2	-14.2	-19.2	-19.2	-10.7
GPW [ms]	2.08	2.1	2.1	1.5	1.5	1.5	1.5	1.66
Disel injection mass (mg/inj)	9.5	9.1	9.1	10.8	11.0	-2.1	10.3	9.6
CNG injection mass (mg/inj.)	200.0	200.1	199.8	189.0	189.9	186.6	188.3	196.3
Equivalence ratio - total	0.67	0.65	0.64	0.66	0.67	0.61	0.65	0.64
EGR Flow Rate (%)	20.4	18.4	18.1	20.8	20.7	19.0	18.6	20.2
Carbon balance ratio	0.98	0.98	0.98	0.98	0.97	1.07	0.98	1.00
CO (g/kW-hr)	6.66	5.11	4.88	8.07	7.84	6.30	6.40	5.37
CO2 (kg/kW-hr)	0.49	0.49	0.49	0.47	0.47	0.46	0.47	0.49
NOx (g/kW-hr)	0.95	1.11	1.15	1.63	1.58	3.24	3.48	1.07
O2 (kg/kW-hr)	0.38	0.41	0.42	0.38	0.38	0.39	0.39	0.40
CH4 (g/kW-hr)	0.68	0.56	0.56	0.80	0.78	0.76	0.78	0.77
nmHC (g/kW-hr,C1)	0.35	0.30	0.30	0.38	0.37	0.37	0.39	0.34
tHC (g/kW-hr,C1)	1.03	0.87	0.85	1.18	1.15	1.13	1.17	1.11
PM TEOM (g/kW-hr)	0.115	0.067	0.072	0.079	0.071	0.041	0.041	0.042
PM DustTrak (g/kW-hr)	0.059	0.052	0.051	0.060	0.047	0.027	0.020	0.031
SMPS Number Concentration (#/kWhr)	1.66E+14	1.74E+14	1.74E+14	1.78E+14	1.55E+14	1.32E+14	1.06E+14	1.45E+14
SMPS Mass Concentration (g/kWhr)	0.213	0.184	0.175	0.240	0.198	0.111	0.088	0.111

Test ID	B75-28-MPa-15-D'	B75-10-EGR-15'	B75-10-EGR-15-D'	B75-10-EGR-10'	B75-10-EGR-10-D'	B75-10-EGR-05'	B75-10-EGR-05-D'	B75-30-EGR-10'
Engine speed (rpm)	1477	1477	1477	1483	1483	1481	1480	1483
Diesel Rail Pressure (Mpa)	28.8	25.8	25.7	25.9	25.8	25.8	25.8	25.9
CNG downstream pressure (MPa)	26.9	25.2	24.9	24.6	24.4	25.3	25.2	25.0
Manifold air temperature (°C)	35.5	31.0	31.1	30.4	30.1	28.6	28.9	40.7
Surge tank pressure (kPag)	190.2	170.7	170.6	167.5	167.2	173.3	173.4	210.2
Exhaust pressure (before BP valve) (kPag)	194.0	172.8	172.6	169.3	168.9	175.5	175.4	214.6
CNG flow (kg/hr)	8.50	9.25	8.97	8.45	8.35	8.79	8.71	8.56
Diesel flow (kg/hr)	0.43	0.66	0.53	0.46	0.45	0.70	0.75	0.48
Air flow (kg/hr)	239.9	247.0	246.9	247.6	247.4	252.8	253.0	223.2
Peak cylinder pressure (bar)	126.2	125.4	124.6	151.5	149.9	174.2	175.3	158.7
Gross IMEP (bar)	16.3	17.2	17.0	16.4	16.3	16.6	17.2	16.7
50% IHR	15.2	15.3	15.4	8.6	8.7	3.9	4.1	10.0
90% IHR	40.0	42.0	41.5	36.0	36.0	31.0	32.5	36.5
PSOI set [deg]	-18	-19	-19	-25	-25	-29	-29	-26
PPW [ms]	0.52	0.58	0.58	0.58	0.58	0.58	0.58	0.65
GSOI set [deg]	-10.7	-11.2	-11.2	-17.2	-17.2	-21.2	-21.2	-17.5
GPW [ms]	1.66	1.9	1.9	1.85	1.85	1.82	1.82	1.83
Disel injection mass (mg/inj)	9.7	15.0	12.0	10.3	10.2	15.9	16.9	10.8
CNG injection mass (mg/inj.)	191.7	208.6	202.4	189.8	187.6	197.7	196.2	192.4
Equivalence ratio - total	0.63	0.68	0.65	0.61	0.60	0.63	0.63	0.68
EGR Flow Rate (%)	20.1	11.2	11.3	10.3	10.2	10.2	10.2	29.4
Carbon balance ratio	1.00	0.98	0.99	1.00	1.01	0.97	0.97	0.98
CO (g/kW-hr)	4.71	6.01	5.18	6.16	5.89	5.83	5.71	8.99
CO2 (kg/kW-hr)	0.49	0.51	0.50	0.49	0.49	0.50	0.48	0.47
NOx (g/kW-hr)	1.11	1.76	1.75	3.62	3.69	6.19	5.96	0.83
O2 (kg/kW-hr)	0.42	0.37	0.39	0.45	0.46	0.45	0.43	0.35
CH4 (g/kW-hr)	0.81	0.39	0.40	0.57	0.60	0.65	0.64	1.24
nmHC (g/kW-hr,C1)	0.35	0.24	0.25	0.31	0.32	0.37	0.35	0.54
tHC (g/kW-hr,C1)	1.17	0.63	0.64	0.88	0.92	1.02	0.99	1.78
PM TEOM (g/kW-hr)	0.046	0.082	0.050	0.055	0.054	0.035	0.035	0.128
PM DustTrak (g/kW-hr)	0.022	0.042	0.028	0.035	0.024	0.019	0.015	0.103
SMPS Number Concentration (#/kWhr)	1.2E+14	1.59E+14	1.32E+14	1.56E+14	1.33E+14	1.11E+14	1.02E+14	1.89E+14
SMPS Mass Concentration (g/kWhr)	0.086	0.135	0.099	0.129	0.108	0.070	0.064	0.394

Test ID	B75-30-EGR-10-D'	B75-MIN-PPW-10'	B75-MIN-PPW-10-D'	B75-MIN-PPW-5'	B75-MIN-PPW-5-D'	B75-MIN-PPW-15'	B75-MIN-PPW-15-D'	B75-15-MG-INJ-15'
Engine speed (rpm)	1483	1488	1488	1491	1491	1485	1487	1484
Diesel Rail Pressure (Mpa)	25.8	25.8	25.9	25.8	25.9	25.8	25.8	25.7
CNG downstream pressure (MPa)	25.0	25.1	25.2	25.2	25.1	24.5	24.2	25.0
Manifold air temperature (°C)	42.4	36.4	36.0	36.9	36.8	36.9	36.9	36.8
Surge tank pressure (kPag)	210.6	187.2	187.4	183.3	183.2	191.2	191.1	194.5
Exhaust pressure (before BP valve) (kPag)	214.6	190.4	190.6	186.7	186.5	194.4	194.4	198.0
CNG flow (kg/hr)	8.54	8.56	8.72	8.45	8.34	8.59	8.43	8.74
Diesel flow (kg/hr)	0.48	0.25	0.36	0.37	0.38	0.42	0.41	1.25
Air flow (kg/hr)	222.8	233.2	233.7	226.1	227.4	235.2	235.4	239.2
Peak cylinder pressure (bar)	160.2	154.7	154.6	174.1	173.7	129.6	126.9	131.2
Gross IMEP (bar)	16.7	16.5	16.4	16.5	16.4	16.3	16.0	16.6
50% IHR	9.7	9.2	9.1	4.7	4.6	14.8	15.1	15.0
90% IHR	36.5	37.0	36.0	32.5	32.0	41.5	41.5	42.0
PSOI set [deg]	-26	-25	-25	-29	-29	-20	-20	-22
PPW [ms]	0.65	0.57	0.57	0.57	0.57	0.57	0.57	0.83
GSOI set [deg]	-17.5	-17.2	-17.2	-21.2	-21.2	-12.2	-12.2	-11.9
GPW [ms]	1.83	1.83	1.83	1.76	1.76	1.88	1.88	1.84
Disel injection mass (mg/inj)	10.8	5.7	8.1	8.4	8.5	9.4	9.2	28.1
CNG injection mass (mg/inj.)	192.0	191.7	195.3	188.9	186.5	192.8	189.0	196.3
Equivalence ratio - total	0.68	0.64	0.66	0.66	0.65	0.65	0.64	0.70
EGR Flow Rate (%)	29.0	19.6	19.4	21.2	20.8	20.5	20.7	20.9
Carbon balance ratio	0.97	1.00	0.98	0.99	0.99	0.99	0.99	0.92
CO (g/kW-hr)	8.41	6.49	7.06	6.17	5.90	5.24	4.85	6.06
CO2 (kg/kW-hr)	0.46	0.47	0.48	0.47	0.46	0.49	0.49	0.50
NOx (g/kW-hr)	0.86	1.89	1.90	2.87	2.96	0.99	0.99	0.96
O2 (kg/kW-hr)	0.35	0.40	0.39	0.37	0.38	0.40	0.42	0.38
CH4 (g/kW-hr)	1.07	0.79	0.80	0.83	0.84	0.75	0.79	0.72
nmHC (g/kW-hr,C1)	0.48	0.41	0.40	0.42	0.42	0.37	0.38	0.35
tHC (g/kW-hr,C1)	1.55	1.20	1.20	1.25	1.26	1.12	1.17	1.08
PM TEOM (g/kW-hr)	0.112	0.068	0.066	0.044	0.043	0.058	0.057	0.051
PM DustTrak (g/kW-hr)	0.070	0.042	0.038	0.027	0.020	0.039	0.029	0.076
SMPS Number Concentration (#/kWhr)	1.72E+14	1.55E+14	1.51E+14	1.23E+14	1.07E+14	1.44E+14	1.35E+14	1.73E+14
SMPS Mass Concentration (g/kWhr)	0.346	0.165	0.179	0.105	0.090	0.120	0.129	0.240

Test ID	B75-15-MG-INJ-15-D'	B75-15-MG-INJ-10'	B75-15-MG-INJ-10-D'	B75-15-MG-INJ-05'	B75-15-MG-INJ-05-D'	B75-093-PPW-10'	B75-093-PPW-10-D'	B75-15-MG-INJ-055-EQR-10'
Engine speed (rpm)	1483	1487	1487	1489	1491	1483	1482	1482
Diesel Rail Pressure (Mpa)	25.7	25.7	25.8	25.7	25.7	26.1	26.1	26.1
CNG downstream pressure (MPa)	25.2	24.9	24.8	24.6	24.5	25.3	25.3	25.5
Manifold air temperature (°C)	37.8	36.9	36.4	36.0	36.8	35.1	35.3	34.9
Surge tank pressure (kPag)	194.9	194.8	194.7	194.5	183.1	193.0	192.6	209.5
Exhaust pressure (before BP valve) (kPag)	198.3	197.7	197.6	197.3	186.5	197.0	196.3	212.8
CNG flow (kg/hr)	9.02	8.43	8.33	8.15	8.15	8.25	8.22	8.22
Diesel flow (kg/hr)	1.25	0.83	0.60	0.61	0.61	1.00	0.66	0.85
Air flow (kg/hr)	238.3	243.3	244.4	244.6	230.3	240.7	240.9	258.8
Peak cylinder pressure (bar)	133.4	158.3	157.6	176.9	171.6	155.5	154.3	160.4
Gross IMEP (bar)	17.2	16.7	16.5	16.5	16.2	16.5	16.4	16.7
50% IHR	15.1	9.2	9.3	4.9	4.8	9.6	9.8	9.8
90% IHR	42.5	37.0	37.0	32.0	33.0	37.0	36.5	36.0
PSOI set [deg]	-22	-27	-27	-31	-31	-27	-27	-26
PPW [ms]	0.83	0.83	0.83	0.83	0.83	0.93	0.93	0.85
GSOI set [deg]	-11.9	-16.9	-16.9	-20.9	-20.9	-16.1	-16.1	-15.8
GPW [ms]	1.84	1.8	1.8	1.8	1.8	1.74	1.74	1.67
Disel injection mass (mg/inj)	28.2	18.7	13.4	13.6	13.7	22.4	14.9	19.2
CNG injection mass (mg/inj.)	202.7	189.0	186.6	182.5	182.2	185.4	184.8	184.9
Equivalence ratio - total	0.72	0.64	0.62	0.60	0.64	0.64	0.62	0.59
EGR Flow Rate (%)	21.4	19.8	19.3	18.9	20.9	20.7	20.4	19.0
Carbon balance ratio	0.93	0.97	1.00	1.00	1.00	0.96	1.00	0.97
CO (g/kW-hr)	7.88	6.03	5.30	4.43	7.04	7.36	7.04	3.62
CO2 (kg/kW-hr)	0.50	0.48	0.48	0.48	0.48	0.48	0.48	0.48
NOx (g/kW-hr)	0.86	1.91	2.02	3.59	2.80	1.80	1.77	2.18
O2 (kg/kW-hr)	0.34	0.42	0.44	0.45	0.39	0.42	0.43	0.50
CH4 (g/kW-hr)	0.72	0.78	0.79	0.83	0.86	0.88	0.84	0.83
nmHC (g/kW-hr,C1)	0.36	0.35	0.36	0.39	0.40	0.47	0.44	0.40
tHC (g/kW-hr,C1)	1.08	1.13	1.15	1.22	1.26	1.34	1.28	1.22
PM TEOM (g/kW-hr)	0.124	0.075	0.063	0.040	0.055	0.147	0.092	0.063
PM DustTrak (g/kW-hr)	0.093	0.063	0.043	0.027	0.034	0.099	0.067	0.045
SMPS Number Concentration (#/kWhr)	1.65E+14	1.62E+14	1.35E+14	1.12E+14	1.28E+14	1.74E+14	1.54E+14	1.32E+14
SMPS Mass Concentration (g/kWhr)	0.300	0.211	0.158	0.094	0.139	0.309	0.255	0.144

Test ID	B75-15-MG-INJ-055-EQR-10-D'	B75-15-MG-INJ-055-EQR-05'	B75-15-MG-INJ-055-EQR-05-D'	B75-15-MG-INJ-055-EQR-15'	B75-15-MG-INJ-055-EQR-15-D'	B75-15-MG-065-EQR-10'	B75-15-MG-065-EQR-10-D'	B75-15-MG-065-EQR-15'
Engine speed (rpm)	1481.3	1483	1483	1480.3	1481.1	1470.5	1470.1	1469.1
Diesel Rail Pressure (Mpa)	26.1	26.1	26.1	26.0	26.1	25.7	25.8	25.7
CNG downstream pressure (MPa)	25.4	25.3	25.2	24.8	24.6	25.0	25.1	25.0
Manifold air temperature (°C)	35.0	35.0	34.9	35.2	35.4	30.8	32.0	34.6
Surge tank pressure (kPag)	210.6	193.5	193.7	204.2	204.5	168.9	169.2	176.9
Exhaust pressure (before BP valve) (kPag)	213.96	197.0	197.2	207.70	208.07	172.76	172.97	180.45
CNG flow (kg/hr)	8.15	8.04	8.00	8.44	8.30	8.56	8.59	8.55
Diesel flow (kg/hr)	0.8	0.6	0.6	0.6	0.6	0.6	0.6	0.6
Air flow (kg/hr)	258.3	243.6	243.2	253.4	252.8	219.9	219.2	222.7
Peak cylinder pressure (bar)	159.9	177.4	176.6	135.4	134.3	147.9	147.4	129.4
Gross IMEP (bar)	16.5	16.4	16.3	16.4	16.2	16.4	16.5	16.3
50% IHR	9.7	4.5	4.5	14.8	14.9	9.5	9.6	14.1
90% IHR	35.95	31.45	31.45	41.45	41.45	36.95	36.95	40.95
PSOI set [deg]	-26	-31	-31	-22	-22	-26	-26	-22
PPW [ms]	0.8	0.8	0.8	0.8	0.8	0.8	0.8	0.8
GSOI set [deg]	-15.78	-20.76	-20.77	-11.79	-11.78	-16.29	-16.30	-12.04
GPW [ms]	1.7	1.7	1.7	1.8	1.8	1.8	1.8	1.8
Disel injection mass (mg/inj)	18.4	14.0	14.0	13.2	14.1	12.6	12.8	12.7
CNG injection mass	183.35	180.6	179.7	189.95	186.82	194.10	194.81	194.10
Equivalence ratio - total	0.6	0.6	0.6	0.6	0.6	0.7	0.7	0.7
EGR Flow Rate (%)	19.31	19.61	19.67	19.46	19.83	19.46	19.40	20.01
Carbon balance ratio	0.98	1.01	1.01	1.01	1.00	0.97	0.96	0.97
CO (g/kW-hr)	3.39	4.86	4.98	4.46	4.20	11.50	11.56	8.63
CO2 (kg/kW-hr)	0.48	0.48	0.48	0.50	0.50	0.48	0.47	0.48
NOx (g/kW-hr)	2.21	3.67	3.69	1.18	1.14	1.63	1.57	1.00
O2 (kg/kW-hr)	0.51	0.46	0.46	0.47	0.48	0.34	0.33	0.35
CH4 (g/kW-hr)	0.85	0.87	0.88	0.71	0.71	0.78	0.78	0.69
nmHC (g/kW-hr,C1)	0.40	0.41	0.41	0.33	0.33	0.36	0.35	0.33
tHC (g/kW-hr,C1)	1.25	1.27	1.29	1.04	1.04	1.14	1.13	1.02
PM TEOM (g/kW-hr)	0.058	0.038	0.041	0.068	0.068	0.110	0.116	0.091
PM DustTrak (g/kW-hr)	0.037	0.028	0.022	0.063	0.052	0.117	0.091	0.096
SMPS Number Concentration (#/kWhr)	1.14E+14	1.1E+14	1.1E+14	1.37E+14	1.43E+14	1.96E+14	1.72E+14	1.87E+14
SMPS Mass Concentration (g/kWhr)	0.121	0.093	0.092	0.171	0.173	0.478	0.385	0.313

Test ID	B75-15-MG-065-EQR-15-D'	B75-15-MG-065-EQR-05'	B75-15-MG-065-EQR-05-D'	B75-15-MG-INJ-23-MPa-10'	B75-15-MG-INJ-23-MPa-10-D'	B75-15-MG-INJ-23-MPa-15'	B75-15-MG-INJ-23-MPa-15-D'	B75-15-MG-INJ-23-MPa-5'
Engine speed (rpm)	1469.3	1471.6	1472.1	1466.3	1466.4	1465.2	1465.6	1470.6
Diesel Rail Pressure (Mpa)	25.7	25.7	25.7	24.2	24.2	24.2	24.2	24.2
CNG downstream pressure (MPa)	24.8	24.5	24.5	23.4	23.4	23.4	23.4	23.4
Manifold air temperature (°C)	34.7	35.0	35.3	35.2	35.8	36.6	37.0	36.7
Surge tank pressure (kPag)	176.70	168.42	168.31	196.71	196.14	196.72	196.83	183.08
Exhaust pressure (before BP valve) (kPag)	180.27	171.93	171.86	200.95	200.27	200.63	200.72	186.98
CNG flow (kg/hr)	8.4	8.3	8.2	8.5	8.5	8.8	8.8	8.3
Diesel flow (kg/hr)	0.6	0.6	0.6	0.6	0.5	0.5	0.5	0.6
Air flow (kg/hr)	222.8	215.3	215.7	239.2	238.8	239.6	239.2	227.8
Peak cylinder pressure (bar)	128.9	167.0	167.2	157.5	156.2	131.8	131.2	172.5
Gross IMEP (bar)	16.1	16.2	16.2	16.6	16.6	16.5	16.5	16.5
50% IHR	14.09	4.73	4.75	9.63	9.85	15.29	15.42	4.96
90% IHR	40.45	32.95	32.95	36.95	37.45	42.45	42.45	32.95
PSOI set [deg]	-22.0	-31.0	-31.0	-27.0	-27.0	-23.0	-23.0	-32.0
PPW [ms]	0.83	0.83	0.83	0.8	0.8	0.87	0.87	0.89
GSOI set [deg]	-12.0	-21.0	-21.0	-17.3	-17.3	-12.7	-12.7	-21.5
GPW [ms]	1.8	1.9	1.9	2.0	2.0	2.0	2.0	2.0
Disel injection mass (mg/inj)	12.53	13.55	13.99	14.02	11.72	11.89	12.34	13.44
CNG injection mass (mg/inj.)	191.6	187.4	186.2	192.2	192.6	199.4	199.6	188.1
Equivalence ratio - total	0.68	0.70	0.69	0.64	0.64	0.66	0.66	0.66
EGR Flow Rate (%)	19.88	19.70	19.58	21.28	21.20	21.08	21.14	21.03
Carbon balance ratio	0.97	0.97	0.96	0.98	0.99	0.99	0.99	0.99
CO (g/kW-hr)	8.42	9.99	9.83	6.77	6.84	7.43	7.47	8.45
CO2 (kg/kW-hr)	0.48	0.47	0.47	0.48	0.49	0.50	0.51	0.48
NOx (g/kW-hr)	1.04	2.79	2.81	1.64	1.62	0.90	0.90	2.63
O2 (kg/kW-hr)	0.36	0.34	0.34	0.42	0.42	0.40	0.39	0.38
CH4 (g/kW-hr)	0.71	0.75	0.76	0.85	0.85	0.78	0.78	0.83
nmHC (g/kW-hr,C1)	0.33	0.33	0.33	0.35	0.34	0.33	0.33	0.33
tHC (g/kW-hr,C1)	1.04	1.08	1.08	1.20	1.19	1.11	1.11	1.16
PM TEOM (g/kW-hr)	0.094	0.072	0.077	0.089	0.097	0.107	0.111	0.078
PM DustTrak (g/kW-hr)	0.083	0.056	0.044	0.084	0.067	0.113	0.091	0.057
SMPS Number Concentration (#/kWhr)	1.65E+14	1.62E+14	1.45E+14	1.71E+14	1.62E+14	2.01E+14	1.79E+14	1.62E+14
SMPS Mass Concentration (g/kWhr)	0.295	0.231	0.207	0.273	0.260	0.362	0.318	0.223

Test ID	B75-NEG-PSEP-BASELINE -10'	B75-NEG-PSEP-BASELINE -10-D'	B75-NEG-PSEP-BASELINE -15'	B75-NEG-PSEP-BASELINE -15-D'	B75-NEG-PSEP-BASELINE -5'
Engine speed (rpm)	1487.1	1487.2	1484.9	1485.7	1489.5
Diesel Rail Pressure (Mpa)	25.8	25.8	25.8	25.7	25.9
CNG downstream pressure (MPa)	25.0	25.0	25.0	24.9	25.4
Manifold air temperature (°C)	34.1	34.7	35.9	36.2	35.7
Surge tank pressure (kPag)	173.98	174.29	191.34	191.59	178.74
Exhaust pressure (before BP valve) (kPag)	177.58	177.98	194.86	195.19	182.08
CNG flow (kg/hr)	8.4	8.4	8.8	8.8	8.3
Diesel flow (kg/hr)	0.5	0.5	0.5	0.5	0.8
Air flow (kg/hr)	225.6	225.3	238.7	238.7	228.3
Peak cylinder pressure (bar)	148.5	147.5	131.9	131.2	176.1
Gross IMEP (bar)	16.3	16.3	16.7	16.6	16.5
50% IHR	9.74	10.12	14.24	14.37	4.67
90% IHR	34.95	35.45	38.45	38.45	30.45
PSOI set [deg]	-20.0	-20.0	-17.0	-17.0	-24.0
PPW [ms]	0.64	0.64	0.64	0.64	0.64
GSOI set [deg]	-17.0	-17.0	-14.0	-14.0	-21.0
GPW [ms]	1.7	1.7	1.8	1.8	1.6
Disel injection mass (mg/inj)	11.31	11.48	11.38	11.35	17.25
CNG injection mass (mg/inj.)	187.5	187.8	196.8	196.8	185.2
Equivalence ratio - total	0.66	0.67	0.66	0.66	0.67
EGR Flow Rate (%)	19.59	19.77	20.08	20.11	19.71
Carbon balance ratio	0.98	0.98	0.98	0.99	0.97
CO (g/kW-hr)	6.46	6.88	6.58	6.35	5.37
CO2 (kg/kW-hr)	0.47	0.47	0.49	0.49	0.47
NOx (g/kW-hr)	2.09	1.99	1.29	1.28	3.64
O2 (kg/kW-hr)	0.37	0.37	0.39	0.39	0.37
CH4 (g/kW-hr)	0.95	0.94	1.03	1.02	0.81
nmHC (g/kW-hr,C1)	0.39	0.37	0.38	0.38	0.36
tHC (g/kW-hr,C1)	1.33	1.32	1.40	1.40	1.17
PM TEOM (g/kW-hr)	0.047	0.049	0.054	0.056	0.032
PM DustTrak (g/kW-hr)	0.042	0.037	0.049	0.036	0.028
SMPS Number Concentration (#/kWhr)	1.31E+14	1.2E+14	1.41E+14	1.22E+14	9.65E+13
SMPS Mass Concentration (g/kWhr)	0.029	0.136	0.122	0.147	0.123